University of Southampton

Initiation of Electrical Degradation in High Voltage Polymeric Cable Insulation: Electroluminescence Detection

by

Nathalie Cariou-Saintemarie

A thesis submitted for the degree of

Doctor of Philosophy

in

The Department of Electronics and Computer Science

March 2001

UNIVERSITY OF SOUTHAMPTON

ABSTRACT

FACULTY OF ENGINEERING AND APPLIED SCIENCE

DEPARTMENT OF ELECTRONICS AND COMPUTER SCIENCE

Doctor of Philosophy

INITIATION OF ELECTRICAL DEGRADATION IN HIGH VOLTAGE POLYMERIC CABLE INSULATION: ELECTROLUMINESCENCE DETECTION

by Nathalie Cariou-Saintemarie

Ageing detection and indications of insulation degradation are often achieved when ageing is already significant, for example when partial discharge (PD) activity is detected from a large enough micro-cavity. Little is known about the degradation before PD activity occurs. Nowadays, long-term degradation in discharge free situations is increasingly the subject of attention. This is because the size level of defects in the insulation has been highly reduced thanks to progress in technology. However the stress increase, due to a reduction of the cable insulation thickness for practical and economic reasons, could amplify the effect of phenomena which were not considered as important until recently. Internal defects cannot be completely eliminated from high voltage cable insulation and one of cable manufacturers' quality tests has revealed the presence of micro-defects in some cross-linked polyethylene (XLPE) transmission cable main insulation. The aim of this study was to investigate the significance of these micro-defects on the degradation of the insulation under ac stresses.

In order to achieve that, a better characterisation and understanding of this phenomenon was primordial. A procedure for the observation of this phenomenon was developed. Since these features were a few microns across, they were likely to induce only a low level of degradation and it was unlikely that they would sustain detectable (electrically) discharges. A method for early detection of electrical ageing before the onset of PD activity was therefore necessary and electroluminescence (EL) was selected. An experimental arrangement was integrally designed to carry out EL measurements on insulating samples in a uniform field configuration at room temperature under ac stress. The experimental system, using a very sensitive cooled CCD detector, made it possible to successfully measure (with short integration time) and monitor the integral electroluminescence in LDPE and XLPE cable insulation samples under relatively low voltages, and to determine the spectral range as well as allowing the imaging of this very low level of light. The difference in temporal behaviour and spectral range of the emission between XLPE cable samples containing micro-defects and samples without micro-defects showed that the degradation of the insulation under ac stresses was accelerated by the presence of the micro-defects.

A ma mère

Acknowledgements

I would like to express my gratitude to Professor Tony Davies for his advice, guidance and encouragement during the course of this research. I would also like to express my appreciation for the valuable help and assistance received from my colleagues within the High Voltage Group, especially to Mr Roland Caldecutt, Mr Neil Palmer, Mr Brian Rogers, Mr Mark Long, and Mr Fred Ho.

My grateful thanks are also extended to Pirelli Cables Company who are funding this research project. Within this organisation, I would like to thank Mr Julian Head, Dr Steve Norman, Mr Malcolm Simmons, and Mr Stewart Walker for their advice and encouragement throughout the project. I am particularly grateful to Mr Stuart Jameson and Mr John Bevis for their help with the work carried out at Pirelli Cables Eastleigh.

I am also grateful to my friends and family. I thank Jacques, my husband, for his love, support and encouragement during this work.

Contents

List of Figures

List of Tables

Chapter 1

Introduction

Polymeric insulation is extensively used in underground high voltage cable insulation. It was in the 1960's that the use of extruded polymeric materials made rapid progress with the use of cross-linked polyethylene [1]. Extruded polymers are gradually replacing the traditional oil-filled cable mainly because of the complexity, the high cost and the relatively high dielectric losses of the latter. Today polymeric cables are rated at all system voltages, from distribution class cables carrying voltages from 5 to 30kV to transmission class cables reaching 400kV and even 500kV [2].

Polymers used as insulation materials in high voltage underground power cables have excellent short-term dielectric properties such as high dielectric strength, ~900kV/mm, low dielectric loss, $\delta < 10^{-3}$, and high dc resistivity, $> 10^{6}$ Ω.m. In addition they have good short term mechanical properties together with high corrosion resistance. They can however be susceptible to long term deterioration due to the application of high electrical stress. For polymeric insulation to be satisfactory in service, scrupulous cleanliness is essential. Improvements in manufacturing techniques and quality control have led to a significant reduction in void size and levels of contamination. However even with present-

day technology, internal defects cannot be completely eliminated and a significant number of service failures are initiated by these inherent defects. These may affect the insulation in many ways by being, for instance, a source of gas discharges, by the enhancement of the local field stress, and causing chemical deterioration or a mixture of all these. The defects could, for example, act as points of electric stress enhancement in the insulation where a tree like growth degradation would initiate which in turn would lead to breakdown [3]. This project examines localised micro-defects which are present in the insulation of power transmission class underground cables and investigates their significance on the degradation of the insulation under ac stresses using a light collection method.

1.1 High Voltage polymeric cable

The design of cables is regulated by a number of industrial, national and international standards and guides [4]. They are related to voltage level, production technology or customer preference. A typical construction of a high voltage (HV) cable comprises a central stranded conductor, which carries the current. Only copper or aluminium are used as conductor material in present day practice. The conductor is surrounded by a semiconducting screen (see figure 1.1).

Semiconducting screens are used in all high voltage cables to ensure a smooth electrical interface between conducting and insulating regions. Indeed the stranded profile of the conductor surface would for example initiate localised field concentrations if interfaced directly with the insulation, with consequent implications in electrical breakdown of the insulation. A smooth semiconducting screen thus removes such field concentrations and ensures a uniformly stressed screen/insulation interface. For XLPE cables the semiconducting layers are formed by extrusion. They are compounds of carbon with polymers chosen to accept a high carbon loading, be bondable to the insulation, be compatible with the extrusion conditions and to be removable when required without damaging the dielectric.

Extruded over the semiconducting screen is the insulating material, which is the most important part of the cable. For cables operating at 66kV and above, the choice of extruded insulation is essentially limited to polyethylene (PE), ethylene propylene rubber (EPR), and crosslinked polyethylene (XLPE). PE is limited to a service temperature of 70°C due to its softening point. XLPE and EPR can withstand the higher operating temperature of 90°C. EPR is inferior to XLPE in loss factor and initial dielectric strength, but has greater resistance to partial discharge and moisture [4].

Surrounding the insulation is another semiconducting screen around which is the metallic sheath, usually aluminium or lead for the UK. This sheath prevents the ingress of moisture into the cable, which could electrically weaken the dielectric. Metal sheaths must be protected against corrosion and for specially bonded systems they must be insulated from earth. The cable is enclosed in a polymer jacket.

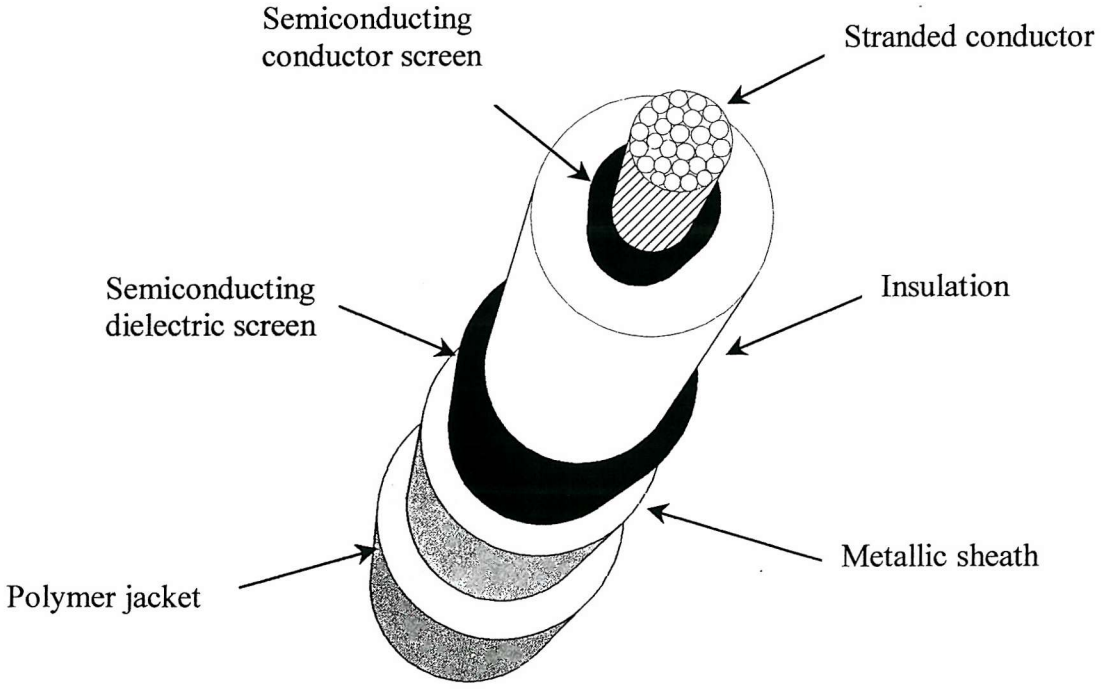

Figure 1.1: typical construction of an HV polymeric cable

Whilst several different materials have been developed and applied, crosslinked polyethylene (XLPE) has emerged as the most favoured extruded insulation material. In this thesis only XLPE insulation has been studied.

1.2 Ageing of polymeric insulating materials

Ageing can be caused by the electrical stress, for example if defects are present in the insulation they will act as points of electrical stress enhancement where the degradation can initiate. Besides the electrical stress, mechanical stresses are sources of ageing due to the bending of the cable or due to vibrations in the ground. The cable is also subjected to thermal stresses due to load cycling and seasonal temperature fluctuations. The cable may also be subjected to environmental stresses due to moisture or gases present in the soil. All these stresses acting singly or in combination cause degradation of the insulation.

In this thesis the emphasis has been placed on electrical ageing, meaning the form of degradation for which an electric field is necessary. Although many physical and chemical ageing processes occur in the absence of an electric field, like for example the formation of free radicals (caused by thermal, oxidation, UV absorption, or mechanical reasons) causing a deterioration of the insulation, the more severe forms of degradation are however visible and specifically electric in origin. In good quality cable insulation it is electrical trees and water trees which lead to the most damaging deterioration during service. As their names indicate, the degradation takes the form of a tree like growth [3, 5].

Electrical trees usually grow in cables operating in a dry environment e.g. when they are enclosed in conduits before they are buried in the ground. Water trees grow in cables which operate in a humid environment where moisture is present. Only electrical tree degradation has been considered as the cables studied in this thesis operate in a dry environment. In recent years [5] some insight has been gained into the growth and the propagation mechanisms of the electrical treeing. Since electrical trees usually start at points of electric stress enhancement in the insulation, such points are simulated in the

research laboratory by embedding sharp needles into a polymer block [6, 51]. It has been shown that electrical treeing has two distinct time periods in its development. The first is the incubation period or initiation phase during which no partial discharges (PD) occur. The second is the propagation period during which PD occur and the tree grows [7]. When large enough cavities are created partial discharges occur in the gaseous contents of microscopic voids when the field exceeds a threshold value depending on the void size and the gas pressure. Once the PD have started, erosion processes will deteriorate the surface of the void and repetitive discharges will cause the tree to grow. The initiation phase of an electrical tree is not well understood.

Several mechanisms have been proposed for electrical tree initiation under ac stresses [8, 9]. These include:

- tree initiation by mechanical fatigue due to Maxwell stresses,
- tree initiation by partial discharges (hot electrons that can break polymer bonds),
- tree initiation by charge injection and extraction.

Once a tree has started to grow it is only a matter of time, sometimes a few power cycles, before final breakdown may occur. Hence a better understanding of the initiation phase is primordial as are possible methods to evaluate the degree of ageing of the insulation.

Physico-chemical analysis such as infra-red spectroscopy or dielectric spectroscopy such as loss tangent measurement can be carried out in order to evaluate material degradation due to electrical stresses. However apart from severe ageing conditions that lead to heavily degraded materials, it is often difficult to reach a conclusion since measurements scatter over a wide range of the sample and the significant parameter which would be related to the degree of ageing of the material is not known. Space charge has been recognised as harmful and different measurement techniques have been developed such as the laser induced pressure pulse technique (LIPP) or the pulse electroacoustic method (PEA) [10]. However doubts exist as to whether or not this method can give useful information on the ageing and pre-breakdown processes [11].

Electrical tree initiation and propagation can be detected by several methods among which are: partial discharge detection, acoustic emission detection, current pulses, light emission detection, optical microscopy, electron spin resonance (ESR) and thermally stimulated currents (TSC) [5]. Light emission or electroluminescence, which is the first observable process, occurs either prior to tree inception or at lower voltages in ramp experiments. This process does not necessarily lead to electrical trees. However a region of degeneration is irreversibly produced during its action [7].

Electroluminescence (EL) is defined as the emission of photons induced by the application of an electric field. EL in this study is the light emitted by a material when an high electric field is applied to it in discharge–free conditions. It is not related to a gaseous discharge but it is a solid state physics effect. EL has been observed during the initiation stage of an electrical tree at a voltage which is significantly below the partial discharge inception level [7]. Therefore EL detection has been successfully used as a method which is sensitive enough to reveal the early stages of polymeric degradation and to give information on possible early degradation mechanisms prior to an electrical tree inception [7, 11].

EL in semi-conducting polymers is an important field of research carried out in order to develop electroluminescent device applications, including displays and lighting. This work deals only with EL from insulating polymers which is an exciting field of research because it has been associated with electrical ageing of polymeric materials and could provide a basis for monitoring the degradation rate.

1.3 Research objectives

Ageing detection and indications of insulation degradation are often achieved when ageing is already significant, for example when partial discharge activity is detected from a large enough micro-cavity. Little is known about the degradation before PD activity occurs.

Nowadays, long-term degradation in discharge free situations is increasingly the subject of attention. This is because the size level of defects in the insulation has been highly

reduced thanks to progress in technology. However the stress increase (due to a reduction of the cable insulation thickness for practical and economic reasons) could amplify the effect of phenomena which were not considered as important until recently.

Internal defects cannot be completely eliminated from high voltage cable insulation and one of cable manufacturers' quality tests has revealed the presence of micro-defects in some cross-linked polyethylene (XLPE) transmission cable main insulation. The aim of this study was to investigate the significance of these micro-defects on the degradation of the insulation under ac stresses.

In order to achieve that, a better characterisation and understanding of this phenomenon was primordial. A procedure for the observation of this phenomenon was developed and is presented in Chapter 2. The microscopic observation techniques of electron, optical and fluorescence microscopy were explored and the most appropriate was retained. Infrared spectroscopy (FTIR) was also used for this purpose. In order to better understand what produced this effect, the influence on the micro-defects of the industrial degassification process parameters as well as the effect of electrical ageing was assessed.

Since these features were a few microns across, they were likely to induce only a low level of degradation and it was unlikely that they would sustain detectable (electrically) discharges. A method for early detection of electrical ageing before the onset of PD activity was therefore necessary and electroluminescence (EL) had been used. The available theory on EL of polymers is presented in Chapter 3 considering that EL of insulating polymers is currently poorly understood. This can be explained by the few research teams specialised in this field and by the difficulty of EL experiments that involve very sensitive optical detection systems performed in an HV environment. The two chapters following present the experimental work carried out on EL.

Chapter 4 describes the design and set-up of an experimental arrangement at Southampton University High Voltage Laboratory in order to carry out EL measurements. This experimental system allows the measurement and monitoring of the integral EL as well as

the imaging of the emission and permits to determine the EL spectral range. The electrical, mechanical and optical aspects of the design are discussed.

Chapter 5 presents and comments on some results obtained from slices of commercial low density polyethylene (LDPE) and samples microtomed from production high voltage cross linked polyethylene (XLPE) cable insulation. The results are classified according to the nature of the experiment:

- imaging of the emission,
- ramps tests with monitoring and measurement of the integral light intensity,
- spectral analysis of the emission at constant voltage.

A comparison is also made between XLPE samples containing micro-defects and samples without micro-defects.

Chapter 6 presents the conclusions of the work carried out and recommendations for further study in the light of the results presented.

Chapter 2

Examination of production XLPE cable insulation

2.1 Introduction

For insulating polymers to be satisfactory in service, a high level of cleanliness is essential both during the fabrication of the polymer and the manufacture of the cable. Improvements in manufacturing techniques have led to a significant reduction in void size and level of contamination. However internal defects cannot be completely eliminated. One of the cable manufacturer's quality tests has revealed the presence of a "smoky" 'halo' effect in some crosslinked polyethylene (XLPE) cable main insulation. Part of the quality test required samples of cables to be subjected to an "oven test", details of which are presented later in this chapter. This test originally revealed the presence of halo bands inside the main insulation.

The aim of this study was to investigate the significance of the features present in the 'halo' on the degradation of the insulation under ac stresses. In order to achieve that, a better characterisation of this phenomenon was primordial. Some original work was

carried out in order to establish a procedure for the observation of this phenomenon as this would allow the study of EL as a function of position within the cable insulation. The microscopic observation techniques of electron, optical and fluorescence microscopy were explored and the most appropriate were retained. Infrared spectroscopy (FTIR) was also used to investigate the halo phenomenon. In order to better understand what produced this effect, the influence on the halo region of the industrial degassification process parameters has been assessed, as has the effect of ageing of cable insulation.

In this thesis the terms micro-void or micro-crack describe cavities probably partly, or wholly, filled with air, methane or peroxide decomposition products.

2.2 Crosslinking of Low Density Polyethylene (LDPE)

2.2.1 Introduction

In a power cable, a high current flows through a central conductor and the insulation surrounding the conductor is subjected to relatively high temperatures together with a temperature gradient. The polymer is therefore crosslinked to provide sufficient mechanical strength to withstand the high temperature. PE is limited to a service temperature of 70^0C due to its softening point. XLPE can withstand the higher operating temperature of 90^0C. Chemical crosslinking is the most commonly used technique, creating by-products in the process (see paragraphs 2.2.2 and 2.2.3).

The crosslinking by-products, such as acetophenone and cumylalcohol, increase the AC breakdown voltage of the polymer and also are reported to cause space charge to be trapped upon the application of DC voltage [12-14]. However, the by-products are volatile and slowly diffuse out of the polymer. By the time the insulation is free of such by-products, the dielectric strength is significantly lowered.

Because the cable user needs to know the ultimate lowest strength of the cable insulation, the general practice is to decrease the concentration of the volatile crosslinking by-products from the newly manufactured cable before they are

commissioned into service. This is carried out by treating the cable directly after production for several days at a sufficiently high temperature, referred to in this thesis as the degassification process. The temperature and the duration will depend on the specifications of the cable. For example for the 132 kV XLPE cable the temperature is 85°C and the degassification duration is around 10 days.

2.2.2 Dicumyl peroxide (DCP) crosslinking chemical process

Dicumyl peroxide (DCP) is the most commonly used peroxide crosslinking agent. All the cable insulations studied in this thesis were cured by adding 2% of DCP added to the polymer.

The crosslinking process presents three different stages (see figure 2.1):

- The thermal decomposition of DCP: the DCP remains inactive at the temperature used for cable insulation extrusion (130-150°C) and when the temperature is raised to about 180°C it quickly decomposes. Cumyloxy radicals are formed by the thermal decomposition of the DCP.

- The initiation: then the initiation of the crosslinking reaction starts, the radicals react with the polymer chain by abstracting a hydrogen atom.

- The crosslinking of polyethylene then starts.

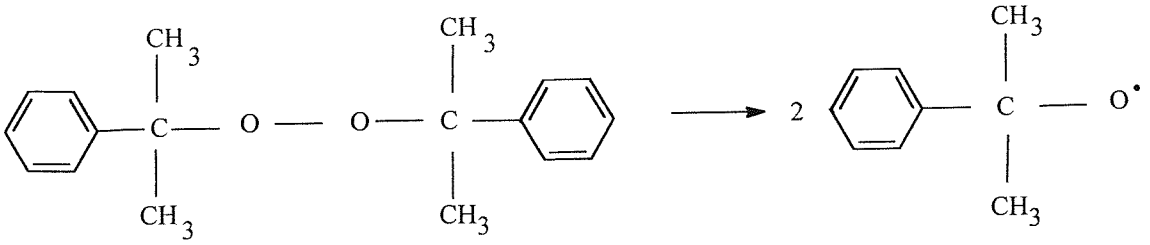

Thermal decomposition of DCP

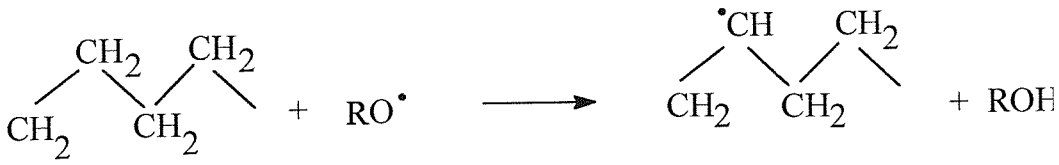

Initiation: R stands for 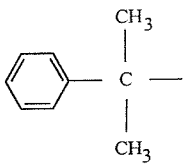

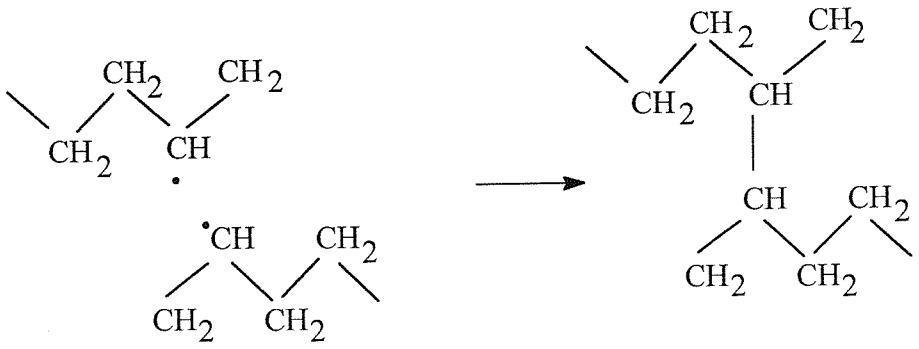

Crosslinking

Figure 2.1: Peroxide crosslinking of polyethylene

2.2.3 Formation of crosslinking by-products

Chemical crosslinking of PE results in several decomposition products. In addition to molecular crosslinks, by-products will be formed (see figure 2.2). The main by-products (in terms of quantity created) are cumyl alcohol, acetophenone and methane. Water and α-methylstyrene are produced in small quantity 0.01% [14] compared to 0.5% for acetophenone and 1.4 % for cumyl alcohol. These by-products are volatile and slowly diffuse out of the polymer.

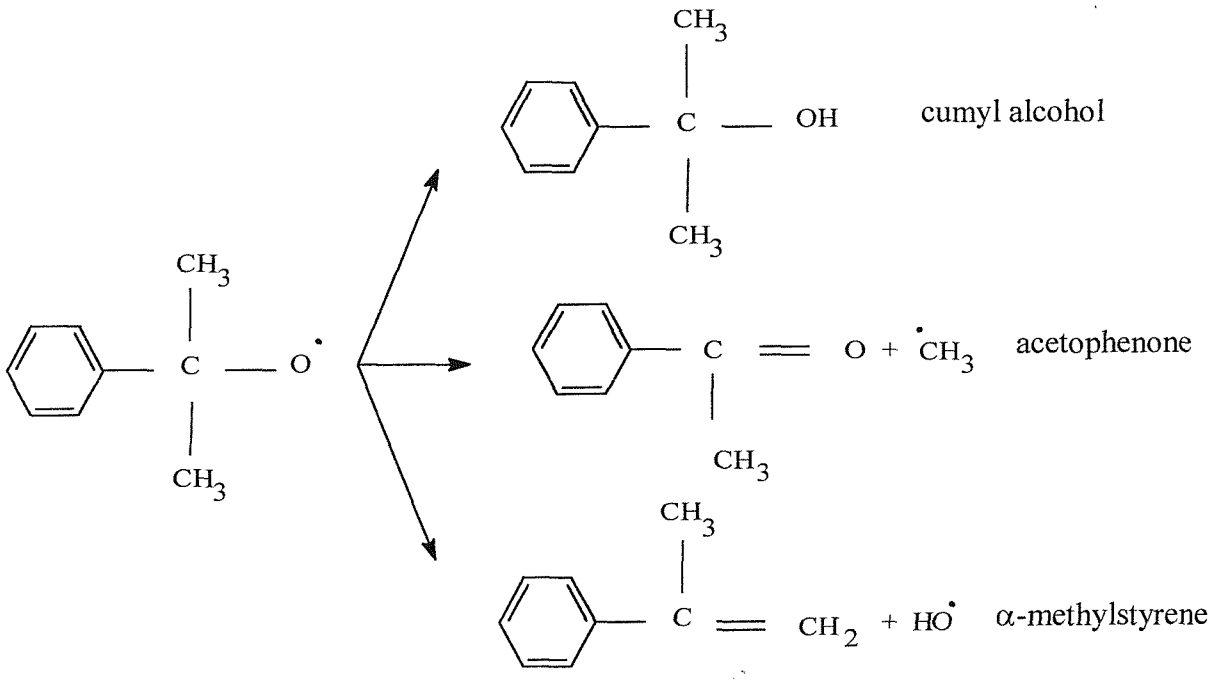

Other possible reactions:

$$CH_3^{\bullet} + H^{\bullet} \longrightarrow CH_4$$

$$OH^{\bullet} + H^{\bullet} \longrightarrow H_2O$$

Figure 2.2: Formation of by-products during DCP crosslinking

2.3 Examination after heating (Oven test)

A cable manufacturer's quality test in order to detect faults in newly manufactured cables is to examine cable samples after heating them in an oven. Samples were examined from cable insulation at two different stages of production: before and after the degassification process, which decreases the concentration of methane and peroxide by-products and water.

2.3.1 Experimental procedure

2.3.1.1 Test

Sections of cable were heated in an oven at 150°C with the central conductor removed. This temperature is higher than the melting point of the insulating polymer making it possible to detect with the naked eye by transparency any defects inside the insulation wall by placing it in front of a lamp.

2.3.1.2 Sample preparation

Table 2.1 gives a range of cables from which 5 cm long wafers were extracted for examination.

Size (mm)	**110 kV**	**132 kV**	**220 kV**	**400 kV**
Conductor diameter	29.9	29.9	44.3	48
min. av. Screen	1.5	1.5	1.6	2.5
min. av. Insulation	15	20	22	28

Table 2.1: Cable specifications

2.3.2 Results and discussion

For cable after degassification, the main insulation showed the presence of one or more halos after 1 hour. A halo consists of a circular band or bands in the bulk of the insulation concentric with the cable cross section. It appears like a smoky or more opaque region compared to the surrounding area (see figure 2.3). This phenomenon was not present in cable insulation immediately after manufacture and before degassification.

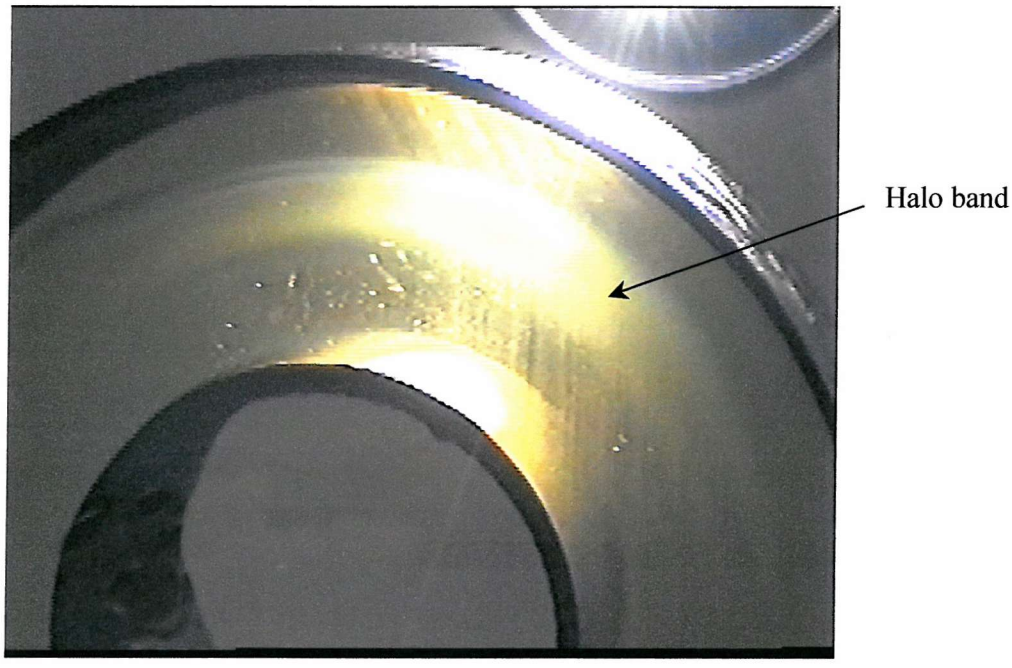

Figure 2.3: Halo effect in the main insulation of 400 kV cable 5 cm section

The appearance of the halo effect changed from sample to sample. The 132 kV degassed cable insulation had a denser and larger halo band (with a higher concentration of defects) than the 220 kV and 400 kV cable insulation, while the 110 kV presented two thin bands.

Some experiments showed that if an undegassed cable insulation sample (with no halo effect present directly after melting of the crystalline phase) was left in the oven for more than two hours, a thin halo started to grow near the outer semiconducting screen. After four hours, two thin halos near each semicon screen were present. For degassed cables (with halo effect present directly after melting of the crystalline phase), the halo grew over a period of hours.

Observations under an optical microscope after samples cooled in air to room temperature showed that the halo region consisted of a high concentration of microfeatures of about 1 micron diameter. These defects were observed to disappear gradually during the course of three hours. One explanation could be that the features were filled by the by-products of the crosslinking process or maybe by low molecular weight material which both have the same refractive index as the crystalline phase. The contrast was maybe simply too low to observe them as the polymer cools down.

In order to render the features visible without heating the samples to 150°C, which could itself create features as these experiments showed, it was decided that some samples should be stained (see section 2.4.2).

2.4 Characterisation of the halo effect

In order to improve the understanding of the nature of the features present in the halo region, FTIR spectra were obtained, together with a mapping of the by-products concentration across the section of the insulation.

2.4.1 Infra-red spectroscopy (FTIR)

In infra-red spectroscopy the energy required to cause a molecule to vibrate by stretching or bending its bonds is provided by infra-red radiation. Precisely what frequency is absorbed gives information which enables to identify the different types of bonds a molecule contains [15]. Infra-red (IR) spectroscopy is used to provide a fingerprint of a molecule or to identify synthesised compound. A monochromator is usually used in a IR spectrometer. More recently Fourier transform IR (FTIR) spectrometry which uses a Michelson interferometer have become common place in research laboratories. The results presented were obtained by FTIR micro-spectroscopy using an optical microscope, which allowed the analysis of sample area as small as 20x20 μm^2.

2.4.1.1 Experimental procedure

A mapping of peroxide decomposition products was carried out on undegassed and degassed 132 kV cable insulation samples. Data were collected every 2mm along a radius line drawn between the two semiconducting screens, starting at the inner screen. The concentration of acetophenone and cumyl alcohol were monitored by integrating the area under the peak corresponding to C=O stretch for acetophenone and to O-H stretch for cumyl alcohol. Then a mapping of the concentration of acetophenone and cumyl-alcohol versus the position along the radius was plotted (figures 2.4 and 2.5).

2.4.1.2 Results and discussion

• FTIR spectra carried out on degassed 132 kV cable insulation revealed no evidence of compositional difference in the halo region as compared to the parent matrix. It could therefore be assumed that the features observed in the halo region were not due to external contamination or particles but was likely due to micro-voids or micro-cracks present.

• The figures below are greatly influenced by sample preparation (a large quantity of by-products diffused out of the sample). The maximum concentrations for undegassed cable were:

- acetophenone ~ 0.35 %
- cumyl alcohol ~ 0.47 %

After degassing, these fell to ~ 0.3 % for acetophenone (see figure 2.5) and ~ 0.35 % for cumyl alcohol.

• FTIR measurements showed that there was a higher concentration of acetophenone and cumyl alcohol in the middle of the degassed cable insulation (see fig. 2.4, 2.5) which corresponds approximately to the region where the halo effect appeared. Two peaks could be observed for both fresh and degassed cable in acetophenone and cumyl alcohol concentration. This appears to be evidence of a relationship between by-products concentration and the halo bands observed after staining.

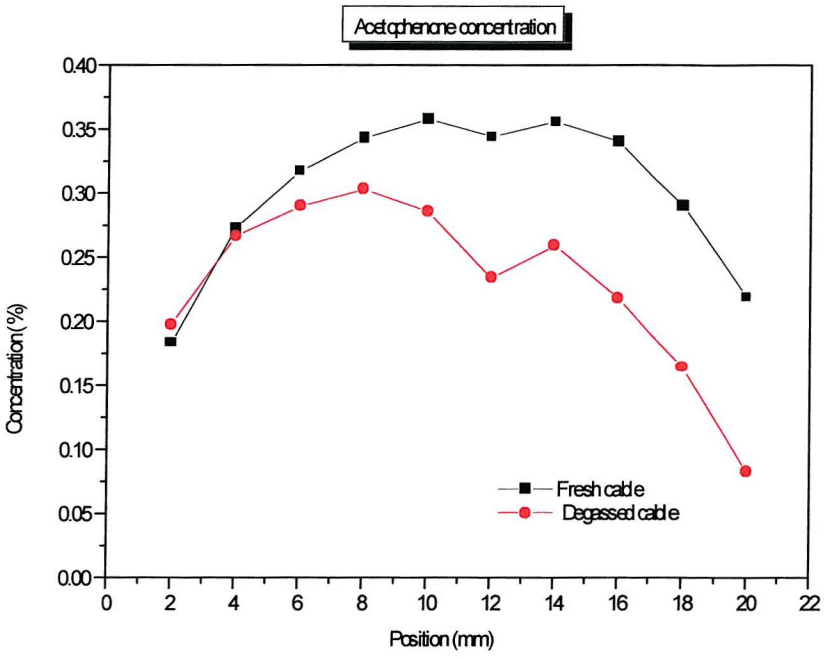

Figure 2.4: Concentration of acetophenone vs position along the radius

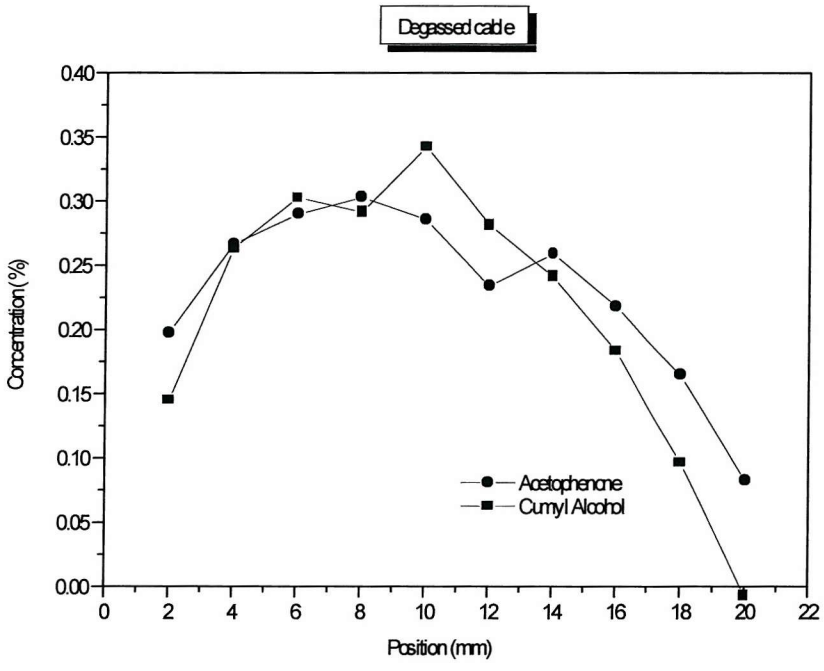

Figure 2.5: Concentration of by-products vs position along the radius for a degassed cable sample

2.4.2 Staining of the cable insulation

In order to render the features visible without heating the samples to 150°C (see paragraph 2.3) contrast enhancement based upon the staining of the polymer cavities with a dye was carried out. To ensure that there was no artefact due to the use of a specific dye several dyes were used:

- methylene blue dye using the Aschcraft procedure [16].This method has been used for rendering water trees permanently visible and has become widely and successfully used for dyeing XLPE as well as PE.
- rhodamine (fluorescent dye) was used in order to ensure that there was no artefact due to the use of methylene blue.

The staining process, like all diffusion processes, is accelerated by increasing the temperature and it is the only possibility for some dyes to penetrate inside the material. However to ensure that the heating process during the staining was not responsible for the presence of microfeatures, a suitable dye, fluorescein isothiocynate (FITC), was found to carry out experiments at room temperature.

2.4.2.1 Staining at elevated temperatures

- *Methylene blue staining*

Both fresh and degassed insulation wafers of similar thickness were stained using this preparation first at the boiling temperature of the solution, then at 70°C. The results obtained were similar for both temperatures, only the duration to reach the same approximate level of stain changed. The duration was of 15 minutes at boiling temperature and near to one hour at 70°C for a sample thickness of approximately 1mm.

- *Rhodamine staining*

In order ensure that there was no artefact due to the use of methylene blue, another dye, rhodamine (fluorescent dye), was used.

Wafers from fresh and degassed cable insulation were stained at 60°C in a solution of rhodamine for three and a half hours.

2.4.2.2 Staining at room temperature

Several dyes were tested: methylene blue, fluorescent dyes used in microscopical biological studies like fluorescein isothiocynate (FITC) and calcofluor.
Wafers from 132 kV degassed cable were soaked for 2 ½ months in a solution of the above dyes.

2.4.2.3 Results and discussion of the naked eye observations after staining

The coloration of samples stained with methylene blue at elevated temperature ranged from pink to a deep blue or violet depending on the thickness of the sample and the temperature at which it was stained. The staining process, like all diffusion processes, was accelerated by increasing the temperature. For comparison all samples were stained at the same temperature with the same duration of impregnation (see paragraph 2.4.2.1) and were of similar thickness. All samples stained with rhodamine were pink.

For methylene blue and rhodamine staining with temperature the observations were similar:

- In samples from cables before degassification the staining was homogeneous.

- In degassed samples, the halo region appeared more stained than the rest of the insulation (see figures 2.6 and 2.7).

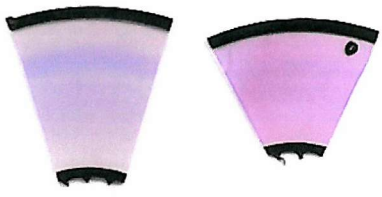

Figure 2.6: Methylene blue staining

Figure 2.7: Rhodamine staining

One question needed to be asked at this stage: does methylene blue or rhodamine fill or mark the defects without modifying them, or worse, does it create them ?
Some physical or chemical effects of methylene blue and rhodamine on polyethylene cannot be excluded at the molecular level, but it is very unlikely that they could induce perturbations at the supramolecular level observed, i.e. in the range of structures that could be detected by optical microscopy (see section 2.4.3). Because the results observed were similar with both dyes it could therefore be concluded that the defects were not created or modified due to an artefact of a specific dye.

For samples stained at room temperature for a long duration, it was impossible to observe anything with the naked eye. This could be because either a low level of dye or no dye had penetrated inside the sample, both cases leading to no colour being detectable with the naked eye at this temperature. These samples were examined in Confocal Laser Scanning Microscopy (CLSM) (see section 2.4.5).

2.4.3 Conventional Optical Microscopy

2.4.3.1 Experimental procedure

Samples stained at elevated temperature using solutions previously described (section 2.4.2) were observed under an optical microscope, equipped with a motorised xyz stage, in both transmitted and reflected light. A computer package allowed the superposition of images captured from different focal planes and an image of large depth of field (referred to later in this section as montage image) was rebuilt in order to obtain a better image since the out-of-focus parts were removed.

2.4.3.2 Results and discussion

Optical microscopy observations in transmission of degassed cable samples after staining at various temperatures were similar to those obtained after the oven test (see section 2.3):

- near the semiconducting layer, there were no features (see figure 2.8),

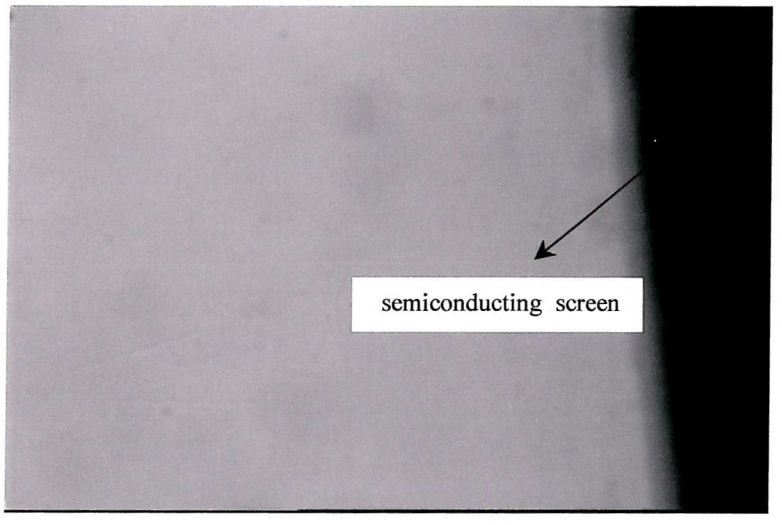

Figure 2.8: Near the semiconducting screen (1cm ↔ 23μm)

- in the halo region (approximately in the middle of the insulation), there was a multitude of micro-features of 1 to 1.5 microns across. These micro-features appeared like isolated micro-voids, clusters of micro-voids and arrays of micro-channels. The first image was captured in one focal plane, the second one corresponds to the superposition of 10 images captured every micron (Figures 2.9 and 2.10) hence showing an unblurred image of features within a 10μm slice. Figure 2.11 presents a cluster of micro-features.

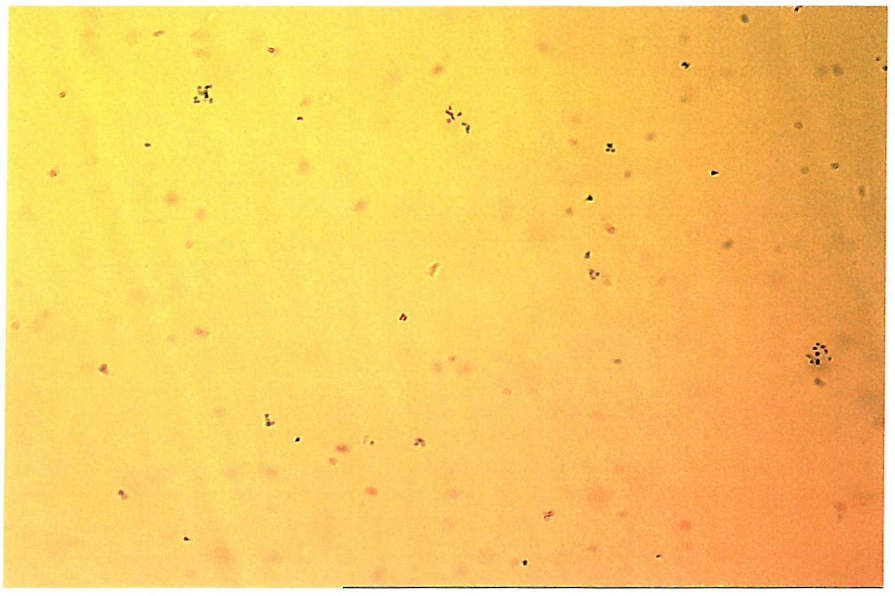

Figure 2.9: Halo micro-features (1cm ↔ 23μm)

Figure 2.10: Montage image (1cm ↔ 23μm)

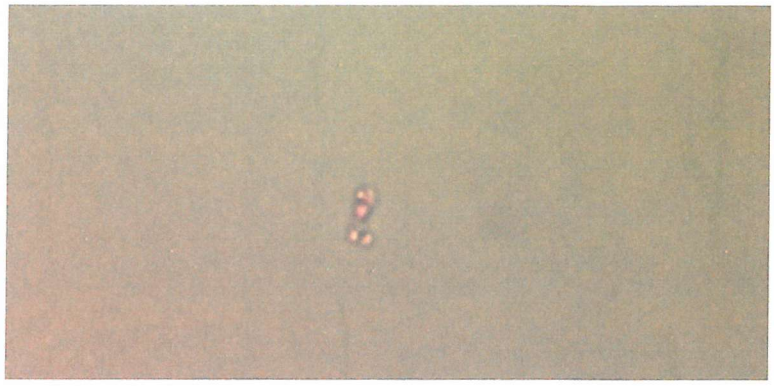

Figure 2.11: Cluster of micro-features (1cm ↔ 8μm)

Due to light scattering, optical microscopy in association with methylene blue and rhodamine staining, did not allow us to distinguish with exactitude the shape of the defects or very small features against the background. Therefore, electron microscopy and fluorescence microscopy observations, which offer the possibility to detect very small objects in the nanometer range, were carried out. The confocal laser scanning microscope (CLSM) used to carry out fluorescence microscopy allows the superposition of optical sections giving a three-dimensional image which permits a better quantification of the number of defects (see section 2.4.5).

2.4.4 Scanning Electron Microscopy (SEM)

The resolving power of the SEM (~5nm) is significantly greater than that of an optical microscope. Therefore it allows more detailed study of surface structure. Another advantage is its large depth of focus giving a clear impression of the three dimensional characteristics of the surface.

2.4.4.1 Cryogenic fracture

Cross sections of 3 mm thick samples from unstained degassed and undegassed 132 kV cable were fractured at low temperature after freezing with liquid nitrogen. The fractured surfaces were coated with sputtered gold and examined using the SEM.

In figures 2.12 and 2.13 a difference of structure is visible. In both cases the fractured surface was rough however in figure 2.13 cavities can be observed which are not visible in figure 2.12. The profile may have been strongly disturbed by the freeze fracture so it was difficult to conclude if the features observed were related to the presence of halo defects or if they were defects created by the freeze fracture. Therefore another technique of sample preparation, the etching technique was also used.

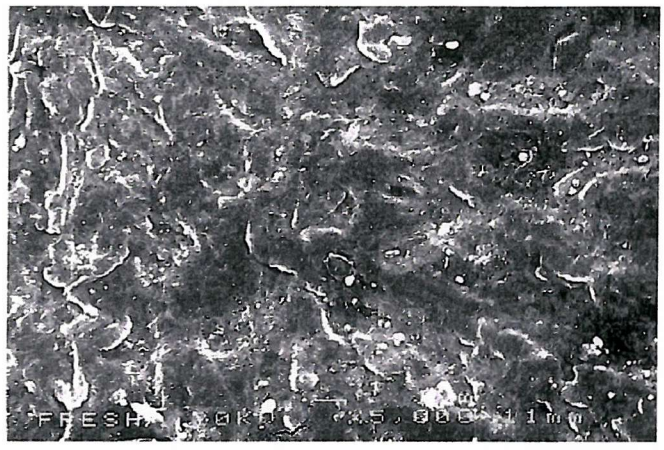

Figure 2.12: Undegassed 132 kV cable insulation sample

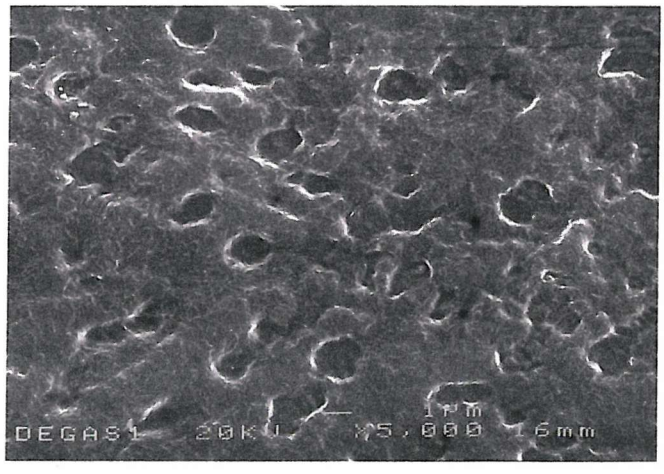

Figure 2.13: Degassed 132 kV cable insulation, halo region

2.4.4.2 Etching technique

- *Sample preparation*

Two series of samples removed from degassed 132 kV cable cross sections were studied. The first one was stained with methylene blue, the other was unstained. Both were microtomed at low temperature to expose a flat, internal surface, which was etched for 3 hours in a 1% solution of potassium permanganate in a mixture of concentrated sulphuric acid, orthophosphoric acid and water [17]. After etching, the surfaces were sputter-coated with gold and imaged with the SEM.

- *Results and Discussion*

All samples presented a uniform fine-scale morphology. Unstained sample surfaces presented no features. Stained sample surfaces presented a few features like microvoids (Figure 2.14) in the area chosen, corresponding to the halo region when observed optically in transmission.

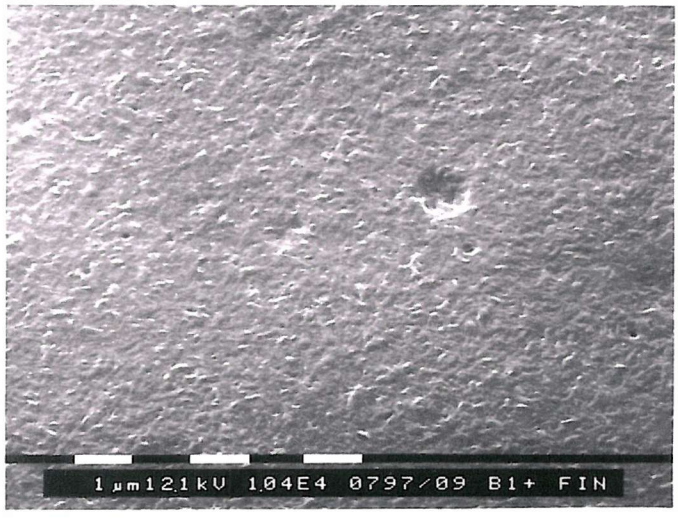

Figure 2.14: Degassed 132 kV cable insulation, halo region

The etching process was likely to flatten voids, this explains why in the unstained etched sample no features were present. For stained samples, the methylene blue (solid at room temperature) could be deposited into existing cavities so the etching could remove it and keep the shape of the cavity observable with SEM. This technique was not the most

suitable for this study because a lot of features could be removed by the etching process. We can conclude that SEM, either by freeze fracturing or etching, was not a suitable technique to study the features present in the halo region.

2.4.5 Confocal Laser Scanning Microscopy (CLSM)

This technique has been largely used in microscopical biological studies. Schematically, a laser source is focused inside the specimen and causes the sample to fluoresce as a result of excitation of the material by light of shorter wavelength (see section 3.2) [18]. Fluorescence is then preferentially collected on a photomultiplier and recorded in a computer. The Confocal Laser scanning microscope (CLSM) allows the superposition of optical sections due to the confocal design, and a three-dimensional image is reconstructed by scanning the specimen, hence allowing the quantification of the number of defects and to obtain a better contrast because the out-of-focus fluorescence is removed.

This technique can be used to produce brightness or colour contrast in the examination of materials. The fluorescence is observed in two different types of specimens. One type of specimen is composed of materials that have an intrinsic fluorescence (or autofluorescence) or fluorescence due to traces of impurities. Other types of specimen exhibit secondary fluorescence, which is the result of treating the specimen with a solution of a fluorescent dye.

One of the most straightforward and useful image manipulations which may be applied to 3D confocal data sets is the generation of stereoscopic pairs of images, permitting the results to be inspected directly in three dimensions. Such stereo image pairs may be viewed in a way that ensures that the right image is not seen by the left eye and vice versa. The images are then displayed as a single red/green anaglyph photograph viewed through red/green spectacles.

2.4.5.1 Specimens

Samples from 132 kV degassed cable were examined. One series was unstained and the other stained:

- with rhodamine and methylene blue at 70 °C during 3 hours,
- with FITC, methylene blue and calcofluor at room temperature for 2 ½ months.

2.4.5.2 Results and discussion

- *Untreated specimens*

Some unstained samples from degassed cable insulation were examined. At visible excitation sources 488nm and 568nm, some autofluorescence (fluorescence inside the polymer) was obtained but the signal was weak, too noisy and the sample became rapidly bleached or photodestroyed during prolonged exposure, hence the resolution was very poor.

A UV laser excitation could elicit enough autofluorescence but a surer way to increase the fluorescent signal is to stain samples with a suitable fluorescent probe [18].This method has been largely used in microscopical biological studies, where the fluorescent dye is generally covalently linked to a drug or an immunological probe.

- *Staining at elevated temperatures*

A good signal was obtained with rhodamine at 543 nm excitation, allowing us to image in fluorescence mode. No fluorescent signal was obtained with methylene blue but it was possible to image in reflective mode (use of the reflected laser light), which brought no more information than conventional optical microscopy. The images obtained are stereo images so red/green glasses are required to see the 3D effect. They are the result of the superposition of 40 optical sections of 0.9 micron each.

In the halo region, many features (Figure 2.15) could be seen. They appeared to be like micro-voids. At higher magnification, we could see isolated micro-voids and some clusters of micro-voids and micro-channels (Figures 2.16, 2.17). The micro-channels appeared to have a random orientation.

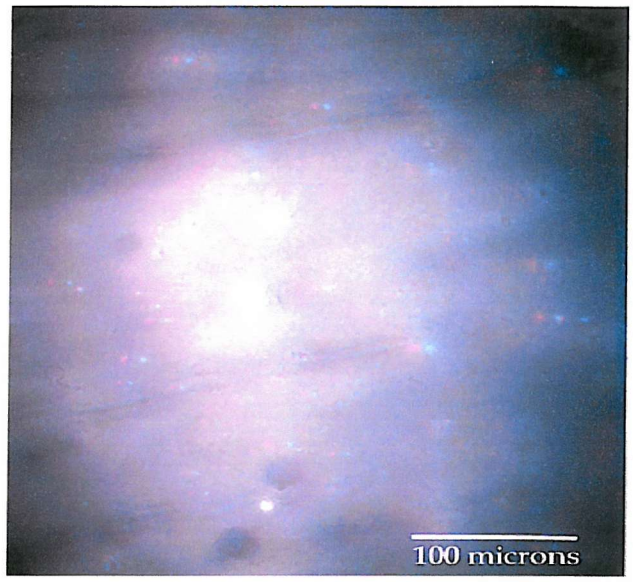

Figure 2.15: Halo region

This technique, unlike previous methods allowed us to observe very fine micro-channels precisely thanks to the better contrast obtained by staining with a fluorescent dye, the three-dimensional effect and also the better resolution achieved with the confocal optical design. The previous techniques did not allow us to distinguish between a cluster of isolated voids and an array of voids connected by micro-channels. An estimated $5x10^5/mm^3$ micro-defects were found.

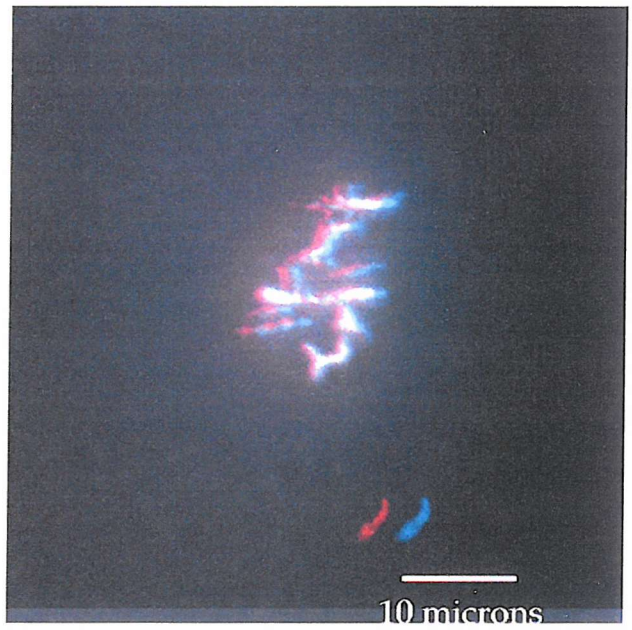

Figure 2.16: halo region, higher magnification

Figure 2.17: Halo region

- *Staining at room temperature*

For specimens stained with rhodamine and calcofluor no fluorescent signal was obtained. Not enough dye had penetrated inside the samples.

It was possible to image the FITC stained sample using the λ488nm laser. The signal was noisy, hence it was more difficult to image than with samples stained at higher temperatures where a lot of dye had penetrated inside the specimen. The images obtained are displayed on the next page (Figures 2.18 and 2.19).

A stereo image of a large area inside the halo region shows a number of micro-features (Figure 2.18). The figure 2.19 is the superposition of 30 optical slices (1 μm each) without stereoscopic effect. The image is viewed with an angle of 0^{o} (flat section) and 90^{o} (cross section). The projection image at 90^{o} ensures that the microfeatures are inside the bulk of the polymer sample and are not due to a surface effect. This image allows the observation of the distribution of the features through the cross section of the sample.

The halo microfeatures were visualised in samples stained at higher temperature as well as in those stained at room temperature. It can therefore be assumed that it was not the temperature during the staining process which caused them. For the following studies only staining with temperature was performed.

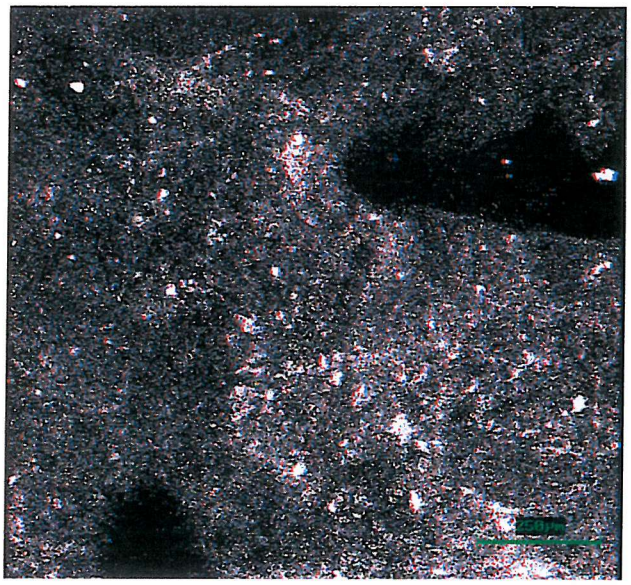

Figure 2.18: Halo region, FITC stained sample

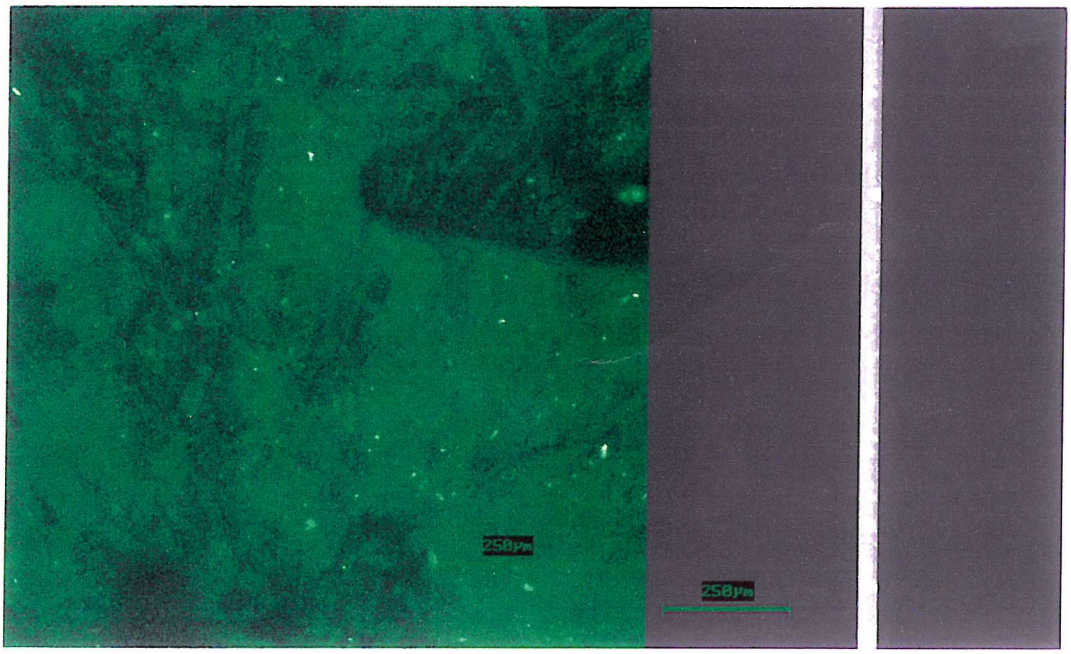

Figure 2.19: Superposition of 30 optical slices, FITC stained sample

2.4.6 Conclusions

• A halo effect appeared in a select number of degassed cable main insulation after degassification. No halo region was present in cable insulation immediately before degassification.

• The halo effect was present in several cables (110 kV, 132 kV, 220 kV, 400 kV) with different geometries: different size of conductor and different insulation wall thickness.

• FTIR spectra carried out on degassed cable insulation revealed no evidence of compositional difference in the halo region as compared to the matrix. So the features observed in the halo region were not due to external contamination or particles but it is likely that they were micro-voids or micro-cracks.

• Observing the concentration of by-products along the insulation wall radius provided evidence of an apparent link between these and the halo bands observed after staining.

• The halo region, when observed by different microscopic techniques after staining or after the oven test, consisted of a multitude of micro-features of 1 to 1.5 microns across. These micro-features appeared like isolated micro-voids, clusters of micro-voids and arrays of micro-channels.

• Staining with temperature followed by Confocal Laser Scanning Microscopy in fluorescence mode was the most suitable way to characterise the halo region. This technique, unlike SEM and conventional optical microscopy allowed us to observe very fine details precisely thanks to the three-dimensional effect, a better resolution being achieved with the confocal optical design which cancels the out-of-focus blurring and also the better contrast obtained by the fluorescence of the specific dye.

• The halo region micro-features were similar when examined after staining with different dyes, so they were not due to perturbations introduced by a specific dye and were visualised in specimens stained with temperature as well as those stained at room temperature so it was not the temperature during the staining process which created them.

2.5 Influence of the degassification process parameters on the halo region

2.5.1 Introduction

The production of micro-features in XLPE cable insulation may be due to several possible causes, among which the more likely are:

- the heat treatment during the degassification process which could be responsible of micro-voids formation for example due to: relaxation of internal stresses frozen in the polymer, difference in thermal expansion coefficient of different concentric layer of the insulation wall and subsequent contraction of the insulation on cooling,
- the non-uniform dispersion of the antioxidant,
- the diffusion of by-products of the chemical crosslinking process through the insulation wall.

In order to better understand what led to micro-void formation in cable insulation, first the influence on the halo region of the parameters of temperature and duration of the industrial degassification process was assessed. In production, cables newly manufactured are degassed at 85°C for several days, the number of which depends on the cable geometry. In order to study the influence of a reduction of the degassification temperature, degassification simulation in an oven of cable pieces (110 kV) was carried out at 65°C. To obtain the same conditions as in production, calculation of the time required to de-methane cables at the chosen temperature was necessary. This calculation is presented in appendix A. In order to observe the effect of the heat degassification treatment duration, cable samples with different degassification time were studied.

2.5.2 Experimental procedure

2.5.2.1 Examination tests

This section briefly summarises the tests used to examine the halo phenomenon. All cable samples were submitted to the same tests: examination after heating, staining of

the insulation with dyes followed by naked eye observation and microscopic examination.

- Examination after heating (oven test):

Wafers (3 cm long) were extracted from all the cable samples and the conductors were removed. All the samples were heated in an oven at 150°C and examined by placing them in front of a lamp in order to detect any defects inside the insulation wall by transparency.

- Staining of the cable insulation:

Contrast enhancement based on the staining of the polymer cavities with a dye was carried out. In order ensure that there was no artefact due to the use of a specific dye, two different dye solutions were used:

- Methylene blue (using the Ashcraft solution [7]),
- Rhodamine B.

Cable slices of thickness varying between 1 and 2 mm were cut from cables. Pieces of these slices were stained at 70°C for three hours.

- Microscopic examination:

  - Conventional optical microscopy:

Stained samples were observed under an optical microscope, equipped with a motorised xyz stage, in both transmitted and reflected light. Software allowed the superposition of images captured from different focal planes and a montage image is rebuilt in order to obtain a better image since the out-of-focus parts are removed (see section 2.3.3.1).

  - Confocal Laser Scanning Microscopy (CLSM):

Fluorescence microscopy was also carried out on samples stained with rhodamine, in order to obtain more information.

2.5.2.2 Effect of the degassification temperature

Two 490 mm cable lengths were placed in an oven at 65°C for the time calculated as in appendix A, that is 16 days. Only samples removed from the middle of the cable lengths were studied. This was to ensure that there were no edge effects and only the diffusion through the semiconducting screens occurred in these specimens.

2.5.2.3 Effect of the degassification duration

In order to observe the effect of the heat degassification treatment duration, some pieces of 110 kV cable were double degassed:

- at 65°C in an oven: after having been degassed once the same cable samples were placed again in the oven for the same period of time,
- at 85°C in production: after having been degassed once a length of cable was cut and placed with new cable drums in the production degassification room for the same period of time .

A degassed 132kV cable insulation sample was also placed in an oven at 150°C and observed over a period of hours.

2.5.3 Results

2.5.3.1 Effect of the degassification temperature

The oven test, methylene blue and rhodamine staining followed by optical microscopical observations showed the presence of the halo region in these wafers. The halo region appeared similar (by its location in the insulation and in its physical appearance) to the one in cable insulations degassed in production at 85°C and studied in sections 2.3 and 2.4.

The degassification temperature appeared to have no influence on the appearance and shape of the halo.

2.5.3.2 Effect of the degassification duration

For both sample series (double degassed at 65°C and 85°C) no difference in the halo appeared after the oven test and the staining compared to single degassed samples at the same temperature.

For the degassed cable insulation placed in an oven at 150°C, the halo band was noted to grow with time for a few hours and then stopped growing.

It seems that an equilibrium state exists, when this state is reached no major evolutions are visible with time. This could explained why no difference was observed between single and double degassed samples. Up to this equilibrium state the halo changed with time and this was observed by monitoring the degassed cable sample placed in the oven at 150°C.

2.5.4 Discussion

The discussion refers to experiments carried out on different series of samples, the history of which is shown in table 2.2:

Cable series	Type (kV)	Degassed in production at 85°C	Heat treatment	Other Information
A	132	No	150°C, 4 Hours	
B	110	No	65°C, 16 days	
C	110, 220, 400	Yes	No	
D	110	No	No	3 ½ months
E	132	No	No	2 years

Table 2.2: Summary of the experiments

The results of experiments carried out at different degassification temperature and for different degassification duration can be summarised as follows:

At 150°C after four hours, a halo region was observed inside insulation samples (A), which were clear before heat treatment (see corresponding table line),

At 65°C after 16 days, a halo region was present in the main insulation of cable samples B.

At 85°C after 6 days a halo was also present in cable samples C.

These results suggest that, given the apparent relationship between time and temperature, a halo should be observed at room temperature in an undegassed cable after a suitable length of time.

In order to verify the hypothesis that the presence of the halo may not be due to a heat treatment but to a diffusion process with time, a 3 ½ months old 132 kV undegassed cable (D) was studied. The oven test at 150°C revealed nothing. The staining at 70°C followed by naked eye observations revealed different results to those produced by the oven test for the first time.

Until now the oven test and staining followed by microscopical observations and naked eye observations had shown the same results. In this case the staining showed two thin concentric bands where the oven test revealed nothing. This implies that to observe a halo in the oven test, the halo band must have a very high density of micro-features in order to be visible (smoky effect) by examination with the naked eye placed in front of a lamp. It was also impossible to observe these bands under an optical microscope because the bands were not sufficiently stained to obtain a good contrast.

A study was also carried out with a 2 year old 132 kV undegassed cable (E) to confirm the previous results. The oven test at 150°C revealed a very thin halo band near the inner semiconducting screen. The staining followed by naked eye observations showed four concentric bands where the oven revealed only one. CLSM observations were carried out since it was impossible to observe them by optical microscopy. It showed few micro-voids in the halo band.

2.5.5 Conclusions

From these series of experiments, it can be concluded that the halo effect appeared not to be due to the heat treatment during the degassification process, since cable insulation which had not undergone this treatment still presented this effect after a period of approximately 3 ½ months. It may be due to the diffusion of by-products inside the main insulation wall, this diffusion process being accelerated by the temperature.
Studies of the effect of the degassification heat treatment duration have shown that an equilibrium state existed and when this state was reached no major evolutions were visible with time. Up to this state the halo grew with time.

2.6 Effect of the crosslinking by-products

2.6.1 Introduction

A high density polyethylene (HDPE) cable (225kV) was examined. The results were then compared to XLPE insulation samples commented on in section 2.3 and 2.4 in order to observe the effect of crosslinking and more specifically the effect of crosslinking by-products.

2.6.2 Experimental procedure

The cable samples were submitted to the same tests: examination after heating, staining of the insulation with dyes followed by naked eye observation and microscopic examination as described in section 2.5.2.

2.6.3 Results and discussion

- Examination after heating:

Because the cable insulation was not crosslinked and hence had no mechanical integrity above the melting point, the cable sample had to be heated at 180°C and had to be turned frequently around its axis in order to be able to observe as quickly as possible the insulation by transparency before the cable sample collapsed under its weight. No 'halo' effect was visible.

- Naked eye observation after staining:

The staining was homogeneous, no halo band appeared in the insulation wall (see figure 2.21).

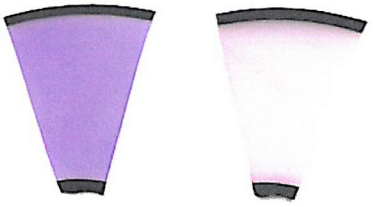

Figure 2.21: Methylene blue and rhodamine staining

- Microscopic examination: No micro-features were present in the insulation wall.

The fact that there was no halo region when the insulation was not crosslinked shows that the halo effect present in XLPE cable insulation is not due to an artefact of the antioxidant such as antioxidant agglomeration but can be explained by the presence of crosslinking by-products.

FTIR measurements (section 2.4.1) showed that there was a higher concentration of acetophenone and cumyl alcohol in the middle of degassed cable insulation which corresponds approximately to the region where the halo effect appeared showing an apparent link between both phenomena.

In the previous section 2.5, it was shown that the halo effect may have been due to the diffusion of crosslinking by-products inside the main insulation wall, this diffusion process being accelerated by the temperature. The fact that there was no halo region when the insulation was not crosslinked confirms this explanation.

2.7 Effect of ageing on the halo phenomenon

2.7.1 Introduction

Two sample lengths of the same 400 kV degassed XLPE cable core were studied:

- one of the sample lengths had not been electrically tested (sample A),
- the other (sample B) was subjected to a year electrical test simulating extreme operating conditions.

Both cable samples were manufactured at the same time. The comparative analyses will reveal the effect of electrical ageing on the halo effect.

2.7.2 Experimental procedure

The cable samples were submitted to the same tests: examination after heating, staining of the insulation with dyes followed by naked eye observation and microscopic examination as described in section 2.5.2.

2.7.3 Results

■ Examination after heating

For sample A (unaged sample):

The main insulation exhibited a smoky 'halo' effect in the middle of the insulation wall consisting of two circular bands concentric with the cable cross section. Compared to the surrounding area, they appeared like smoky or more opaque regions, separated by a narrow clearer region.

For sample B (aged sample):

The halo region appeared like a wide band instead of the two bands observed in cable A.

■ Naked eye observation after staining:

For sample A:

The staining of the cable insulation with methylene blue and rhodamine revealed the same effect. The halo region appeared more stained than the rest of the insulation (see Figure 2.22). However it was difficult to distinguish the two bands observed after the oven test.

For sample B:

The halo region seems more stained and wider than in sample A.
For comparison, figure 2.22 shows sample A on the left and sample B on the right.

(a) (b)

Figure 2.22: Methylene blue (top) and rhodamine (bottom) staining
(a) untested
(b) tested

■ Microscopic examination after staining:

For sample A:

The halo region consisted of a multitude of micro-features of 1 to 1.5 microns across. These micro-features appeared like isolated micro-voids, clusters of micro-voids and arrays of micro-channels. Figure 2.24 corresponds to the superposition of 10 images captured every micron.

For sample B:

The halo region was made up of a multitude of micro-features of 1 to 1.5 microns across as in sample A. Closer examination seemed to suggest that at the densest point in the 'halo' the micro-features were longer, about 6μm, and appeared to be oriented in the direction of the electrical field as figure 2.25 shows. These kind of features were not present in sample A.

At higher magnification and using only reflected light, these elongated features appeared to be made of clusters of micro-voids arranged in the direction of the field (Figure 2.23).

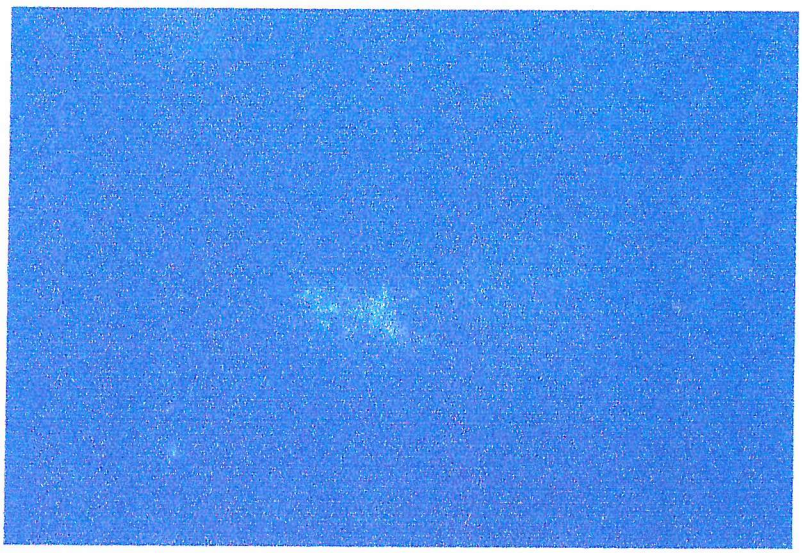

Figure 2.23: Tested sample, halo micro-features, reflected light (1cm ↔ 7μm)

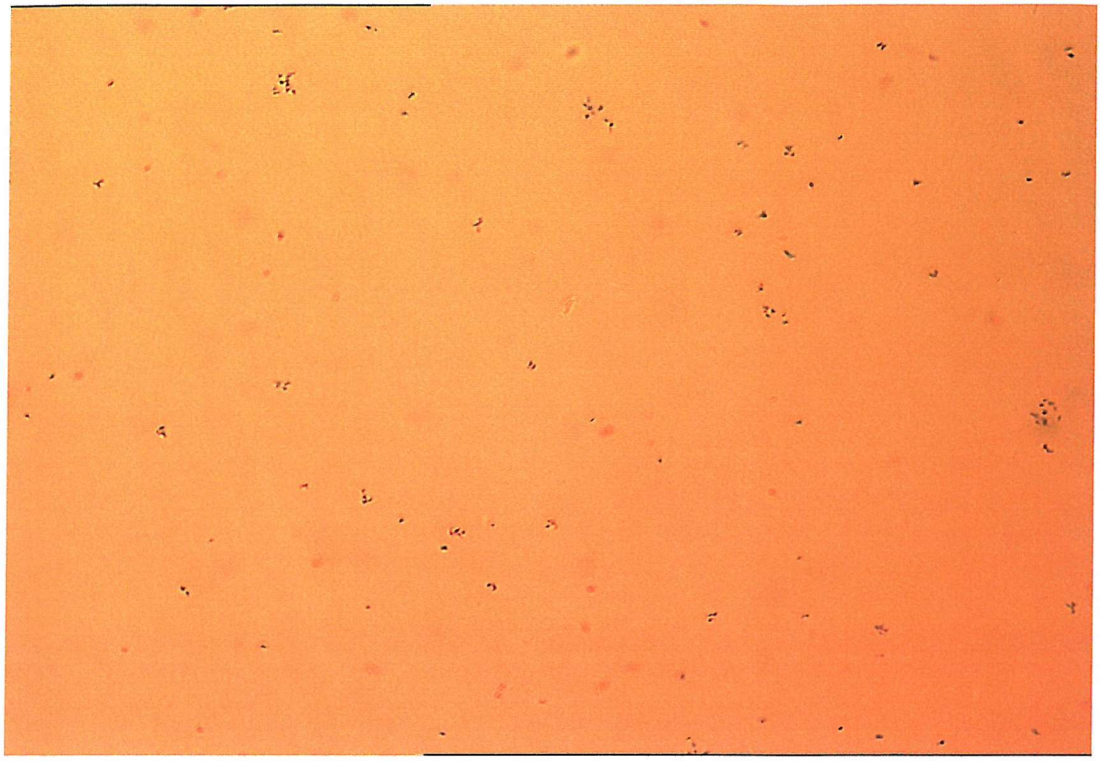

Figure 2.24: Untested sample, montage image (1cm ↔ 23μm)

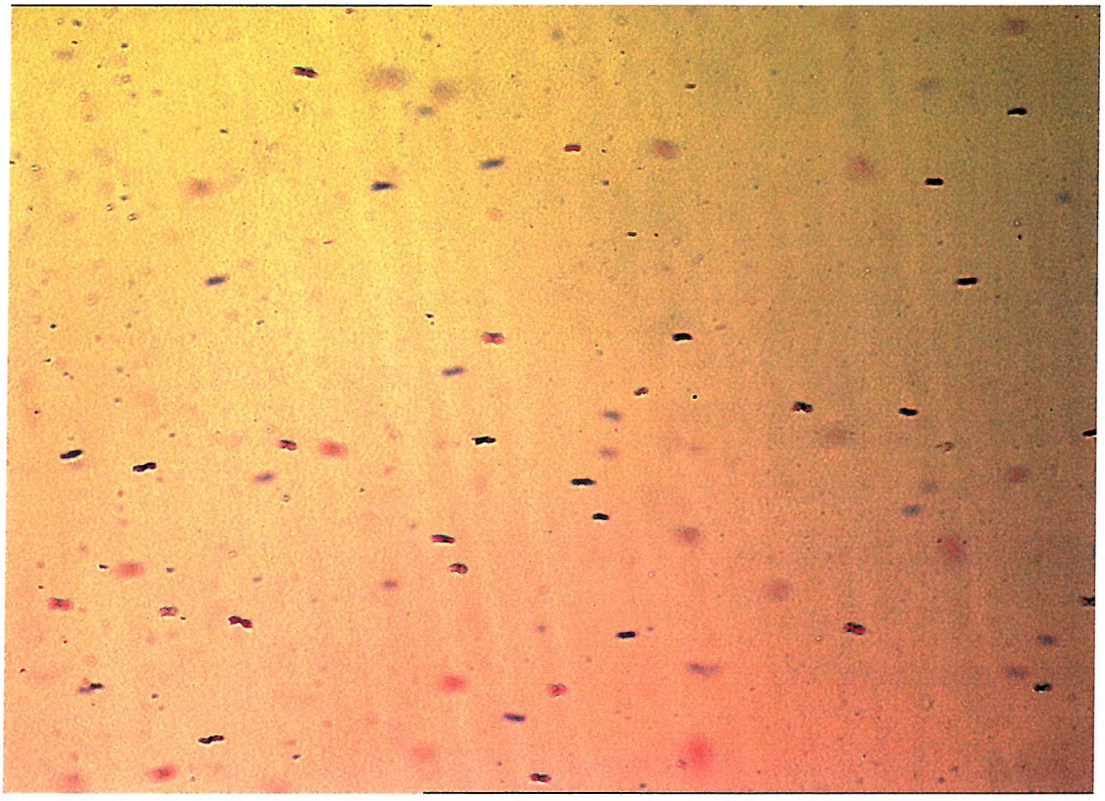

Figure 2.25: Electrically aged sample (1cm ↔ 23μm)

The image in figure 2.26 was obtained from a slice cut in the direction of the electric field, in figure 2.27 from a slice cut in the direction perpendicular to the electric field. The micro-defects were oriented in the direction of the field.

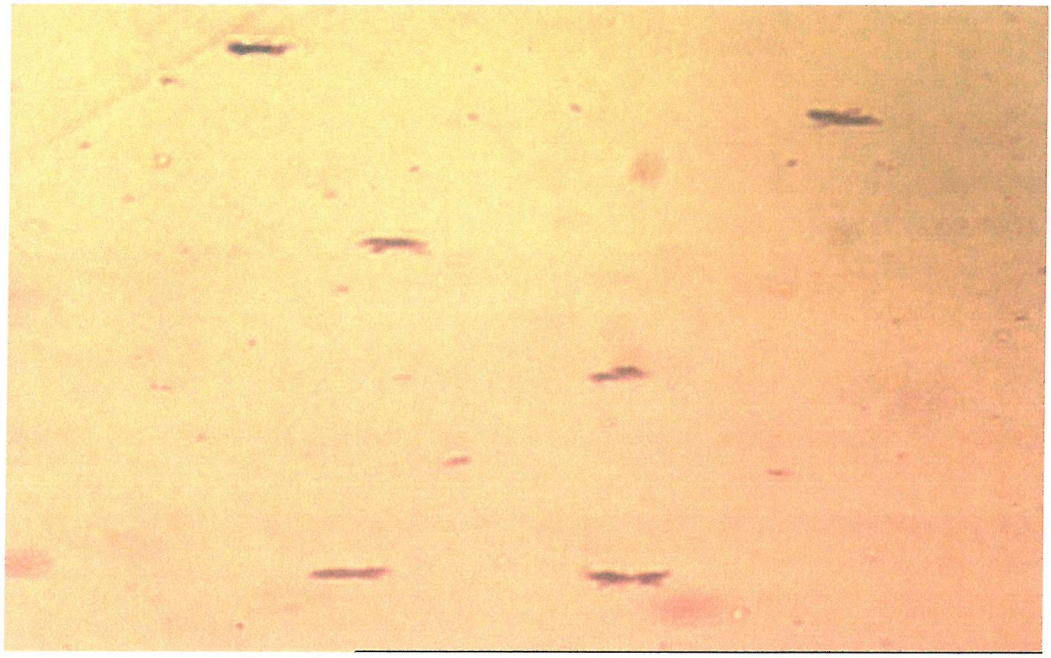

Figure 2.26: Slice cut parallel to the electric field, transmitted light (1cm ↔ 7μm)

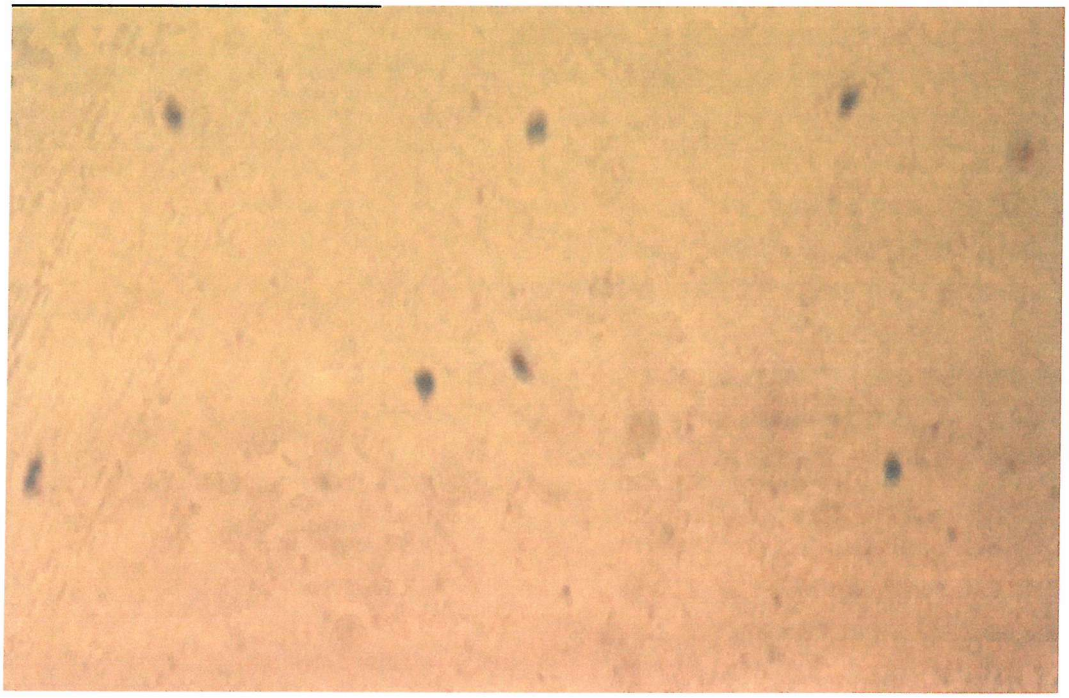

Figure 2.27: Slice cut perpendicular to the field, transmitted light (1cm ↔ 7μm)

Confocal Laser Scanning Microscopic (CLSM) observations in fluorescence mode showed the same tendency, the micro-features were oriented in one direction only (Figures 2.28, 2.29).

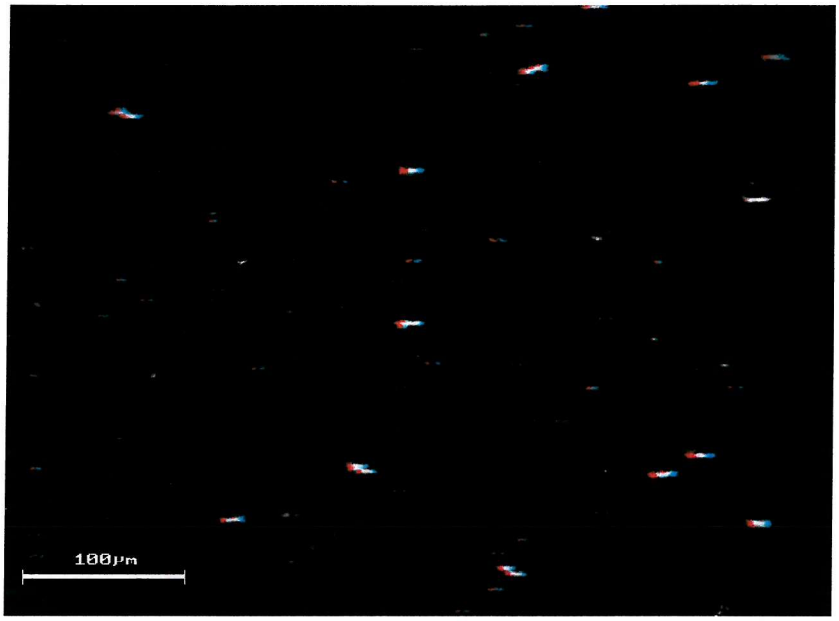

Figure 2.28: Stereo image, halo micro-features

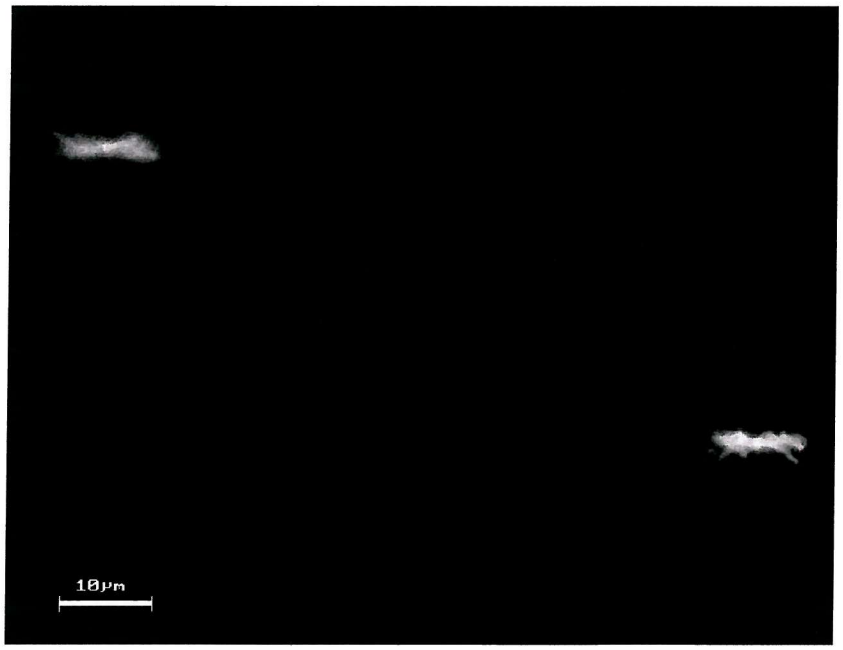

Figure 2.29: Halo micro-features

Figure 2.30 shows a 3D rotation carried out by the imaging software on one micro-feature. Each image, read from left to right, follows a successive rotation, turning the feature through a total of 180°. It starts with an image at an orientation parallel to the field, passes through an image of the feature oriented at 90° to the field and returns to the original alignment. No oriented micro-channels or crazes were observed in the direction perpendicular to the electrical field.

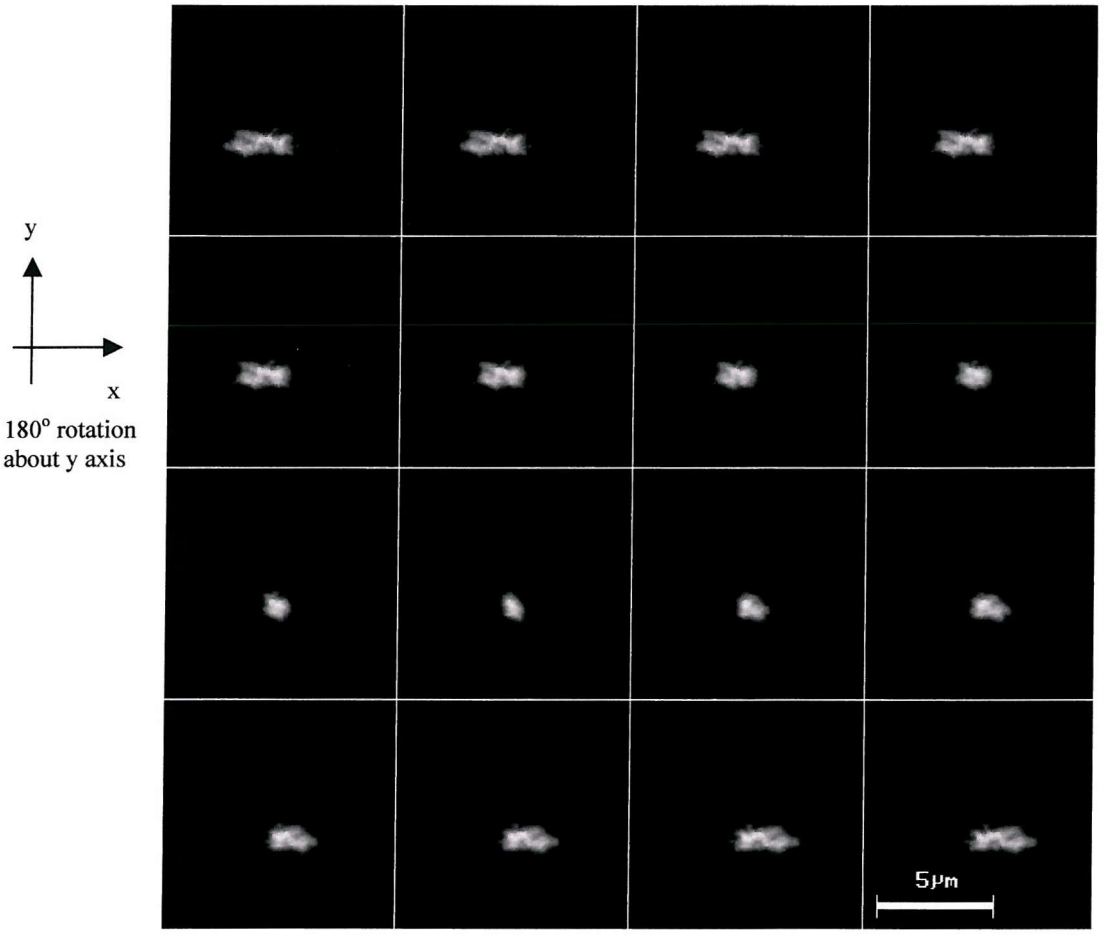

Figure 2.30: 3D rotation

2.7.4 Discussion

A difference in the 'halo' effect has been found in the cable insulation sample after electrical testing. The halo region seemed more dense and wider than in the sample from the same cable before electrical testing. At the densest point in the 'halo' the micro-features were longer, about 6μm, and oriented in the direction of the electrical field. At

higher magnification, these elongated features appeared to be made of clusters of micro-voids and micro-channels arranged in the direction of the field.

We can try to explain the effect of the field on the halo micro-features using a mechanical approach because it calls to mind the formation and propagation of crazes when a mechanical stress, σ, is applied (see figure 2.31). It seems that in the presence of electrically-caused (e.g. by Maxwell forces) mechanical stresses, the 'halo' micro-features grow and are oriented in the direction of the electric field. This phenomenon may possibly be explained by micro-void coalescence due to a mechanical tensile stress.

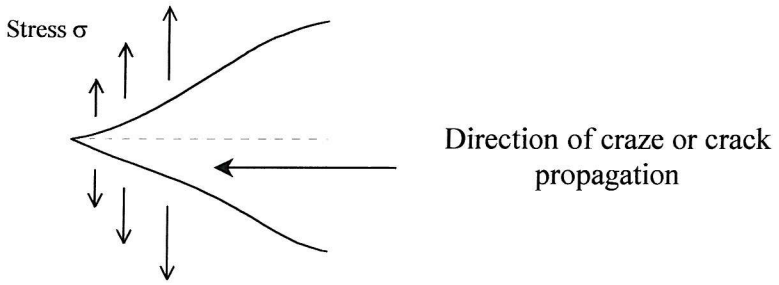

Figure 2.31: Craze and crack propagation

It has been shown that a dielectric sample of macroscopic thickness d between metal electrodes satisfying the condition that the field is zero in the regions z<0 and >d will be subjected to stresses tending to expand it against its cohesive forces in directions everywhere normal to the field. This has been generalised to three-dimensions. When a field is applied as shown in figure 2.32, then the dielectric is subjected to a mechanical stress σ over a surface whose normal is collinear with the field. Thus stress surfaces will exist orthogonal to the field at every point [19, 20].

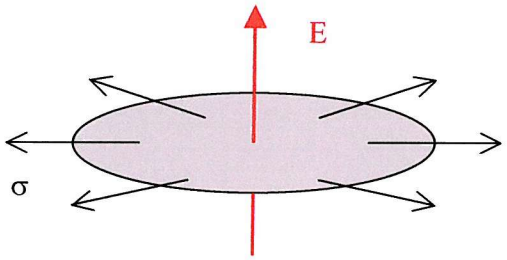

Figure 2.32: Mechanical stresses induced by an electric field E [19]

The stress is a tensile one so if imperfections like the halo micro-features exist, the energy associated with the stress might be sufficient to extend them or create crazes via micro-void coalescence in the direction of the electric field.

2.8 Conclusions

■ A halo effect appeared in some cable main insulation after degassification. No halo region was present in cable insulation immediately before degassification. The halo effect was present in several cables (110 kV, 132 kV, 220 kV, 400 kV) with different geometries: different size of conductor and different insulation wall thickness. The halo region, when observed by different microscopic techniques, after staining or after the oven test, consisted of a multitude of micro-features 1 to 1.5 microns across. These micro-features appeared like isolated micro-voids, clusters of micro-voids and arrays of micro-channels.

■ Staining with temperature followed by Confocal Laser Scanning Microscopy in fluorescence mode was the most suitable way to characterise the halo region. This technique, unlike conventional optical microscopy allowed the observation of very fine details precisely thanks to the three-dimensional effect, the better resolution achieved with the confocal optical design which cancels the out-of-focus blurring and also the better contrast obtained by the fluorescence of the specific dye.

■ In order to better understand what produced this effect, the influence on the halo region of the parameters of temperature and duration of the industrial degassification process has been assessed. After this campaign of experiments, it was possible to conclude that the halo effect appears not to be due to the heat treatment during the degassification process, since cable insulation which had not undergone this treatment still presented this effect after a period of approximately 3 ½ months. It might be due to the diffusion of by-products inside the main insulation wall, this diffusion process being accelerated by the temperature. The fact that there was no halo region when the insulation was not crosslinked showed that the halo effect present in XLPE cable insulation was not due to an artefact of the antioxidant, such as antioxidant agglomeration, but could be explained by the presence of crosslinking by-products.

FTIR measurements showed that there was a higher concentration of acetophenone and cumyl alcohol in the middle of degassed cable insulation which corresponded approximately to the region where the halo effect appeared, showing an apparent link between both phenomena.

■ A difference in the 'halo' effect had been found in the cable insulation sample after electrical testing. The halo region seemed more dense and wider than in the sample from the same cable before electrical testing. At the densest point in the 'halo' the micro-features were longer, about 6μm, and oriented in the direction of the electrical field. At higher magnification, these elongated features appeared to be made of clusters of micro-voids and micro-channels arranged in the direction of the field.

■ It seems that in the presence of electrically-caused (e.g. by Maxwell forces) mechanical stresses, the 'halo' micro-features grow and are oriented in the direction of the electric field. This phenomenon may possibly be explained by micro-void coalescence due to a mechanical stress. The stress is a tensile one, so if imperfections like the halo micro-features exist, the energy associated with the stress might be sufficient to extend them or create crazes via micro-void coalescence in the direction of the electric field.

■ In order to assess the significance of these halo micro-features on the degradation of the insulation when an ac stress is applied, a method which allowed the detection of the early stages of the degradation well before partial discharges occur, was required. The micro-voids observed being very small they were likely to induce a low level of degradation. Electroluminescence (EL) measurements are known (see chapter 3) to provide such a method.

Chapter 3

Electroluminescence from insulating polymers

3.1 Introduction

In general, luminescence is defined by the emission of light in the ultraviolet (UV), visible and infrared (IR) ranges by an excited material. Depending on the origin of this excitation several forms of luminescence exist. For example, photoluminescence results from an excitation by photons in the UV or visible range, triboluminescence is induced by the friction of two materials and chemiluminescence occurs during chemical reactions. Finally electroluminescence (EL), which is the topic of this study, is a consequence of the excitation by the application of an electric field. EL phenomena were first found in organic materials in the 1960s [21, 22]. The basic mechanisms of luminescence are the same for all forms of excitations. These mechanisms are described accurately using theories of quantum mechanics while introducing the general principles of these theories [23, 24] the development of the phenomenon of EL in polymers is expanded.

3.2 General mechanisms of luminescence

In atomic or molecular systems luminescence is linked to the successive excitation and de-excitation of their valence electrons. In order to understand these processes, a brief summary of atomic and molecular energy structure is given.

■ In an atom, the energy states are determined by the distribution of the electrons in the atomic orbitals. The Pauli exclusion principle states that only two electrons can be accommodated by a given atomic orbital and their spins must be paired. In the ground state the electrons fill the lowest orbitals with two electrons per orbital. When the atom is excited the electron can reach higher free orbitals and according to different possible configurations multiple excited states are formed. The lowest excited states correspond to the elevation of one electron to a higher orbital.

In the ground state the electrons have opposite spins and consequently their total spin is zero. The ground state is called a singlet state (denoted S_0). When an electron quits the ground state it can either keep a spin parallel to the first or undergo a reversal of spin or spin-flip. In the first case the resultant spin remains zero: the excited state is also a singlet state (denoted S_1). In the second case the resultant spin is equal to 1: the excited state is then called a triplet (denoted T_1). The triplet states are referred to as such because they are degenerated three times, that means they correspond to three distinct sub-states.

■ In a molecule, the energy states are described in a similar fashion by the theory of molecular orbitals. According to this theory molecular orbitals can be obtained by the linear combinations of the different constituent atoms' orbitals. According to their nature they are then labelled under the name of the orbitals σ, π, n... and to each of them (except for n orbitals) there are corresponding superior orbitals called antibonding molecular orbitals, denoted σ^*, π^*...

In polymers, π orbitals are important. They are present at each double bond. The n orbitals (or non-bonding orbitals) are present when there is a free pair, for example in the case of a ketone groups (>C = O). Finally the σ orbitals are the most common in polymers but they do not intervene in luminescence.

Similarly to atoms, a molecule reaches an excited state when an electron reaches a free higher orbital. In organic molecules the first excited states generally correspond to n - π^* and π - π^* configurations, which explains why the σ orbitals play no role in luminescence. The excited molecular states are spread between singlet and triplet states.

Figure 3.1 shows a simplified energy diagram on which all the possible transitions between lowest energy states are represented: radiative transitions are represented using solid lines, while non radiative transitions are represented with dotted lines. The ground state S_0 is represented with the first excited state singlet S_1 and a little lower is the first excited state triplet T_1.

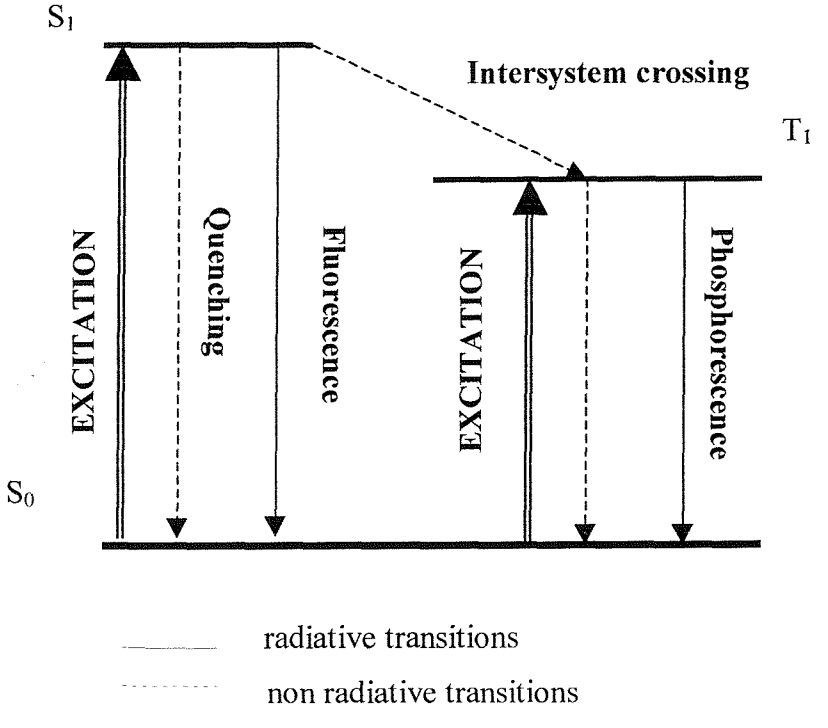

Figure 3.1: Energy level diagram

Fluorescence is defined by the transition from state S_1 to the ground state S_0. Phosphorescence is defined by the transition from state T_1 to the ground state. It should be noted that phosphorescence is characterised by a long life, typically 10^5 times more than that of fluorescence. In the solid state non radiative transitions compete with radiative ones. The description of these processes will not be presented, only their names will be mentioned. The non radiative transition between the state S_1 and S_0 is called quenching while the one between S_1 and T_1 is called intersystem crossing.

Several studies show that EL in polyolefins seems to be dominated by phosphorescence. As excited triplets can decay unimolecularly, mostly by bond cleavage and rearrangements involving breaking and formation of new chemical bonds, their detection in EL is a signature of irreversible reactions [11, 25].

3.3 EL in polymers

Given the general description of luminescence, it is possible to extend the discussion of the mechanisms of EL in polymers and more particularly in insulating polymers.

3.3.1 Band theory applied to polymers

The EL mechanisms are considered in the framework of electronic band theory which is generally used for inorganic semiconductors. This is a big approximation because this model assumes that the molecular orbitals are delocalised on the total "network" of molecules, which is not the case in reality. The periodic potential resulting from a chain of mers will set-up bands of extended electronics states and these bands are established with only a few mers in the polymer chain. However we shall see that this model allows a satisfactory description of EL phenomena. In this model one does not consider energy levels but energy bands, which are made up of many electronic states. One should recall that there are two energy bands, which are separated by a band gap sometimes known as the forbidden band gap. The highest filled band at absolute zero is known as the valence band, and the first unoccupied band as the conduction band.

According to band theory, the conductivity in the material is linked to the increase in energy of the electrons which pass from the valence band to the conduction band (see figure 3.2). This process depends strongly on the width, Eg, of the gap, which can be used to classify materials as either insulating (Eg > 5eV), semiconducting (Eg ~ 2eV) or conducting. The band gap for PE is assumed to be ~ 8eV to 10eV [5]. The fundamental ground state is usually situated at the top of the valence band while the excited state is situated near the conduction band.

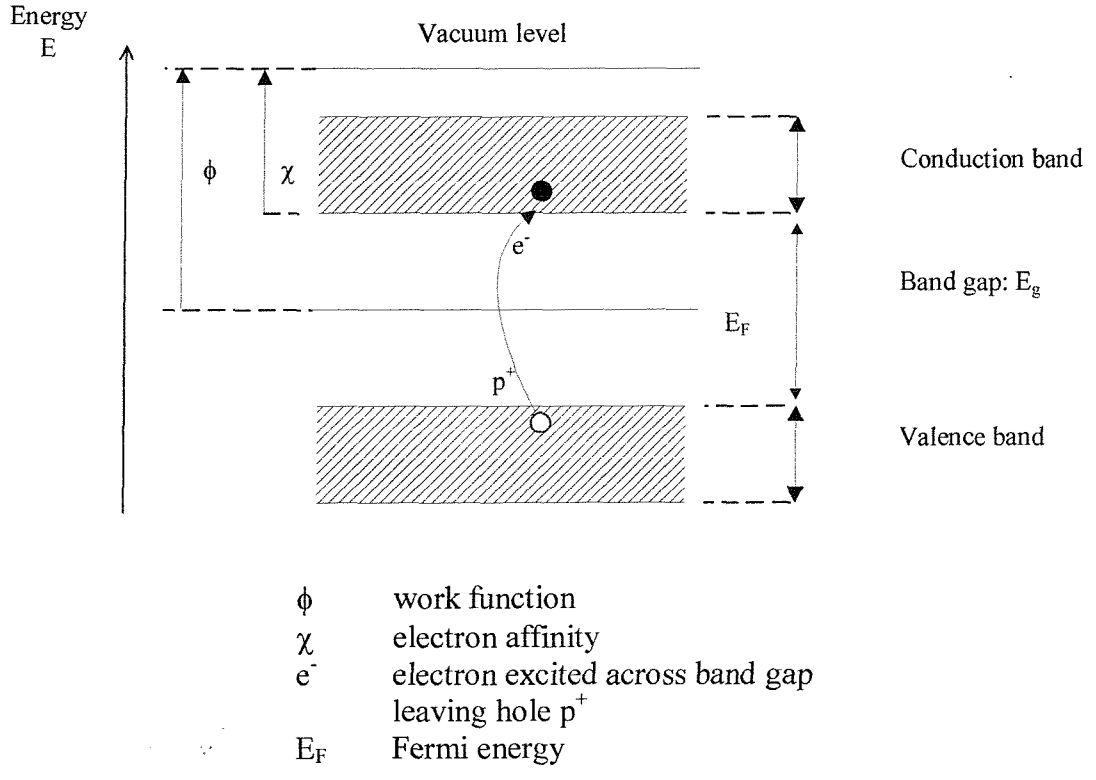

Figure 3.2: Energy-band diagram for a covalently-bonded crystal

In polymers (amorphous or semi-crystalline) the valence and conduction bands are less clearly defined, and temporal and spatial inhomogeneities cause localised energy states (charge traps) to occur in the band gap [5, 26]. Interruption of the periodicity of the potential by chain irregularity (such as folds, chain ends, foreign atoms...) gives rise to a localisation in space of the energy states.

Every polymer has chemical entities which can act as traps for electrical charges. For example every time a polymer bond is broken, it gives rise to a free radical, which has a great affinity for electrons and hence acts as a trapping centre for negatives charges. Moreover, attachment of electrons can occur at regions of low electron charge density *e.g.* at the carbonyl groups, or they can be caged within groups of atoms. There are traps for both electrons and holes; for example, while free radicals act as traps for electrons, the hydroxyl (-OH) groups act as traps for holes. Charge trapping may take place not only at chemical groups, but also at physical irregularities and amorphous-crystalline boundaries in the semi-crystalline polymer. Traps are also classified as shallow and deep, depending on their energy level. The depth of a trap is defined as the energy needed to liberate a charge carrier. Trapped charges are released relatively more easily from the shallow traps (0.1eV to 0.3eV from the conduction band in PE) than from the deep traps (0.8eV to 1.4eV in PE) [27].

3.3.2 Charge injection mechanisms

For EL to occur, charge injection at the electrode–polymer interface is necessary. The nature of the electrode-insulator interface is complex. The energy-band diagram is complicated by the presence of physical, chemical and electrical defects such as: surface roughness, imperfect contact, chemical impurities and local polarisation resulting in band bending, trap states...etc.

The shape of the injection barrier and the two mechanisms usually invoked to explain electric field-assisted charge injection based on a simplified energy-band diagram is briefly described.

When a contact between a polymer and a metal conductor is made, a state of equilibrium across the interfaces has to be reached such that the vacuum and Fermi energy levels of the insulation and metal become continuous across the interface. Electrons will flow from one to another until the Fermi levels coincide.

The nature of contact will depend on the relative work functions of the metal and insulation [27]:

- if the work functions are equal the contact is called neutral,

- if the work function of the metal is less than that of the insulation then the contact is called ohmic contact,

- if the work function of the metal is greater than that of the insulation the contact is called blocking contact.

The following diagram (Figure 3.3) represents the two classical shapes of potential energy barrier at the interface metal/insulator when an electric field is applied [28]:

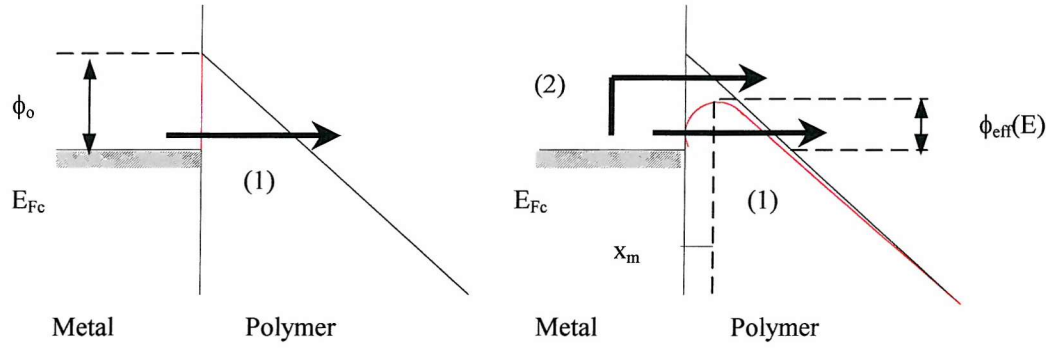

(1) tunnelling effect
(2) thermionic emission

(a) (b)

Figure 3.3: Metal-polymer interface energy barrier
(a) triangular barrier
(b) barrier lowered by Schottky effect

■ In the first case the potential barrier is triangular. The theories were initially developed for electron injection from the metal into a vacuum in which case the barrier height was equal to the work function of the metal ϕ_m. In the case of the metal-polymer interface this

barrier height is modified by the local conditions. In an ideal case the electrons have to be excited into the conduction band in the polymer in which case the barrier height would be decreased by the electron affinity χ of the polymer:

$$\phi_0 = \phi_m - \chi \tag{3.1}$$

where ϕ_m is the electron work function of the metal and χ the electron affinity of the polymer.

• When the electric field is high enough (E> $3x10^8$ V/m [29]) the process of field emission occurs, in which charge carriers enter the insulator by tunnelling of the interfacial barrier. This mechanism, called, the Fowler-Nordheim effect, is characterised by the following expression of the current density [28, 29]:

$$J \approx E^2 \exp\left(-\frac{B}{E}\right) \tag{3.2}$$

where E is the intensity of the electric field,
B a parameter which depends on the barrier shape.

For a triangular barrier shape B is given by:

$$B = \frac{8\pi\sqrt{2m^*}\phi_o^{3/2}}{3eh} \tag{3.3}$$

where m^* is the carrier effective mass in the insulator,
ϕ_o the barrier height,
e the electron charge,
and h the Plank constant.

■ Generally, it is assumed that the barrier at the interface between metal and insulator is not triangular but gradually lowered under the effect of the coulombic image force (figure 3.3 (b)). This effect is called Schottky effect. The barrier is assumed to be due to the electrostatic attraction between the electron and the metal, the latter being positively charged since the electron has left it. This attraction gives rise to a gradually changing barrier due to the potential energy of the electron.

Because of this effect the barrier height is reduced by $\Delta\phi$ which is a function of the electric field intensity:

$$\Delta\phi(eV) = \left(\frac{e^3 E}{4\pi\varepsilon_0\varepsilon_r}\right)^{1/2} \qquad (3.4)$$

where ε_0 is the dielectric permittivity in vacuum,

ε_r the relative dielectric permittivity.

Above high field values [29] Fowler-Nordheim injection is more likely.

The effective barrier height is:

$$\phi_{eff} = \phi_o - \left(\frac{e^3 E}{4\pi\varepsilon_0\varepsilon_r}\right)^{1/2} \qquad (3.5)$$

Figure 3.3 shows that the maximum of the barrier is now situated at the distance x_m from the interface metal/insulator, which is a function of the applied electric field given by the formula:

$$x_m = \left(\frac{e}{16\pi\varepsilon_0\varepsilon_r E}\right)^{1/2} \qquad (3.6)$$

• Charge carriers can enter the insulator by tunnelling of this type of interfacial barrier. Then the current density variation is given by a relation similar to (3.2) in which we take into account the reduction of the barrier height.

• Charge carriers can be thermally activated over the barrier, entering the sample with some kinetic energy which is dissipated over a discrete distance. This mechanism by thermionic emission is called Richardson-Schottky emission.

For this injection mechanism the current density expression is given by:

$$J = AT^2 \exp -\left(\frac{\phi_o - \beta_S E^{1/2}}{kT}\right) \qquad (3.7)$$

$$\text{with } \beta_s = \frac{1}{2}\left(\frac{e^3}{\pi\varepsilon_0\varepsilon_r}\right)^{1/2} \text{ and } A = \frac{4\pi mk^2}{h^3}$$

where A is the Richardson-Schottky constant,

β_s is the Schottky constant,

m the electron mass,

and k the Boltzmann constant.

In order to verify Richardson-Schottky injection, the plots of log (J/T^2) versus $E^{1/2}$ are often constructed. These yield straight lines although at low fields space charges and surface inhomogeneities tend to cause deviations.

The relation of the EL intensity versus the applied electric field has been fitted to that of the injection current versus the electric field given by the charge injection mechanisms presented above, assuming that the EL intensity I is proportional to the injection current [29, 33].

In the case of the Fowler- Nordheim injection mechanism (equation 3.2) by field emission, the relation between I and E could be written by:

$$I\alpha E^2 \exp\left(-\frac{B}{E}\right) \tag{3.8}$$

In the case of the Richardson-Schottky injection mechanism (equation 3.7) the relation between the EL intensity I and the electric field E was given by:

$$I\alpha \exp\left(\frac{\beta_S E^{1/2}}{kT}\right) \tag{3.9}$$

It has been shown from EL experiments in LDPE samples using a pin-plane electrode geometry (see section 3.4.1.2) giving a divergent field configuration that the Richardson-Schottky plot (plot of ln I versus $E^{1/2}$) gives a good fit to the experiment in the lower field region, and the Fowler-Nordheim plot (plot of ln (I/E^2) versus 1/E) in the higher field region [29, 33]. Thus it is possible to follow charge injection by monitoring the EL intensity.

3.3.3 Mechanisms of EL

By its nature EL involves the excitation of electronic states by a voltage applied to the material. Two processes are involved [11, 30]: the excitation process or how the radiative system is excited, and the relaxation mechanism or how the light is emitted.

3.3.3.1 Excitation mechanisms

The general phenomena of EL can be classified according to the mode of excitation [30].

- The high-field EL is defined by the assumption that an external electric field excites states directly. This effect involves electron tunnelling from the valence to conduction band (Zener effect) or field ionisation of impurity centres. Because of weak inter-molecular interactions in organic solids the more probable excitation would be a result from an electric field-induced perturbation of well–localised (practically intra-molecular) electronic states.

In a large band gap insulator this mechanism could not play a role as calculations [31] show that the field required to induce this effect is in excess of the breakdown field.

- Collision of accelerated charge carriers (hot carriers) generated in the bulk or injected at the interfaces of the sample with luminescent centres, chemical and physical defects or unperturbed molecules can lead to their excitation and subsequent radiative decay. The emitted light is called impact EL.

- If electrons and holes are injected into the materials at their interfaces (i.e. electrical contact) or are generated and their recombination generates excited states which give rise to emission, we then have recombination EL.

The threshold fields required for EL distinguish between the three excitation mechanisms [31]. Approximate local fields of 10^7 and 10^5 volts/cm are necessary for the direct field ionisation and the impact excitation mechanisms respectively. The recombination mechanism does not have a field threshold.

The different excitation mechanisms are represented schematically in figure 3.4.

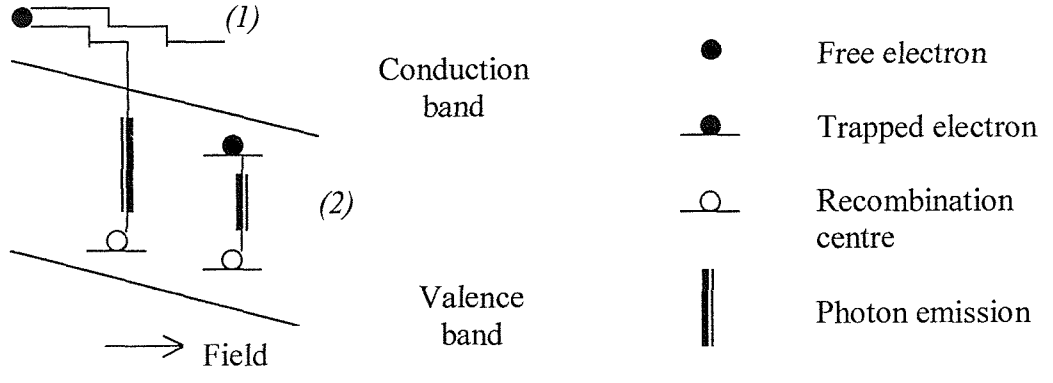

Figure 3.4: (1) impact-dominated luminescence
(2) recombination-dominated luminescence

3.3.3.1.1 Impact EL

In this type of EL, the bulk created or injected charge carriers are accelerated out of equilibrium with the material structure, so that they undergo inelastic collisions with molecules and excite them (or ionise) to states from which radiative de-excitation results (see figure 3.5).

■ Impact ionisation mechanism

A mobile space charge is able to generate electron-hole pairs across the gap.A molecular approach can be written as:

$$AB + e^-_{hot} \rightarrow AB^+ + 2\,e^-_{th}$$

where e^-_{hot} and e^-_{th} stands for hot and thermalised electrons and AB is a molecule.

This mechanism would require at least three conditions:

- high-field regions capable of accelerating charge carrier to large kinetic energies must be produced,
- free charge carriers must be present,
- and the interaction with the luminescent centre must absorb a significant fraction of the energy extracted from the field by the charge carriers.

Free charge carriers can be supplied by injection from an electrode (see section 3.3.2), by field- or thermal-detrapping, or by some other mechanism.

■ Impact excitation mechanism

Electrons are brought into excited states of the molecule without being free to move in the conduction band while the electrostatic interaction is still binding them to the centre.

This excitation is referred to as an exciton and is well documented in the literature [32].

A molecular approach can be presented as such:

$$AB + e^-_{hot} \rightarrow AB^* + e^-_{th}$$

where AB, a molecule, is excited in a state AB^*, e^-_{hot} and e^-_{th} stand for hot and thermalised electrons.

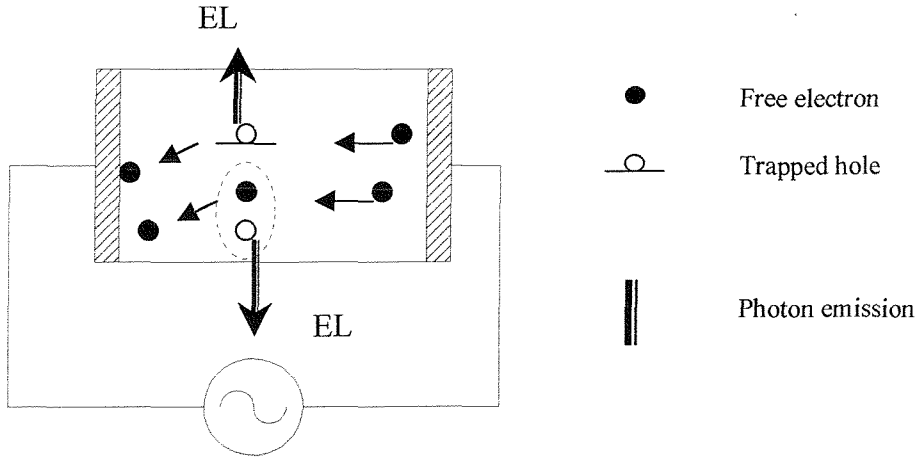

Figure 3.5: Model of impact EL

3.3.3.1.2 Recombination EL

This process can take place at low fields and does not require any sort of threshold although bipolar charging must be achieved. Under dc stress, space charges of opposite polarity can be injected from anode and cathode. Under ac voltage, bipolar charging can be achieved by injection in the vicinity of the same electrode acting as anode and cathode alternately.

A trapped space charge is characterised by carriers which reside for a long time on their trapping site. Their kinetic energy is zero, but electronically excited states can be generated upon their recombination with carriers of opposite polarity.

Recombination can involve:

- band to band transitions,
- transitions between free carriers and deep traps acting as recombination centres,
- transition between two trapping levels.

These can be represented (respectively) by the following:

$$A + e^-_{th} + p^+_{th} \rightarrow A^*$$

$$e^-_{th} + A^+ \rightarrow A^*$$

$$A^+ + B^- \rightarrow AB^*$$

where p^+_{th} stands for thermalised hole.

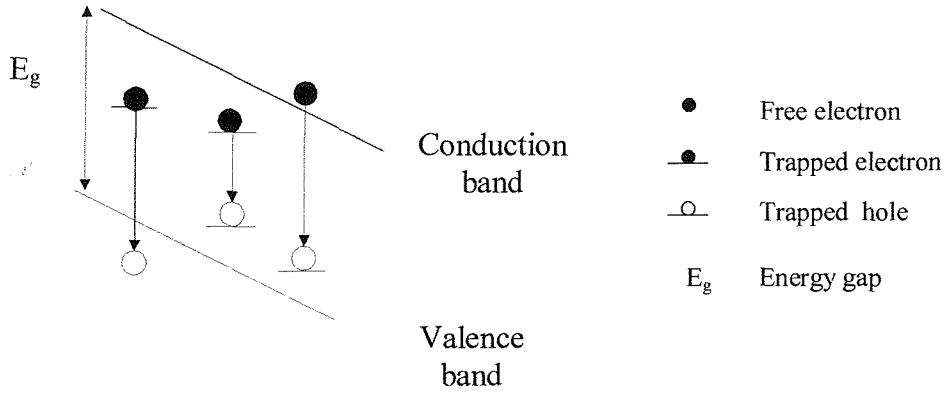

Figure 3.6: Recombination EL

3.3.3.2 Relaxation mechanisms

Once the excited state has been formed, its de-excitation involves radiative and non-radiative transitions (see section 3.2). Among the radiative transition, two main pathways can be distinguished: a physical and a chemical one.

In a physical process, the excited states return to their ground state without any chemical reaction by a purely reversible effect and give rise to fluorescence emission (singlet to

singlet transition), phosphorescence (triplet to triplet) transition (see section 3.2). The relaxation can also be by quenching or energy transfer.

In a chemical process, the excited states can dissociate into molecular fragments which can be very reactive and lead to further degradation reactions.

Possible chemical processes are:

$$AB^* \rightarrow A + B^*$$

$$AB^* \rightarrow A + B$$

$$AB^* \rightarrow A^+ + B^-$$

where AB^* is a molecular excited state.

The balance between these two mechanisms is obviously very important for the relationship between electrical degradation and EL emission. This relationship will be discussed later in this thesis (see section 3.4.7).

3.3.4 Polymer luminescent properties

Chromophores are certain chemical groups in the polymer which absorb characteristic radiation in comparison to the rest of the compound. It is useful at this point to distinguish between two main classes of polymers: polymers that can emit light through chromophores present in the monomer unit that form the backbone structure of the polymer (e.g. aromatic polyesters) and polymers that can emit light through isolated impurity chromophores (e.g. polyolefins).

Polyolefins are typical polymers which do not contain chromophores in the repeat units of the macromolecule, but contain chromophores as defects. These defects could be:

- intrinsic as unsaturated species strongly bonded to the chain (*e.g.* vinyl, vinylene, carbonyl *etc.*) situated in-chain, side-chain, or end-chain groups
- extrinsic as additives weakly coupled to chain (*e.g.* additives, antioxidants).

Saturated polyolefins such as polyethylene (PE) in their pure form do not absord light of wavelength > 300nm. However, commercial PE absorbs light in the near-UV range between 270 and 400nm and this is because of impurity chromophores. They can be introduced during the various compounding and manufacturing stages of the polymeric insulation. For example, during polymerisation Ti or Al catalytic residues or carbonyl and hydroperoxides are introduced. During extrusion some oxide groups (OOH, -O-O-) are formed due to thermal oxidation and metal oxides from the corrosion of the apparatus are also introduced into the polymer. During storage poly-nuclear aromatics such as naphthalene and anthracene, as well as charge transfer complexes are formed.

When crosslinked polyethylene (XLPE) is considered, chemical by-products of crosslinking reactions can be another source of chromophores. Some studies have shown that the presence of antioxidant in the polymer does not affect the EL spectrum [33]. The spectrum is also similar when XLPE with residual acetophenone is considered [11, 33]. Aromatic structures do not seem to be involved in EL emission even if they are readily excited by UV irradiation [33].

3.4 Literature Review

3.4.1 Electroluminescence detection and sample configurations

3.4.1.1 Detection

EL in insulating polymers is very faint, and hence very sensitive optical detection methods have to be used. Sensitive photomultiplier tubes (PMT) are usually used to detect and measure the integral EL. They have a high sensitivity, a low background noise and an extended wavelength response (250 to 900nm).

Interference optical filters are used in the light path of the PMT in order to determine the spectral range of the light emission [7]. Lenses or ellipsoidal mirrors [34, 35, 74] have been used to focus the active area of the sample onto the PMT photocathode.

More recently, sensitive cooled detectors based on charge-coupled device (CCD) technology, which have virtually no background noise, have been used as an imaging camera [36-41, 43] or a multichannel optical analyser for spectral analysis of the emission [42].

3.4.1.2 Sample configuration

Two electrode configurations are generally used to study EL from polymers: the divergent field configuration and the uniform field configuration. A different type of configuration is used to study EL from a surface layer of polytetrafluoroethylene (PTFE) [44] which consists of two concentric electrodes and also a planar surface model has also been used to study EL from alumina ceramic's surface [45, 46].

- Divergent field configuration or pin-plane electrode geometry

Because EL was detected prior to electrical tree inception, a considerable amount of work has been carried out to study EL in situations usually adopted for treeing experiments, i.e. the divergent field configuration. The sample consists of a needle electrode inserted into the material (see figure 3.7). The ground electrode is usually a conducting plane ~2mm from the tip electrode but a double-needle configuration has also been used in the past [47].

Different sample preparation procedures have been adopted. Metallic electrodes were either inserted in the polymer block at elevated temperature or compression moulded in the sample (sandwiched between pre-moulded polymer plaques) or the polymer is injection- moulded around the needle. Some tests have been performed with embedded semi-conductor electrode tips made from partially crosslinked ribbons of carbon loaded polymer [51].

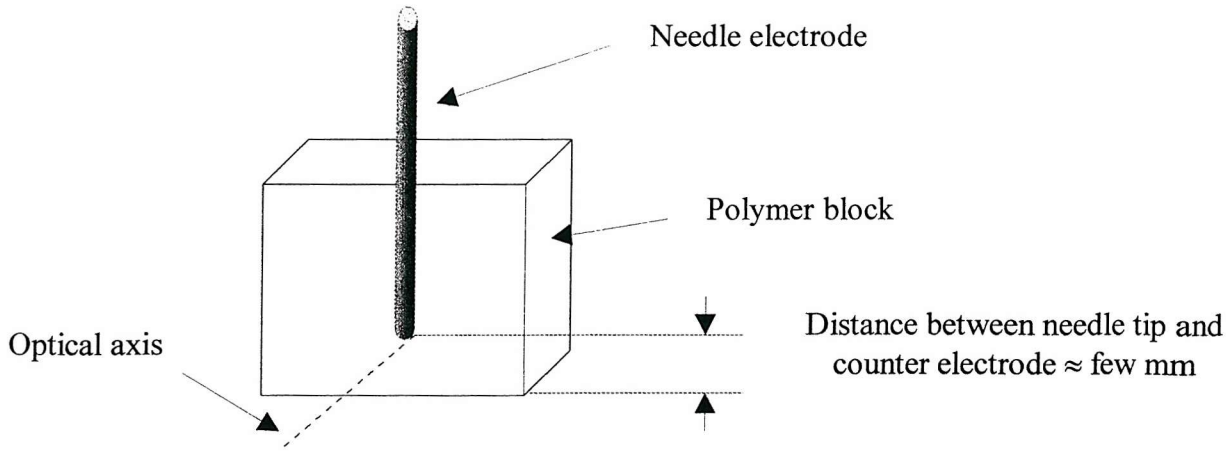

Figure 3.7: Diagram of needle-plane geometry

This configuration is well adapted to correlate EL with ageing since the volume under stress is well identified and the degraded region corresponds to the small emitting volume near the needle tip.

■ Uniform field configuration or plane-plane electrode geometry

Polymer films are sandwiched between two electrodes. Previously, one was a glass electrode covered with a transparent conducting layer [21]. The light was detected through the glass electrode. The use of semi-transparent metalised electrodes was subsequently preferred [48] because the interface between the polymer and the electrode is more efficiently controlled. The semi-transparent conducting layer is deposited by thermal evaporation [49], or by metal sputtering which avoids heating during sample preparation. Gold and aluminium are currently chosen as metal electrodes. Light can be detected directly through the metallic layer by using a ring electrode [76, 78].

This configuration is well adapted to the obtaining of a fundamental understanding of EL, such as the nature of the chemicals involved in the emission process and the excitation mechanisms (in relation to the space charge distribution).

3.4.2 Influence of different gases on EL emission

When the material under examination contained a dissolved gas in equilibrium, the behaviour of the solid was found to depend on the chemical reactivity of the gas and on its electron affinity [50]. For semi-crystalline polymer, gases are localised solely in the amorphous regions of the material and have zero solubility in the crystalline regions. In LDPE and XLPE, it was shown that dissolved and adsorbed gas molecules changed the emission threshold and light amplitude [29, 50-52]. However, it is important to point out that it has been shown that EL is not due to radiative phenomena affecting the gas phase (ionisation or excitation of the gas dissolved in the polymer under the influence of high electric field). If it was the case, the spectra of the light obtained should be characteristic of electronic de-excitation of the gas molecules. The spectra from samples impregnated with various gases are identical which suggests that the gas phase is not responsible for EL [50].

The influence on EL of Oxygen (O_2), Sulphur Hexafluoride (SF_6), and nitrogen (N_2), gases which are currently used in high voltage applications is of importance.

3.4.2.1 Influence of electronegative gases: O_2, SF_6

The influence of oxygen is specifically considered because of its high reactivity and strong electronegativity. It exists in the bulk as dissolved molecules and at the electrode-polymer interface as adsorbed layers.

In the bulk, a lower oxygen concentration induces an increase in the time to electrical tree inception, an increase in the tree inception voltage and a decrease in the photodegradation due to UV emission [51]. This suggests that the oxygen present in the free volume of the polymer plays an important role in the deterioration of LDPE insulation subjected to high electric stress.

Hence an increase in the concentration of O_2 in polyethylene gives rise to two effects:

- the material is degraded more quickly due to the strong reactivity of O_2: radical sites are created on the polymer chains and oxygen will react on these radicals to produce new breaks in the bonds and the formation of carbonyl groups. These oxidation reactions are well understood.

- the light emission is reduced, partly due to (i) the strong electron affinity of oxygen (it will capture injected electrons), and partly due to (ii) quenching (see section 3.2 figure 3.1) by this gas of excited states responsible for the luminescence.

Oxygen also plays a role at the metal-polymer interface by introducing localised electronic states thereby modifying the injection mechanisms [29]. Interfacial electronic states are important in charge transfer at the metal-dielectric interface. They can be natural polymer states due to either a structural disorder in the interfacial region, or to a higher degree of oxidation of the polymer surface. They can be introduced through the existence of gaseous atoms or molecules adsorbed at the polymer surface and trapped between the metal and the dielectric. The contact is then metal-gas-dielectric. The surface states yielded by O_2 give rise to the enhancement of charge injection from the electrode into the surface states. However the electrons which are injected into the surface states yielded by O_2 contribute little to the EL processes such as radiative recombination. Therefore, the presence of O_2 gas results in a decrease of EL intensity but an enhancement of the electron injection [29].

The same behaviour was observed for SF_6. The reactions were less efficient than in the presence of oxygen [51].

3.4.2.2 Influence of N_2 gas

This gas is chemically inert so it does not react with the radicals created by the breaking of polymer chains, neither does it capture electrons since it has no electron affinity [50, 51]. Hence it does not interfere with the light emission process (it does not change the EL inception voltage and barrier height). Therefore, the EL characteristics from N_2 impregnated samples are similar to that of degassed polymers [51].

3.4.3 Model of EL in PE

Models proposed for EL emission under ac and dc stress and impulse voltages are well documented. These models do not take into account the presence of gas molecules which interfere with the mechanisms of EL according to their electron affinity and chemical reactivity as developed in section 3.4.2. The experimental conditions usually adopted to study EL are degassed samples in order to avoid the complicated effect of oxygen in the bulk and at the metal-polymer interface. Some experiments were carried out at atmospheric pressure using the pin-plane geometry but a large scatter in inception field and light intensity was noted [51, 53].

3.4.3.1 AC voltage

A model has been proposed to explain EL when an ac voltage is applied to the polymer. It has been proposed for polyethylene (LDPE and XLPE) by Laurent *et al* [50] and Bamji *et al* [7, 52, 53].

They have assumed that hot-electrons mechanisms are impossible. They suggest that at voltages just above the light inception level, EL is not due to hot electron impact (impact EL, see section 3.3.3.1.1). It is almost impossible for electrons to gain sufficient energy (> 3.5 eV) from the electric field to cause impact ionisation or break bonds of the polymer chain. It suggests that EL is most likely due to the recombination of charges (recombination EL, see section 3.3.3.1.2) at the trapping centres in the polymer.

For light emission, charge injection at the electrode polymer interface is necessary (see section 3.3.2). The shallow and deep trapping levels (see section 3.3.1) in the band gap can be separated by the so-called demarcation levels (figure 3.8). The shallow levels act as traps for charge carriers while the deep traps act as recombination centres. Volume traps due to methylene and carbonyl groups yield shallow trapping levels, while structural defects located particularly at the interfaces of the amorphous and crystalline regions are responsible for deep traps.

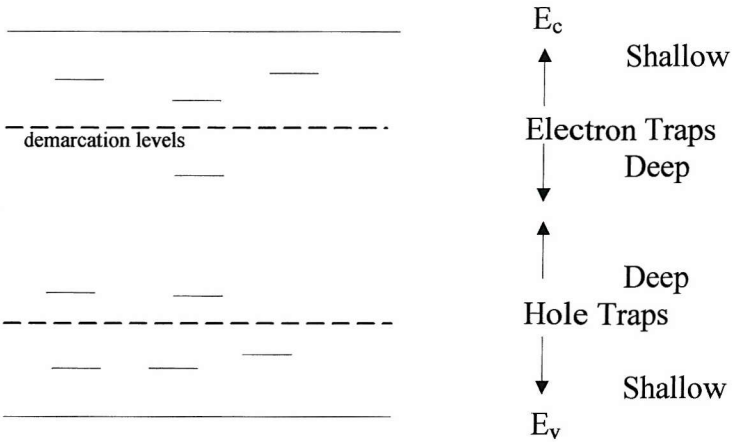

Figure 3.8: Trapping centres

For electrons, the variation of the field causes injection during the negative half of the cycle and extraction during the positive half. The proposed model is represent in figure 3.9.

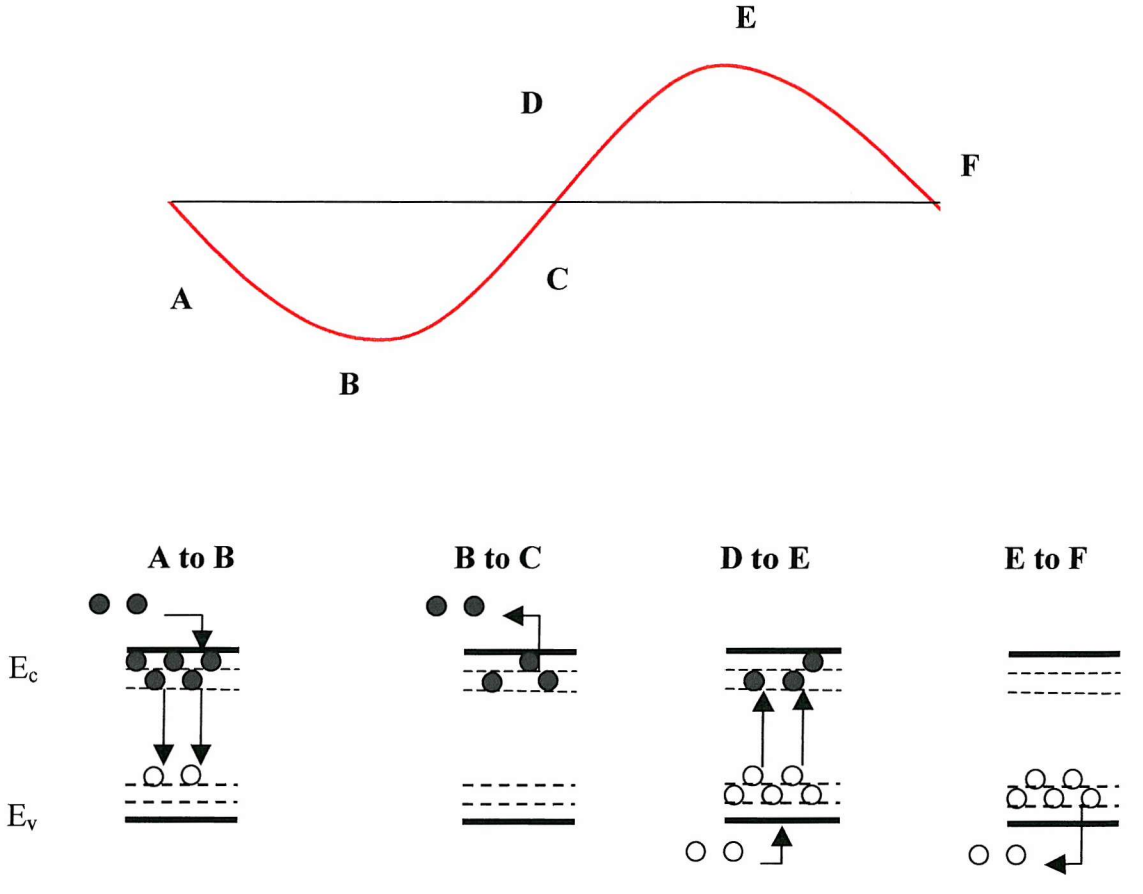

Figure 3.9: Model of EL under ac

During the negative half cycle, above a certain threshold voltage level, denoted by the letter A, electrons are injected into the polymer because of the high electric field. These electrons get trapped into the shallow and deep traps of the polymer. Some of these electrons recombine with the holes which were injected into the polymer during the previous half cycle and which could not detrap when the polarity was reversed. The recombination of the electrons and the holes gives rise to light emission.

During the decreasing portion of the negative half cycle (B to C) the electrons in the shallow traps detrap but those in the deep traps cannot. When the polarity reverses holes are injected into the polymer and are trapped in shallow and deep traps of the polymer. Some of these holes will recombine with the electrons in the deep electron traps and light is again emitted (D to E). When the voltage decreases the holes in the shallow traps will detrap but those in the deep traps remain and recombine with the electrons emitted when the polarity is reversed. This process is repeated every cycle of the ac voltage.

3.4.3.2 DC voltage

EL has never been observed for a constant dc voltage using a pin-plane geometry (divergent field). The field is reduced at the tip due to the localisation of the injected space charge cloud and the system evolves towards the space charge limited case with space charge spreading throughout the insulation with a low mobility [54].

The occurrence of light emission following double injection from anode and cathode and subsequent bulk charge recombination has been investigated under a plane-plane geometry in PE [55]. The effect was attributed to radiative recombination between trapped electrons and trapped holes rather than to impact excitation.

A substantial amount of work has been carried out on polyethylene naphthalate (PEN) and polyethylene terephtalate (PET) because the level of EL is higher than in PE making spectral analysis under DC easier [56-59]. The results are in agreement with a model of EL involving inelastic collisions of hot electrons with the polymer molecules.

3.4.3.3 Impulse voltage

EL has also been investigated under impulse voltage because underground power cables in service are inadvertently subjected to impulses generated by lightning and switching surges and also in order to better understand the temporal behaviour of carriers injected into the polymer. It has been shown that during each impulse, EL appears within two distinct periods between which there is no EL activity and this is described fully in literature [60-68].

3.4.4 Discrimination between EL and discharge light

It has been shown that optical methods are more sensitive to detect discharges than electrical methods [69]. In order to distinguish between two different light emitting phenomena, EL and discharge light, comparative studies have been carried out. The first difference is that EL is about two orders of magnitude less intense than the light of partial discharge (PD) during electrical tree growth. Reliable ways of discrimination between the two processes rely on optical analyses in both energy and time domains [11].

■ Spectral analysis of the light explores the energy domain. The light from discharges has a maximum in the UV region (300 - 400 nm) of the optical spectrum which is due to CO_2 and H_2 gases formed by the decomposition of the polymer due to the PD. EL in PE peaks between 500 and 600nm. The clear separation between emission of light from PD and EL denotes two different origins of the emission.

■ Analysis in the time domain when samples are submitted to a constant stress level shows high stability of the EL intensity *vs.* time, contrary to what is observed for discharge light emission. In the latter case, strong fluctuations of the amplitude of the light signal are recorded because the discharge activity in microvoids depends on the internal void pressure and the electrical conductivity of the cavities [69, 72, 73]. Similar conclusions were obtained from epoxy resin [36, 70, 71]. The phase angle dependence of the light emission is another way that has been used to differentiate between the two processes [69, 74].

3.4.5 Identification of the components of the EL emission of PE excited under ac voltage

Different processes can contribute to the emission involved in EL as developed in section 3.3.3.1. Hot electrons can be involved through inelastic collisions with the molecules of the dielectric. They can induce electronic excited states with or without the mediation of pairs of charges (impact ionisation and impact excitation respectively). Light is then emitted during charge recombination (for impact ionisation) or during relaxation of the excited molecule (for impact excitation). Charge recombination on luminescent centres can be responsible for EL in the absence of hot carriers if electrons and holes can be injected from the interfaces or generated inside the material by electro-dissociation.

The emitting centres could be chromophores originally present in the polymer before voltage application, or new chromophores formed during ageing of the material. Moreover recent research [75], has shown that there is a component in the EL spectrum which is due to a pure electrode effect. EL detected under uniform field configuration (plane-plane electrode geometry), when polymer films are metalised on both sides, has two different physical origins, each mechanism being characterised by a typical spectral distribution. One is associated with the EL of the polymer and peaks between 500 and 600nm, the other is due to a pure electrode effect and peaks between 700 and 800nm, i.e. in the red part of the spectrum. The light from the metallic electrodes is due to radiative decay of surface plasmons (SP) excited by injection current. This component is not present when the material is excited under dc voltage.

The material EL is enhanced with respect to the red emission as the thickness of the film increases for a given thickness of the metal layer. Moreover the two components do not have the same field dependence [78]. At low field the red emission is dominant, while as the field increases the polymer EL increases.

Another possible explanation of the red component of the EL spectrum is the existence of interfacial electronic states at the metal-dielectric interface [76, 77]. These states could be

populated during charge injection, and neutralised during voltage polarity reversal, the excess energy being released by photon emission. Experiments carried out by Laurent *et al* argue in favour of the SP explanation. Polypropylene (PP) films were surface grafted with acrylic acid leading to a surface layer of poly(acrylic acid), $-(CH_2CHCOOH)_n-$, chemically attached to both sides of the polyolefin film. No differences were detectable in the red domain of the EL spectrum between PP and grafted PP which shows that the surface states and the interfacial region are not involved in the emission process in that part of the spectrum [78]. Interfacial states common to many different polymers could exist if they are due to the metal deposition procedure. They used two kinds of metal as electrodes [66], gold and silver, deposited either by sputtering or by thermal evaporation. Despite very different interfacial characteristics for gold and silver electrodes they obtained similar red components in the EL spectrum.

The EL of the polymer can be analysed after correction of the spectra of the light radiated by the electrodes, which can be carried out easily because the two phenomena have different spectral range and field dependence. The EL spectra assigned to the polymer is identical to the spectra obtained with the pin-plane electrode geometry which reconciles the research made on the two geometries (divergent field configuration and uniform field configuration) by different research groups.

In order to identify the luminescent centres and to understand their role in the ageing process Laurent *et al* have compared the spectral features of the light emitted by polyethylene naphtalate 2,6 dicarboxylate (PEN) and polyolefins when the emitting states are created by different excitation sources: UV irradiation, cold plasma interaction, thermal oxidation and electric field [11, 25, 79-90]. Each source is characteristic of a particular mechanism and, except for the electric field, they all excluded the electrode effects since they were carried out on non-metallised samples.

■ By using mild UV irradiation, they were able to record the Photoluminescence (PL) spectrum of the polymer. They considered it to be the fingerprint of the physical de-

excitation path (see section 3.3.3.2) involving the chromophores that are initially present in the polymer before ageing.

- The luminescence due to the recombination of trapped charges (Plasmaluminescence (PIL)) was studied after implantation of electric charges of both polarities at the surface of the film by a cold helium plasma.

- Thermal oxidation gave access to the emission spectra (chemiluminescence) characteristics of a possible chemical pathway.

In EL where highly conjugated polymers are being used as the emitting medium, the EL spectrum closely resembles the polymer's PL spectrum, indicating that the same excited states give rise to both. The non-matching between the two kind of spectra in insulating polymers can be considered as an indication of the occurrence of irreversible reactions. It leads to the following options: either the chromophores involved in EL are specially excited by the electric field or they are the products of a degradation reaction (chemical process section 3.3.3.2). Similar chromophores can be involved in both photo- and electro-stimulated emissions, but the balance between singlet and triplet electronic transitions (see section 3.2) is not the same. They have shown that EL in polyolefins favors triplet states which are long-lived states and are chemically reactive.

The spectral components involved in recombination-induced luminescence (PIL) are present in the EL emission indicating that some EL does indeed arise from charge recombination. They have concluded that unsaturated carbonyl of the dienone type (poly-enone sequences) seems involved in the recombination processes. EL would be due to charge recombination on these chromophores (deep traps for electrons and holes) and can possibly also be emitted during their creation by chemiluminescence but a definitive interpretation would require further work.

3.4.6 Imaging the emission

The use of cooled CCD detectors has allowed imaging of the emitting volume in epoxy samples using a divergent field configuration [36]. The intensity is maximum at the interface between the electrode and the polymer but extends to 10 μm away inside the resin. An extension of the bright volume is observed as a function of the stress duration.

Recently, imaging of a uniform field configuration has been carried out by Laurent *et al* for polyethylene naphtalate 2, 6 dicarboxylate (PEN) [59] and LDPE [38, 91].
- Under ac stress, the emission pattern consists of a homogeneous emission level on which are superimposed brighter spots. These spots are mainly responsible for the red emission and appear at low field whereas the homogenous EL appears in the spectral range of the material luminescence (see section 3.4.5) [91]. Surface plasmons are preferentially excited in the vicinity of local defects of the metal-polymer interface that provide enhanced charge injection.

- Under dc stress, the emission spreads over all the surface and the bright spots are not observed. The absence of such localised emitting area together with the absence of the red component confirm that surface plasmons are not excited under dc because the injection is space charge limited.

3.4.7 Threshold voltage/field

EL starts above a certain voltage called threshold voltage (V_{thres}). The search for a physical emission threshold is the subject of some controversy in the literature. It is difficult to define a threshold since any observation depends on the limited sensitivity of the detection set-up. In this section we will differentiate between EL experiments using the divergent field configuration and the uniform field configuration.

3.4.7.1 Divergent field geometry

Baumann *et al.* claim [92] that EL in epoxy is emitted above a material-dependent threshold which defines the onset of material ageing. They found that space charge and EL appear at the same physical threshold which is the onset of a high mobility regime. This interpretation is in conflict with the results of Champion *et al.* on epoxy [70]. They found an acceptable fit with injection laws (see section 3.3.2) and a dependence of emission thresholds on radius of curvature of the needle electrode. Their conclusion is that charge injection and EL occur as soon as an electric field is applied. There is no field (or voltage) threshold.

For PE, Lebey *et al.* [47] found that the onset of the space charge effect and EL are reasonably well correlated. Similar conclusions were drawn by Piestsh [93]. Bamji *et al.* argue in favour of a decoupling between the onset of a charge injection effect and the onset of EL. Their light inception field is 300 kV/mm while they found that a field of 100 kV/mm under ac stress is usually required to induce space charge accumulation [52, 94].

3.4.7.2 Uniform field geometry

In the case of uniform geometry, thresholds are well below those obtained for divergent field experiments. In epoxy resin, *Coisson et al.* [95] report values of the order of 10 kV/mm for a frequency of 200 Hz. For PE (LDPE and XLPE) Laurent *et al.* report values of 10 kV/mm under ac stress. Under dc stress the values are higher, 110 kV/mm for LDPE and 80 kV/mm for XLPE. For dc stress the onset of EL is related to a drastic change in the conduction process, current and EL being proportional above a field threshold value. Then the dc threshold are considered as physical thresholds corresponding to the onset of hot electron effects [25, 96].

Under ac, the situation is more complex because of the two contributions to the light emission, which are:

- surface plasmons excited by the injection current which dominates at low field,

- the EL due to the material excited by charge injection/extraction.

Then the threshold values derived from metallised polymer films stressed under ac are 'apparent' thresholds [96].

3.4.8 Relationship between EL and ageing

Different authors have proposed a mechanism of initial degradation based on the characteristics of light emission with applied stressing voltage. This section will deal with different observations and mechanisms postulated.

■ Using the divergent field electrode geometry, it has been shown that the degraded volume, which is correlated to the emitting volume at the tip of the needle, presents a higher degree of unsaturated bonds, and free radicals [97-99].

Champion *et al.* [36, 70] proposed a mechanism for the initiation of electrical trees in epoxy resin. They have found four regions of behaviour leading to the formation of an elemental electrical tree and they are represented in figure 3.10.

Region (i) is characterised by EL concentrated at the pin tip (< 3μm).

Region (ii) a steady but generally slower increase in the EL intensity may be due to progressive material degradation at the pin tip-resin interface. This may occur because of high energy injected charge carriers breaking bonds in the resin network. Alternatively UV-induced bond scission could occur if the EL spectrum has components with energies greater than 4 eV. To account for the intensity increase, bond breakage may lead to an increase in the number of deep trap recombination centres.

Region (iii) is a transition region where the light emission intensity decreases sharply. The most likely explanation is that gradual interface failure occurs, leading to a reduction in the charge injected into the bulk of the resin.

Region (iv) is associated with the formation of micro-void and micro-channels at the pin tip and micro-discharge activity.

After region (iv) once the breakdown channels are greater than about 10μm more conventional discharge appear (PD activity in growing tree) but this is not represented on the diagram that follows.

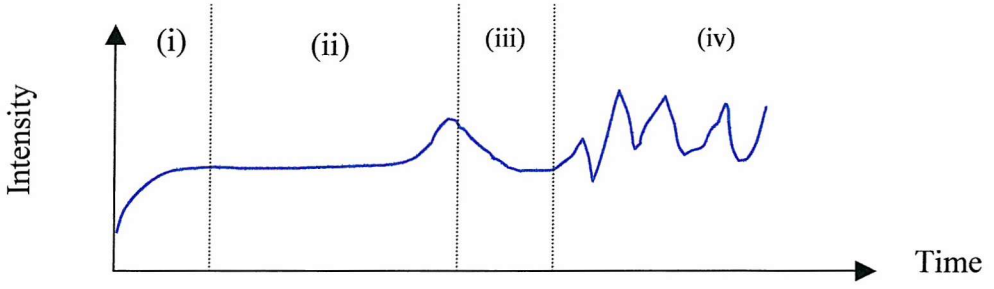

Figure 3.10: Typical long term light emission behaviour in an epoxy resin

For PE (LDPE and XLPE) a similar mechanism was proposed by Kaminaga *et al.* [72, 73, 98] which takes into account the important action of oxygen in polyolefins. However, the EL intensity has been found to decrease with time of voltage application [43]. This decrease could be attributed to the decrease of the luminescent centres and to a change of the molecular structure of the luminescence region, but the mechanism of EL did not change with time since the spectra do not change.

■ Using the uniform field electrode geometry, attempts were made to estimate the dependence on ageing conditions of EL excited under ac stress in polyolefins. The thermal and UV ageing of PP films lead to a decrease of the EL intensity as compared to unaged samples excited under the same conditions [100]. Similarly electrical ageing of samples leads to a lower EL intensity compared to a virgin sample [101, 102]. This could be due to a disappearance of the chromophores involved in light emission or to quenching mechanisms occurring when their concentration reaches a critical level. Only EL investigation has revealed a difference between these electrically aged and unaged films. Chemical analysis could not differentiate the two series of sample. This shows that EL is a powerful ageing diagnostic tool.

These observations do not however give the exact relationship between EL and ageing. The question of EL being a cause or a consequence of ageing is the subject of debate in the literature.

■ Using a divergent field electrode geometry in their experiments, Bamji *et al.* postulate that EL in PE is a cause of ageing [52, 103-106]. They suggest that the injection of electrons and holes and their recombination at luminescent centres gives rise to EL having spectra in the visible and the near-UV ranges. The UV light causes photodegradation of the polymer which results in bond scission and the formation of a microvoid in which PD can occur and cause tree propagation. The degradation is rapid in the presence of oxygen because the free radicals generated react with oxygen. They claim that the light inception voltage is the threshold voltage at which the polymer starts to degrade. They have shown that specimens held below the light inception voltage did not initiate electrical trees even after long periods of voltage application (13 000 hours), while those held above the light inception voltage always developed trees within a few hours and the time to treeing depended on the voltage level at which the polymer was held [94].

■ Using a uniform field electrode geometry, Laurent *et al.* show that EL may be a consequence of ageing but not the driving force. They base their approach on the postulated steps in electrical ageing described in figure 3.11 [25].

Initially, the potential energy supplied by the voltage source has to be converted into some sort of electronic excitation (conversion stage controlled by the local field). To be channelled into bond breaking reactions (dissipation stage), the energy has to be localised at a specific centre on the polymer chain (localisation stage). Ageing thus proceeds through the molecular dissociation of some of the original constituents of the material and the formation of new chemical bonds, necessitating the mediation of electronically excited states. These states have a non-zero probability of relaxing photons. Once the excitation has been localised on a given molecular orbit, either its relaxation can be radiative or non radiative following a purely reversible effect (see section 3.3.3.2), or the excited states dissociate into molecular fragments that can be reactive and lead to further chemical reactions.

It has been established (see section 3.4.5) that EL favours triplet states in polyolefins. They are chemically reactive, especially in the presence of oxygen. As a result of degradation reactions, new species are created amongst which are new chromophores. Evidence has been obtained that EL is associated with degradation reactions (see section 3.4.5).The implication is that the inception of EL, if it can be defined, would be the onset of the degradation as well.

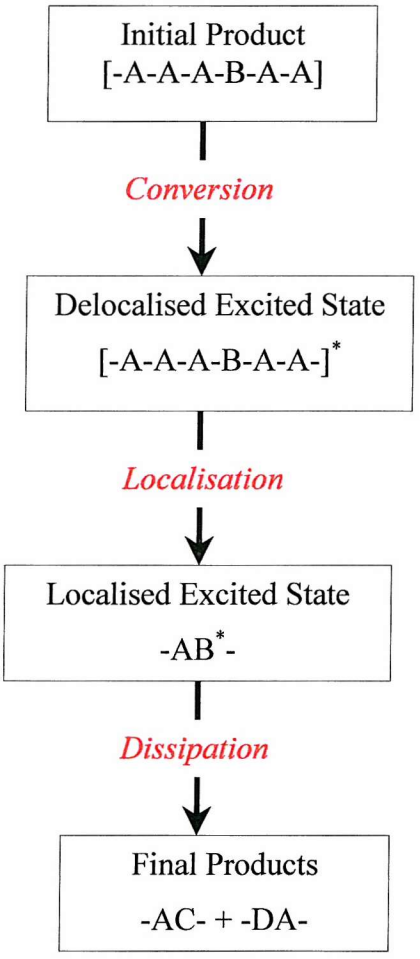

Figure 3.11: Postulated steps in electrical ageing

A: repeat unit of the chain
B: chain defect

3.5 Conclusion

EL of insulating polymers is currently poorly understood. This can be explained by the few research teams specialised in this field and by the difficulty of EL experiments that involve very sensitive optical detection systems performed in an HV environment. The nature of the luminescent centres, the excitation mechanisms and the existence of a threshold voltage or field value for EL are all currently the object of research in this field.

A considerable amount is known about tree growth but little about the degradation before PD occur. Ageing detection and indications of insulation degradation are achieved when ageing is already significant. For example when partial discharge activity is detected from a large enough micro-cavity. Due to this lack of understanding of the initial degradation mechanism, EL of polymers is a subject of great interest and EL has been used successfully to detect the very early stage of insulation degradation. It has been shown that EL detection is at least two orders of magnitude more sensitive than PD detection and can detect the initiation of polymeric degradation much before partial inception. Moreover, EL analysis is a useful method for understanding charge injection and transport in insulating materials.

EL can be detected under divergent and uniform field geometries (using a needle or metallic layers as electrodes). A considerable amount of work has been carried out using a divergent field geometry because this geometry is well suited for tree studies and until recent years partial discharges and treeing phenomena were considered to be the main sources of the degradation and breakdown of HV polymeric insulation. A reasonable description of the deterioration mechanism is available. Nowadays, long-term degradation in discharge free situations is increasingly the subject of attention. This is because the size level of defects in the insulation is highly reduced thanks to progress in technology and the stress increase (due to a reduction of the cable insulation thickness) could amplify the effect of phenomena which were not considered as important until recently. The uniform field geometry is well suited for a fundamental understanding of EL and permits the study of cable insulation directly by microtoming insulation slices. Hence in order to assess the significance of the micro-features present in the halo region (see chapter 2) on the degradation of the insulation

under ac electrical stresses which are likely to induce a low level of degradation, the study of EL appears to be the right approach. This study of light emission from HV cable insulation films containing micro-defects which are not sufficiently large to support partial discharge activity of an intensity which could lead to electrical tree initiation is important.

Recently, sensitive, cooled detectors based on charge-coupled device (CCD) technology, which have very low background noise, have been used as an imaging camera or a multichannel optical analyser for spectral analysis of the emission. However they have not yet been used to measure and monitor the integral EL. A new experimental set-up has been designed using a cooled CCD device to detect and measure the integral EL which also allows the determination of the spatial and spectral analysis of the light emission [107, 108].

Chapter 4

Design and set-up of an EL detection experimental arrangement

4.1 Introduction

An experimental arrangement was integrally designed as part of this project to carry out EL measurements on insulating samples in a uniform field configuration at room temperature under ac stress.

The novel experimental arrangement, shown in the diagram in figure 4.1 and in the photograph 4.1, which is designed to measure and monitor the integral electroluminescence in polymer insulation, is presented. The determination of the spectral range together with the imaging of EL emission is also possible. The different aspects of the design are described and discussed.

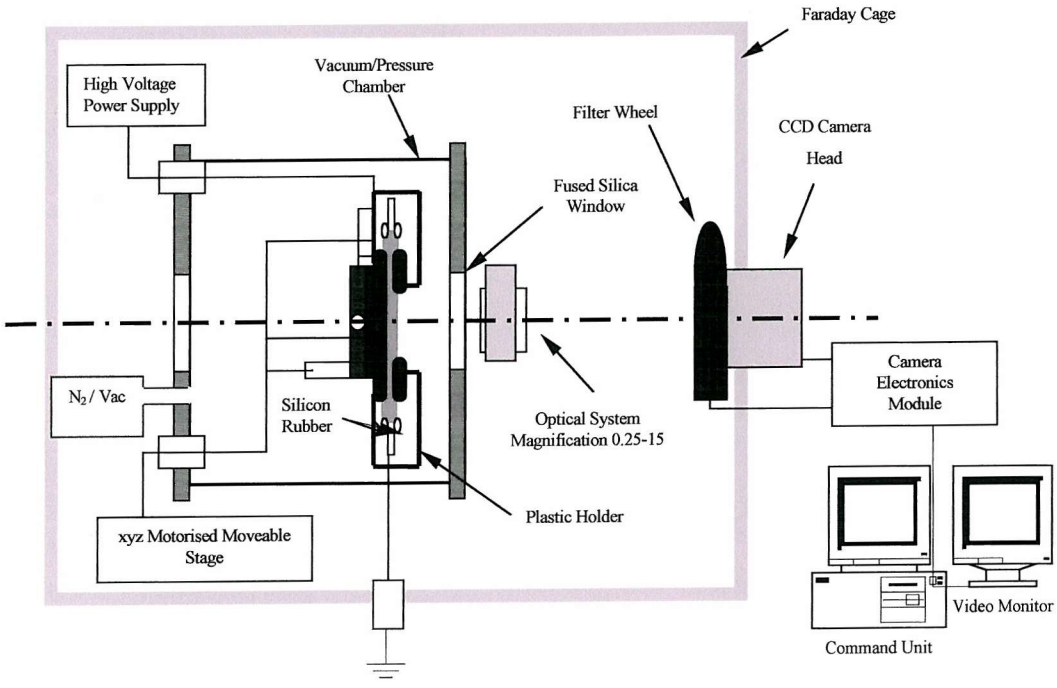

Figure 4.1: Experimental arrangement

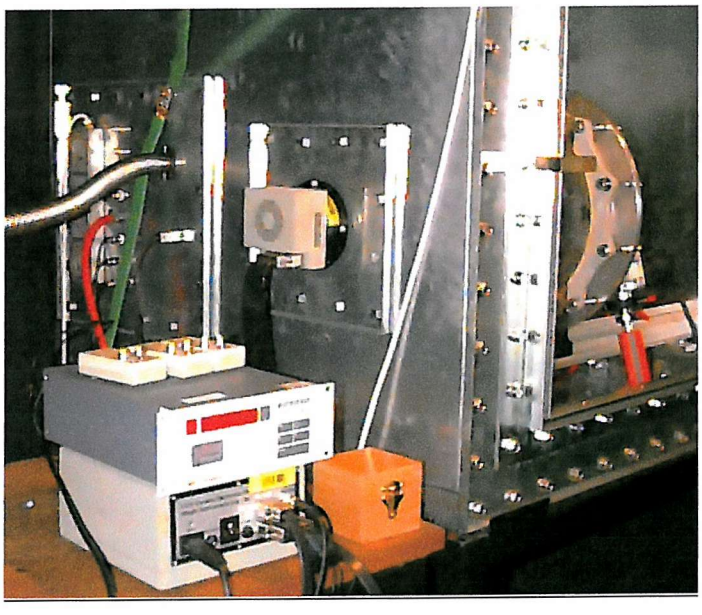

Photograph 4.1: Experimental system with the camera head fixed on the Faraday box, part of the pressure chamber, the vacuum system and, in the foreground, the camera electronics module.

4.2 EL detection experimental arrangement design

4.2.1 Sample configuration

A sample holder was designed and constructed as shown in figures 4.2, 4.3 and in the photograph 4.2.

On both sides of a polymer film (100-200 μm), a semi-transparent gold layer (30nm-80nm) was deposited by sputter coating in order to avoid sample heating compared to thermal evaporation technique. This method was selected in order to ensure a better control of the interface between the polymer and the electrode. The metalised polymer sample was sandwiched between two stainless steel electrodes with polished surfaces as follows: a ring electrode to detect the light directly through the gold layer and a plane electrode in order to avoid light emission in the other direction. The ring electrode was spring mounted to ensure a good electrical contact.

The main difficulty arose from the presence of the electrode edges. Discharges and unwanted light phenomena had to be avoided. Therefore the edges were covered with silicone rubber to prevent light detection from this zone and a plastic cover was used to detect only the light emitted from the centre of the film.

Photograph 4.2: Sample cell fixed on a 3D motorised moveable stage

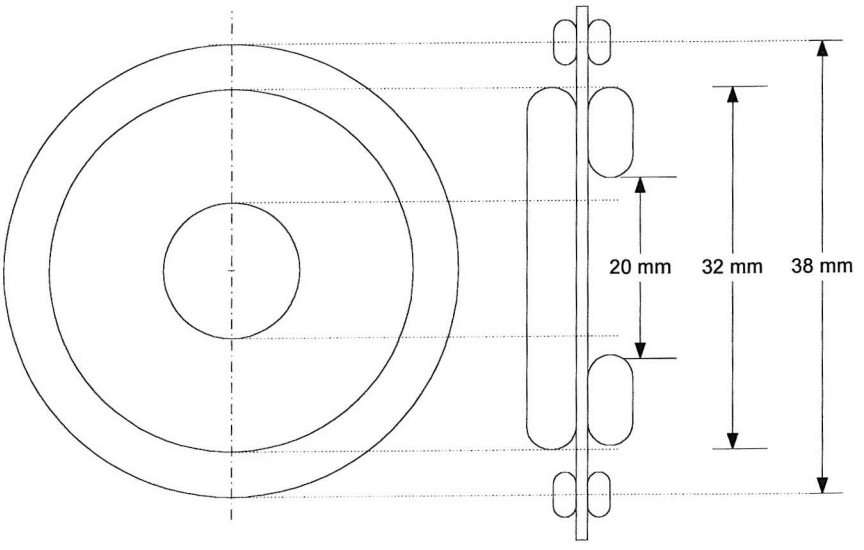

Figure 4.2: Sample geometry

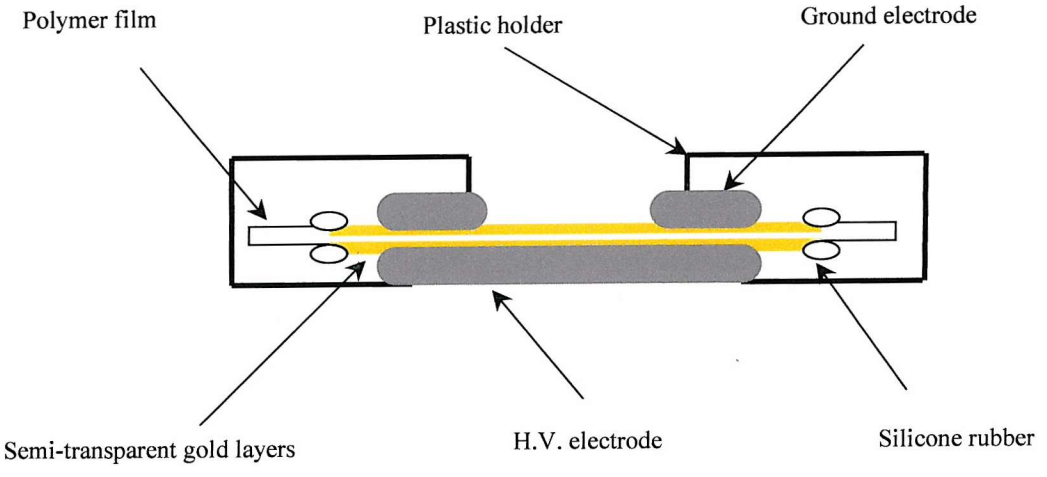

Figure 4.3: Sample arrangement

4.2.2 Light collection device: Charge-Coupled Device (CCD) detector

Although a sensitive photomultiplier tube (PMT) is usually used to detect the integral EL light, the results of simultaneous measurement of EL using both a PMT and a very sensitive detector based on charge-coupled device (CCD) technology have shown that EL is detected by the CCD detector at voltages lower than when first detected using the PMT [36]. Hence in order to carry EL measurements, a high sensitivity CCD camera was used.

The light was collected using a Wright Instrument Peltier cooled CCD camera. This comprises the camera head with the CCD, cooler and shutter, the camera electronics unit, and the computer interface [109].

4.2.2.1 CCD operation

CCDs are semiconductor devices made up of an array of photosensitive elements. These elements, or pixels, carry out light-to-charge conversions on incoming photons and store the converted charge in discrete potential wells consisting of metal-oxide-semiconductor (MOS) capacitors associated with each pixel. The charge in each storage element may then be clocked through to an output stage where it is converted to a voltage proportional to the number of photons striking that pixel. When they are moved, the potential wells carry with them any electronic charge which they may have collected. The organisation of our CCD detector is shown in figure 4.4.

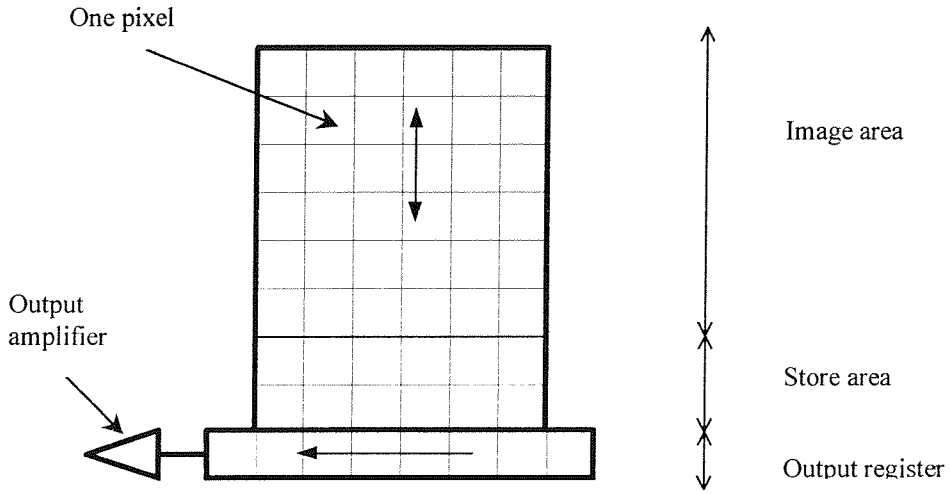

Figure 4.4: CCD array schematic

The device uses three separate sets of clock electrodes. The image electrodes cover the top half of the device (the image area), the store electrodes cover the bottom half of the device (the store area), and the output register electrodes run along the output register at the bottom of the device.

Reading out data from an exposure is accomplished by simultaneously moving all the charges in the CCD array down their respective columns, one element at the time, towards the output register. Once in the output register, a row of charges is shifted in a serial manner to the output amplifier from where it can be converted into a digital number and transmitted to the computer.

4.2.2.2 CCD cooling

Thermal excitation produces signal charge in a CCD, even in the absence of light. This effect is known as dark current. It mimics the charge produced by incident light and adds both an offset and noise to the data being collected.
Dark current in CCDs is reduced by cooling. The camera head uses a four stage Peltier cooler with fan assisted waste heat removal to give a CCD temperature of around 200K, with a cool down time of around 10 minutes.

4.2.2.3 Electronics unit

The camera electronics module contains all the circuitry to read out the CCD, and to process and digitise the data it produces. It also controls the cooler and the camera shutter.

4.2.2.4 AT1 system software

The CCD array contains 512 x 455 pixels, each capable of producing a single output, so an enormous quantity of data can be produced by a single exposure. The AT1 system comprises all the hardware and software necessary for collecting and analysing images and spectra from the CCD camera: an AT computer with a 16 bit image display board attached to a suitable monitor and the CCD camera connected to the computer via the camera board. Communication between the user and the system is via two monitors. The

standard PC (Pentium 133 MHz) monitor displays textual information for control purposes, and an additional screen displays image and graphical data output from the systems image display board.

4.2.2.5. Performance of the CCD used: comparison with other detectors

Performance can be assessed using the Quantum Efficiency (QE) of the CCD chip, the dark current obtained and the CCD resolution.

■ Quantum efficiency

QE expresses the number of charge packets generated from a given exposure and is defined as the ratio of stored charge packets to incident photons per pixel area. It varies with the wavelength of the incident photons.

The quantum efficiency of the THX7395 CCD used in our detector has a peak value of 70.6% at 550nm and is greater than 45% between 400 and 750nm. Thus over the spectral range used for EL measurements the CCD detector has a considerable advantage over a PMT which has a maximal QE of 25% [70, 71] or a photodiode used with an electronic gated intensifier system. Intensifiers use the same photosensitive materials as photomultipliers [110].

The QE data given by Wright Instruments Ltd. are plotted in figure 4.5.

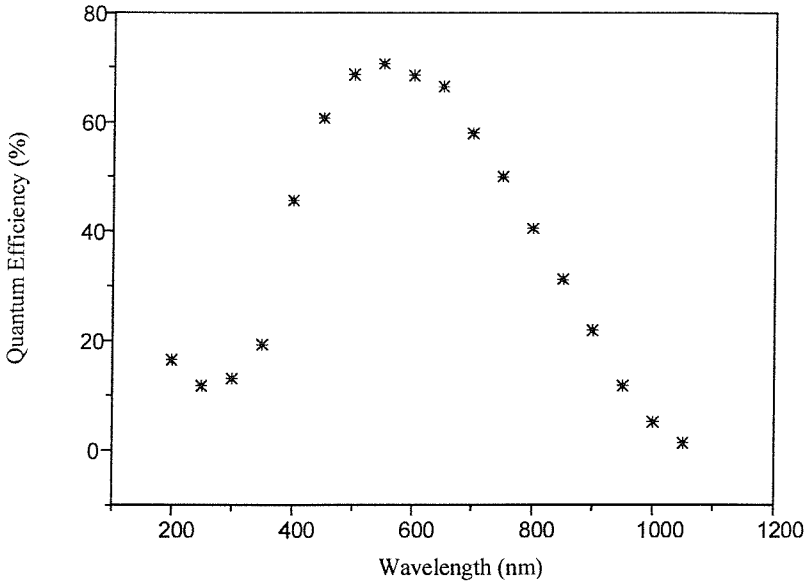

Figure 4.5: QE vs wavelength of the CCD used

■ Dark current level

The low noise in the cooled CCD detector is probably the greatest advantage this detector has over other detectors. This low noise is very important when measuring EL, which is normally a weak signal. Dark current is the name given to thermally excited signals mimicking incident radiation and increases with the exposure length. The architecture of the silicon substrate layer of which the sensor is made has a great effect on its performance. The MPP (multi-phase pinning) architecture of the CCD used ensures an extremely low dark current level of 4.5×10^{-3} e^-/pixel/second.

■ Resolution

The CCD chip is made of 512 horizontal by 455 vertical pixels. The pixel size is 19 μm square.

4.2.3 High Voltage system

A 50 Hz ac voltage was applied to the samples. The plane electrode was connected to the HV power supply while the ring electrode was connected to the ground (ref. to

4.2.1). Both electrodes had polished surfaces. In order to avoid earth loop interference produced by improper electrical grounding of the test system, a proper one point grounding had been connected. The whole set-up was inside a Faraday cubicle and all the power supply connections through the box were filtered in order to protect the detection system from external noise as shown in figure 4.7.

The transformer used was rated for a maximum secondary voltage of 20 kV. The transformer was calibrated using the ac voltage across the meter with a digital voltmeter. The calibration is shown in figure 4.6.

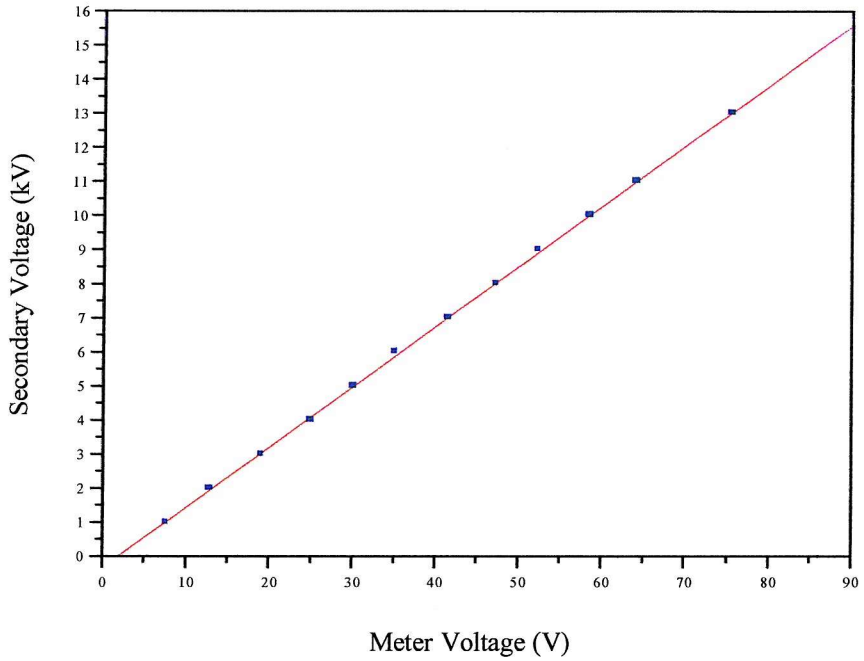

Figure 4.6: High Voltage transformer calibration

A bushing was built from PTFE material to allow high voltage to pass safely into the gas/vacuum chamber's wall separating the two media: the atmospheric medium and nitrogen pressure medium. The length of the bushing was sufficiently long to prevent flash-over at the surface and the ends were modified for stress control.

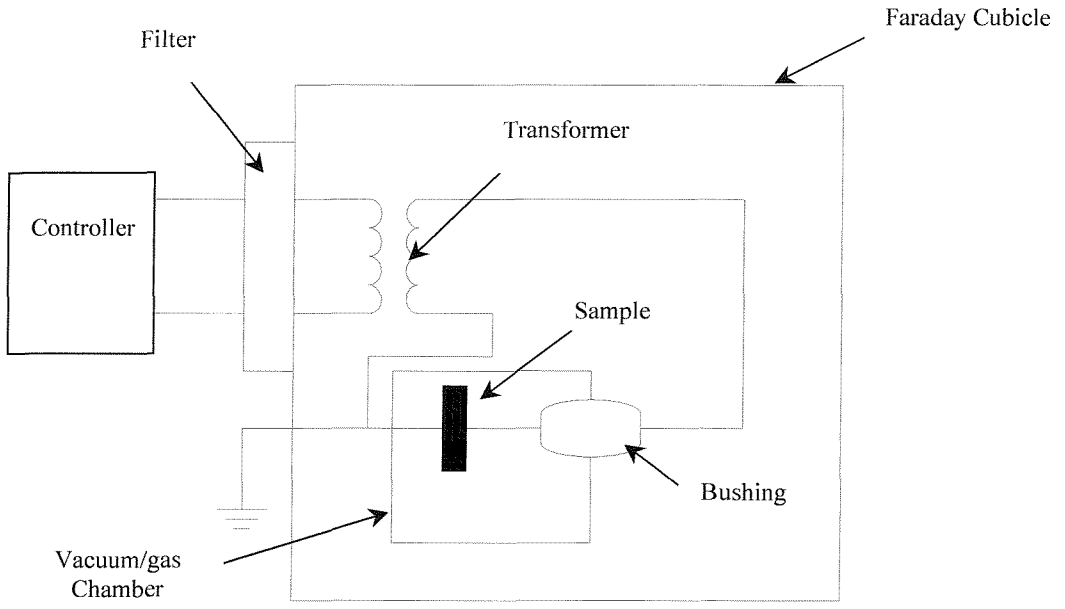

Figure 4.7: High Voltage system

4.2.4 Vacuum/Pressure chamber design

The samples were tested inside a vacuum/pressure chamber, which allowed work under atmospheric as well as under low or high pressure conditions to be carried out. For most of the experiments, the chamber was evacuated to a rough vacuum of 10^{-3} Torr and then pressurised with 1 bar of high purity nitrogen gas in order to avoid discharges around the electrode's edge while applying high voltage and to avoid the complicated effects on EL emission of oxygen at the electrode-polymer interface. Nitrogen was selected because of its low electron affinity and its high chemical stability. It does not therefore interfere with the EL processes in contrast to Sulfur Hexafluoride, SF_6, which is currently used in high voltage application (see Chapter 3 section 3.4.2).

The chamber was built using a borosilicate glass pipeline component manufactured by QVF Ltd.. Its diameter of 300 mm was determined such that it could accommodate a motorised movable stage (see figure 4.8). The transparency permitted visual monitoring of the sample cell displacement during positioning.

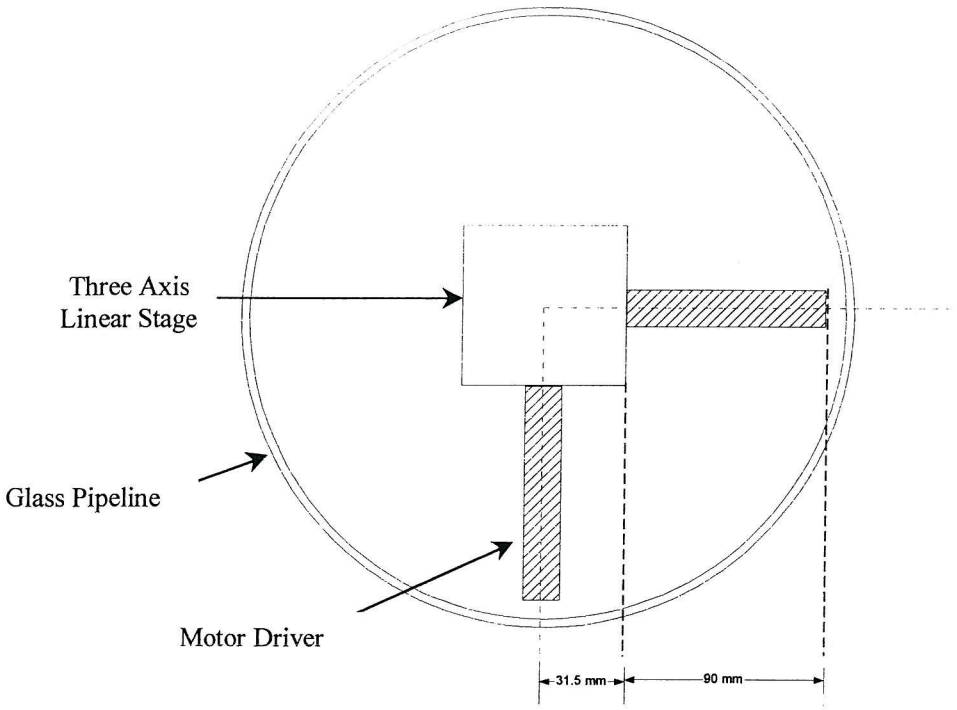

Figure 4.8: Section through the glass pipeline

The complete couplings joining the glass pipeline to the stainless steel plaques used as the walls of the chamber included:

- two backing flanges made from cast iron and epoxy resin coated to improve their resistance to corrosion,
- four inserts fitted between the flanges and the glass,
- two gaskets manufactured from high quality PTFE in order to obtain a good seal between glass and stainless plaques (see diagram figure 4.9).

The chamber was connected to a turbo molecular pump system allowing operation down to around 10^{-4}Torr. The system was fitted with a Pirani gauge for use during the evacuation phase controlled by an Edwards automatic gauge controller.

The chamber was equipped with a quick release bayonet fitting which allowed its pressurisation with gas.

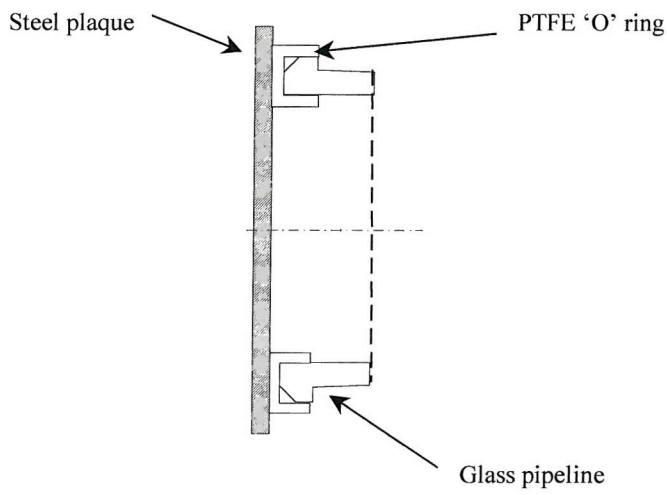

Figure 4.9: Couplings

4.2.5 Optical Design

Given that the EL spectrum is in the UV and the visible range, all the detection set-up was to be effective in this range of wavelength (300-900nm). The sensitivity of the CCD detector in this range is shown in figure 4.5.

■ The vacuum chamber was equipped with two windows made of fused silica since this material transmits in the wanted range (see figure 4.10) [113].

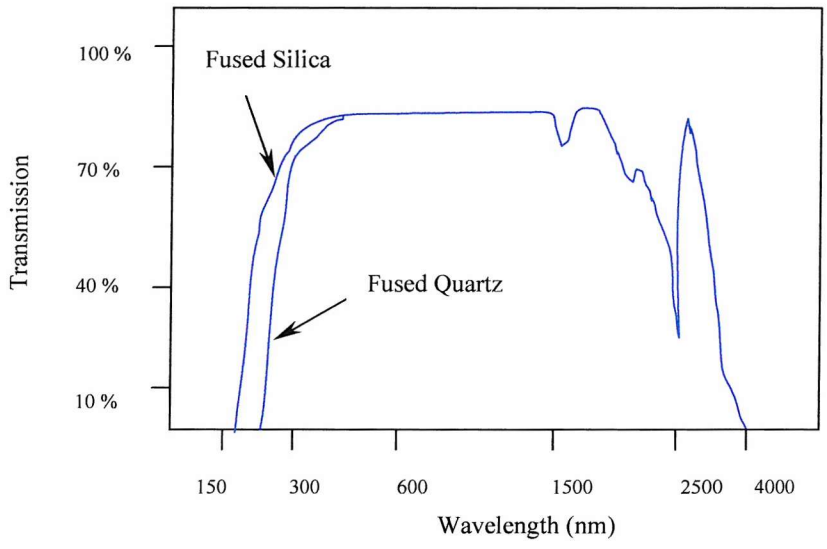

Figure 4.10: Transmission of Fused Silica and Fused Quartz (10 mm thick sample)

■ Since the overall sensitivity of the optical detection was a critically important parameter, an optical system was used to focus the light emitted onto the CCD camera chip. Depending on the magnification required a fused quartz lens or a reflecting objective (transmission from the UV to the far IR due to its all reflective construction) could be used, both of which transmit in the range of wavelength required (see figure 4.10). Until now all the experiments have been carried out using a quartz equi-convex lens which allowed us to collect the light emitted from a larger area.

The distance between the sample arrangement and the focal plane of the CCD detector relative to the lens was calculated using the set of equations below:

$$\begin{cases} \dfrac{1}{f} = \dfrac{1}{s} + \dfrac{1}{s'} & \Leftarrow \text{thin lens equation} \quad (4.1) \\ m = \dfrac{s'}{s} & (4.2) \end{cases}$$

where s is the object distance, s' the image distance, m the lateral magnification wanted, f the focal length of the lens (f=50.8mm in our case).

Note: An ellipsoidal mirror has been used by others workers [34, 35, 74] in order to increase the efficiency of the light collection system when using a pin-plane (needle) geometry where the light was emitted on all sides of the sample. The light was collected over a solid angle of 3π for this type of mirror when the tip of the needle was located at the focal point of the mirror. But with this optical component it was not possible to image as the ray construction on figure 4.11 illustrates.

This construction is based on the equation 4.3 of the ellipsoidal profile and the law of conservation of the angle in a pure reflection.

$$\frac{x^2}{a^2} + \frac{y^2}{b^2} = 1 \qquad (4.3)$$

$$\text{where } a = \frac{s+s'}{2} \text{ and } b = \sqrt{ss'}$$

The image of the object primary focal point is the secondary focal point. This is determined using two different rays (black rays). The intersection of the two rays starting from the object point gives the position of the image point. The construction of the images of two other points (red and blue rays) demonstrates the impossibility to image with such a device. An ellipsoidal mirror can only be used to collect light, not to image and hence was rejected for our purpose.

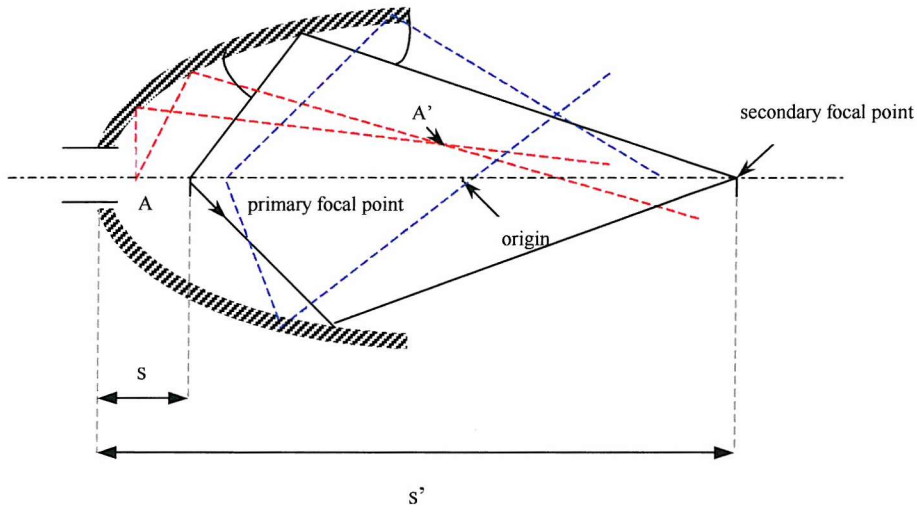

Figure 4.11: Ellipsoidal mirror, ray construction

■ The transmittance of the gold layer, for the thickness we used, had been estimated using a theoretical case illustrated in appendix B.

Published values for the refractive index of gold were used [112]. The transmittance was calculated for different wavelengths and it is shown next page in figure 4.12.

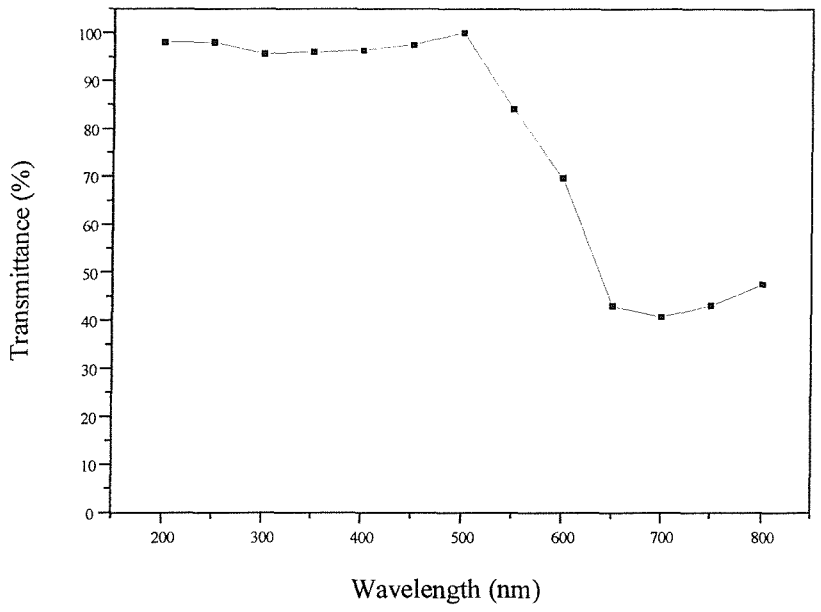

Figure 4.12: Transmittance of gold layer for thickness range 25-50nm

The calculated transmittance considering the optical properties of bulk gold predicted more absorption in the red region of the spectrum between 650nm and 800nm so a correction should be applied to take this into account. However, in the case of EL experiments, light is emitted in the region limited by two layers so that multiple internal reflections between the two layers may produce a different apparent transmission spectrum. The correction that should be applied to take into account the optical absorption of the metallic electrodes cannot be done directly. Laurent *et al* have compared the photoluminescence spectrum of a given polymer with and without metalisation on both sides of the film [75] and little distortion was observed. It turned out that the correction was much less important than expected from transmittance measurements. The use of the transmittance-based correction led to an overestimate of the light in the red part of the spectrum. In the spectral analysis results presented in this thesis no correction for the gold layer was applied to the spectra.

■ The wavelength distribution of the light emission was analysed using a set of interference optical filters to obtain an estimate of the spectrum of the light emitted. In order to do that, a filter unit was fixed inside the Faraday cubicle in front of the CCD detector (see figure 4.13). It was driven from the camera electronics module. The filter unit accommodated a rotating filter wheel holding up to 6 x 50.8mm square standard

sized filters. It allowed the filters to be selected under computer control and to be inserted into the optical path between the collecting lens and the CCD camera chip.

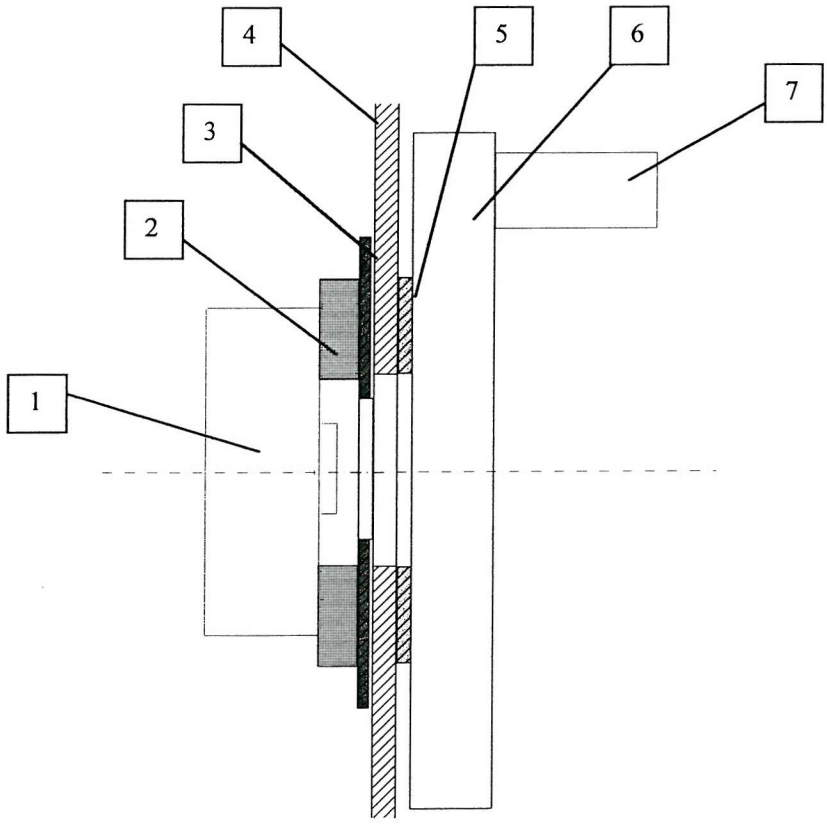

1 CCD camera head
2 Insulation plaque
3 Metal plate
4 Faraday cubicle
5 Flange
6 Filter Unit
7 Filter Unit Motor

Figure 4.13: Diagram of the filter unit fixing

Spectra were measured by using seven bandpass interference filters. These transmitted light only within a defined spectral band. Table 4.1 gives information on the filters used to cover the entire range of EL emission.

Centre Wavelength (nm)	Bandwidth (nm)	Peak Transmission (%)
365	10.7	37
450	40	67
500	40	72
550	40	79
600	40	76
650	40	76
700	40	80

Table 4.1: Bandpass filters specifications

4.3 EL detection experimental arrangement set-up

4.3.1 Detection system performance

The overall sensitivity of the EL detection arrangement depends on the quantum efficiency and the noise level of the CCD detector (see paragraph 4.2.2), the light collection efficiency of the optical system and the transmittance of all the optical components of the measuring system.

Both quantum efficiency and transmittance are wavelength-dependent as shown in section 4.2. All the optical component materials (lens, chamber window) have a flat response in the domain 300nm-900nm with a value of transmittance around 90% (see figure 4.10). The quantum efficiency of the CCD detector falls below 20% above 900nm and below 350nm (see figure 4.5). Hence light will only be efficiently detected within this wavelength range. The spectral range of the light detection system is shown in figure 4.14 where the optical components' absorption and quantum efficiency have been combined and plotted against wavelength.

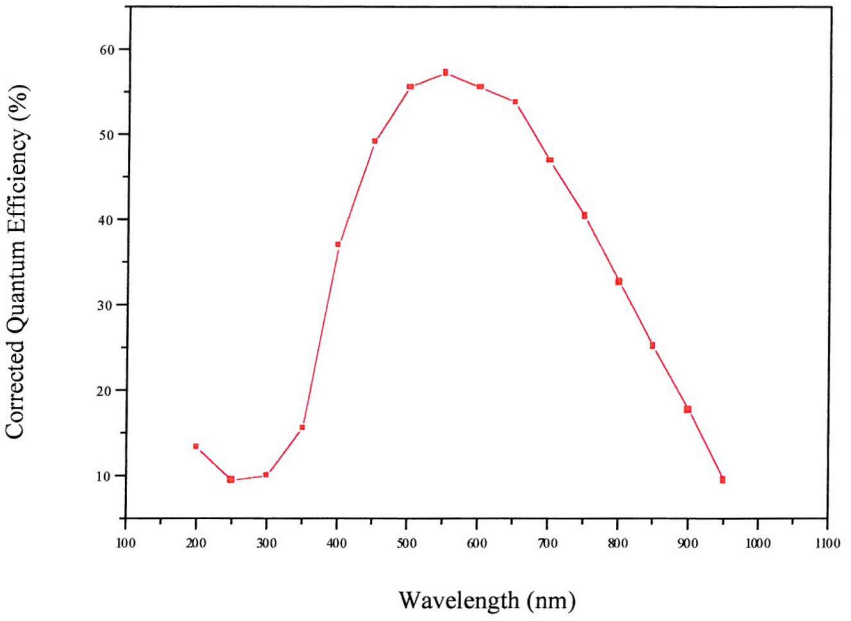

Figure 4.14: Spectral sensitivity of the light detection system

The optical collection efficiency was calculated as follows. It is given by the ratio of the solid angle of the lens aperture to 4π when light is emitted in all directions. In our experimental design, a ring electrode was used to detect the light directly through the gold layer and a plane electrode was used in order to avoid light emission in the other direction. Hence the light collection efficiency was the ratio of the solid angle of the lens aperture to 2π.

The solid angle is given by the formula:

$$d\Omega = \frac{dS}{r^2} \Rightarrow \Omega = \iint_R \frac{dS}{r^2} \tag{4.5}$$

where Ω is the solid angle, r is the radius from the focus to the area element dS, and the domain of integration R is the radius of the lens.

In the case described in figure 4.15 the expression of Ω is given by formula 4.6 where f is the focal length of the lens (in our case: R = f =50.8mm) and α is the angle of light accepted by the lens:

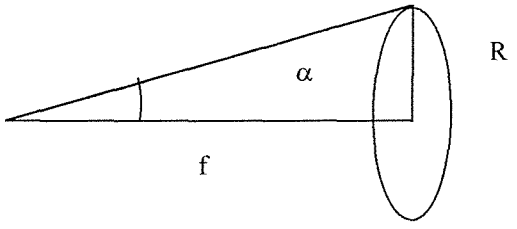

Figure 4.15: Solid angle calculation

$$\Rightarrow \Omega = 2\pi(1-\cos\alpha) = 2\pi(1-\frac{f}{\sqrt{R^2+f^2}}) \qquad (4.6)$$

This calculation gives a value of 10%. Assuming that the emitted photons have a wavelength of 550nm (at the peak of the curve figure 4.14) the overall detection efficiency is 5.7%. This corresponds to one photon being detected for 18 photons emitted.

4.3.2 CCD readout set-up

Thanks to its two dimensional array the CCD detector has been used to allow (i) the imaging of the light emitted, as well as permitting (ii) the detection and measurement of the integral light intensity versus time. CCDs are integrated circuits (see section 4.2.2.1) which contain potential wells which can be moved around the CCD by suitably varying the potential of clock electrodes on the surface of the device. When they are moved, the potential wells carry with them any electronic charge collected as a result of light falling on the device. The total active area of the CCD chip (512 horizontal x 411 vertical) was used as image area. The signal gain of camera electronics had been set-up to the maximal value of 4 which corresponds to 2.5 e^- per count. Hence a signal of 100 counts means 250 e^- being generated. Assuming the incident photons wavelength is 550nm then 355 photons would have to be detected by the CCD sensor in order to obtain 100 counts.

(i) In order to read it, the image was shifted down by one row so the charge in the bottom row fell into the output register. The time taken for the 411 vertical transfer was 411 x 16 μsec = 6.6 msec. Following that the output register was shifted one pixel to the left and read from the output amplifier. This was repeated for the whole row, taking 512 x 5.4 μsec = 2.8 msec, and then the next row was shifted into the output register. This process was repeated until the entire device had been read out.

(ii) The CCD chip was read out as one single point which was repeated as many times as had been requested in order to obtain a plot of signal against time (1D data scan compared to imaging). This was obtained by cumulating the whole of the charge using a 'binning' function in the area defined to produce a single point. To read the whole image area as one pixel the image area was shifted down by 512 rows so that the charge from each column was accumulated into the output register, then the output register was shifted of 512 pixels and all the charge was accumulated in the output amplifier from where it was read as a single pixel.

4.3.3 Analysis of noise

4.3.3.1 Noise Sources

The main sources of noise in the experimental arrangement are detailed below.

■ Photonic noise

This noise is a consequence of the quantum nature of light, which gives rise to shot noise (statistical fluctuation). Photonic noise constitutes the major source of noise at low illumination levels.

■ Dark current level

This noise is generated in the CCD chip silicon by thermal agitations which energise some electrons into the conduction band. These electrons are trapped in the potential

wells and assimilated with the signal. This thermal charge is proportional to time and is a strong function of temperature; the dark signal doubles for every 8 to 10°C rise in temperature above –25°C. Our CCD sensor operates at 200K and the MPP (multi-phase pinning) architecture of the CCD used ensured an extremely low dark current level of $4.5x10^{-3}$ e^-/pixel/second.

■ Readout noise

This noise originates in the transistors in the CCD output amplifier during readout. It is present on each signal value produced by the CCD camera and is independent of exposure length. It has a Gaussian distribution with a standard deviation which can be specified as equivalent to a certain number of signal electrons. For our detector the readout noise amounts to 7.8 electrons RMS for the low speed setting.

■ Fixed electronic noise

This refers to the temperature and illumination as well as time independent noise contributions such as spurious clock transients and due to charge transfer in our detector. 0.05 electrons per pixel are generated in the output register due to charge shift.

■ Cosmic ray

Cosmic ray muons incident on the CCD will produce detectable signals. Cosmic ray muons occur at a rate of about 2/minutes/cm^2. Cosmic ray will typically show as spikes in a scan. To correct this an option in the AT1 software can be selected, when each point is collected twice and the lesser value is used.

■ Interference

Another source of noise within the system is interference from external signal sources. This can take many forms and enter the system at any stage. In order to protect the detection system from external noise the whole experimental arrangement was inside a Faraday and light tight cubicle and all the ac signals through the box were filtered.

Careful design of the experimental arrangement as explained in paragraph 4.2 had removed a great deal of interference.

Noise sources and strategies used to reduce them include:

- mechanical vibration: with a Peltier camera the cooling fan can affect associated equipment by vibration. However the vibration amplitude is very much less than 20 microns and so will not affect the camera directly and, as the camera head is fixed on a plastic plaque, will not affect the rest of the equipment.

- ambient light: this level was reduced by the light tight box but the CCD detector being so sensitive low leakage cannot be excluded completely.

- earth loops: in order to eliminate earth loop interference produced by improper electrical grounding of the test system, a proper one point grounding was connected to the Faraday cubicle, and the camera head was insulated from the system with a plastic plaque (see figure 4.13).

- layout: leads were kept as short as possible to avoid interference.

- interference due to the application of high ac voltage such as discharges (sharp edges on electrodes or poor electrical contact) was eliminated.

4.3.3.2 Measurement of noise level on data

An estimate of the CCD noise level on 1D scan measurement was important in order to separate the noise from the signal. In spectral analyses, it was also important to apply corrections for filter transmittance and detector QE to the signal and not to the noise which had to be subtracted from the reading.

Figure 4.16 shows a schematic of the decomposition of the signal and indicates how to access experimentally the value of the different parts of the signal.

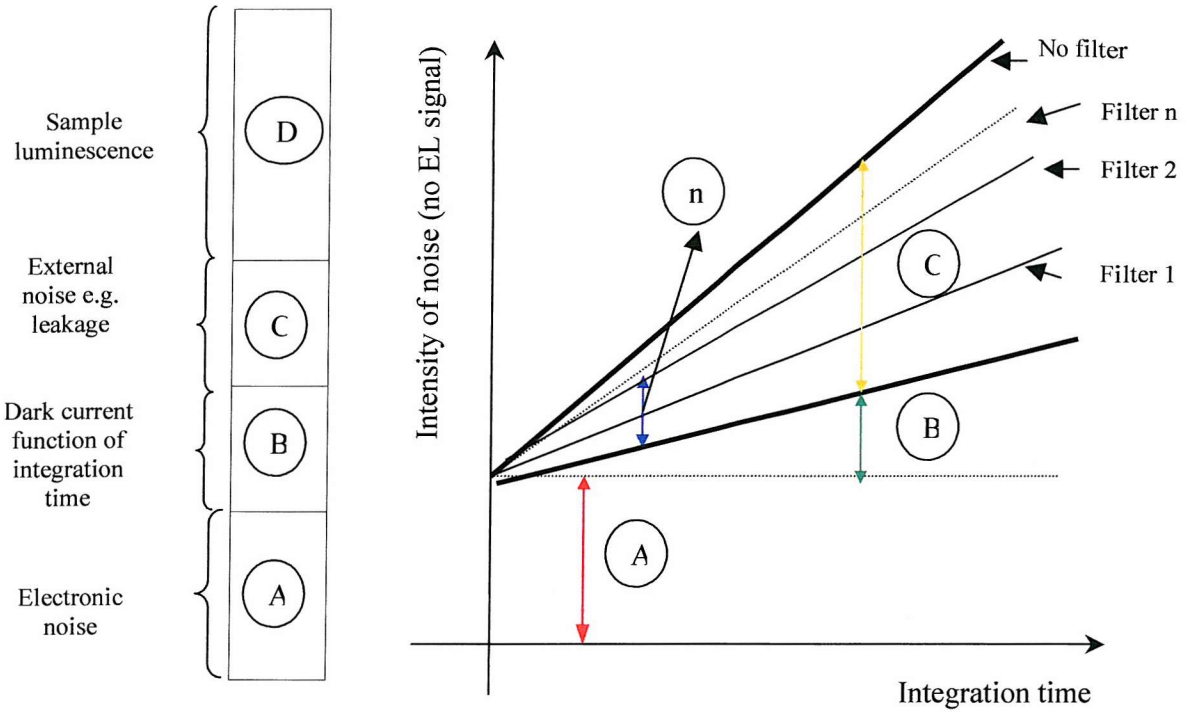

Figure 4.16: Decomposition of the CCD camera signal

In order to decompose the camera signal, five different integration times were selected: 0.1, 1, 5, 10, 15 second. For each integration time, the noise level (without high voltage application) detected by the CCD detector during 1D scan was measured in different conditions.

- the evaluation of (B) was obtained by fixing a light tight cap in front of the CCD chip and by subtracting (A)..

- (C) was the signal obtained without putting any filter in the filter unit in front of the CCD detector (and by subtracting (A)) and corresponded to the light leakage of the Faraday cubicle.

- (n) the noise with each filter: 365, 450, 500, 550, 600, 650, 700nm.

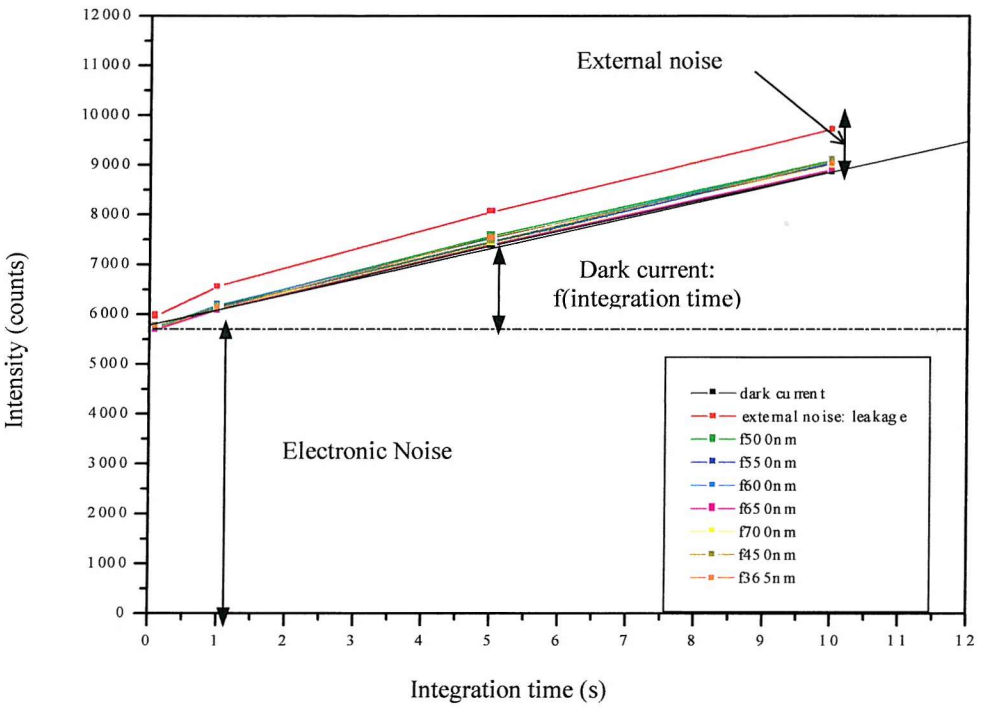

Linear Regression for data with cap:

Y = A + B * X

Parameter	Value	sd
A	5783.64796	30.35585
B	307.83795	3.62299

R = 0.99979 SD = 45.47803

Figure 4.17: Experimental evaluation of the noise level

A linear regression on the data obtained with a light tight cap in front of the chip gave an estimate of the electronic noise (A=5783.6 counts) which is independent of the exposure length.

For 10s integration time the value of the noise was 8884.4 counts. This level subtracted from the electronic noise gave a total of 3101 counts for 10s.

Hence the dark current was:

$$\Rightarrow \frac{3101}{(512x411)x10} = 1.5.10^{-3} \text{ count/pixel/s} \Rightarrow \sim 4.10^{-3} \text{ e}^{-}\text{/pixel/s.}$$

The corrections for filter transmittance and detector QE which must be made on spectra must therefore only be applied on (D) and (C) of the figure 4.16.

4.3.4 Impregnation time of polymer sample in the chamber

Some measurements were carried out at atmospheric pressure while others were performed under N_2 pressure, when the chamber was first evacuated to a rough vacuum of about 10^{-3} Torr and then pressurised with 1 bar high purity nitrogen gas. Nitrogen was selected because of its low electron affinity and its high chemical stability. It did not therefore interfere with the EL processes as compared to Sulfur Hexafluoride, SF_6 (see Chapter 3 section 3.4.2), currently used in many high voltage applications.

Another option for the study of EL processes due to the polymer itself would have been to work under secondary vacuum. However it has been shown recently that unlike the tests in pressurised gas which always result in a light emission from inside the specimen, the tests in vacuum can lead to light emission from the specimen surface. Electrons are emitted from the metallic electrodes into the high vacuum and they can achieve mean free paths of several meters and gain high energies from the electric field. High energy electrons can bombard the surface of the sample and cause luminescence or secondary electron emission. They can also bombard the metallic electrodes or the walls of the chamber to produce UV or X-ray emission that can produce photoluminescence on the surface of the sample [37].

Between the pressurisation and the beginning of each experiment, a settling time, as the following calculation shows, was required in order to ensure that the thermodynamic equilibrium of the polymer-gas mixture was reached.

The calculation of the time depends on the thickness of the sample d, and the diffusion constant D of nitrogen gas in polyethylene.

For a plane sheet geometry a solution of Fick's 2nd law of diffusion (see appendix A) is given by:

$$\frac{M(t)}{M(\infty)} \cong \frac{4}{d}\sqrt{\frac{D.t}{\pi}} \qquad (4.7)$$

where M(t) is the total amount of diffusing substance at a time t, d the thickness of the plaque, D the diffusion coefficient,

at equilibrium :

$$\Rightarrow \qquad t = \frac{\pi.d^2}{16.D} \qquad (4.8)$$

Taking $D_{N2} = 5.16 \times 10^{-7}\ cm^2 s^{-1}$ in PE of density 0.923 [50] and d =180μm then a settling time of 124 seconds is required for thermodynamic equilibrium.

In all the experiments carried out under nitrogen pressure, after the filling with nitrogen gas a period of 10 minutes was allowed before commencing an experiment.

Chapter 5

Electroluminescence measurements: results and discussion

5.1 Introduction

Experiments were carried out using the Electroluminescence experimental arrangement described in Chapter 4 in a uniform field electrode configuration under ac voltage. Initially samples were prepared from commercially available LDPE films in order to obtain a benchmark against which to compare future experiments. Samples from production cables were prepared by microtoming using a peeling technique. EL measurements were carried out on these, the bulk of the results being classified into three different sections according to the nature of the experiment: first the imaging of the light emission, then the measurement and monitoring of the integral light intensity, finally the spectral analysis of the light emission.

5.2 Sample preparation

5.2.1 LDPE films

In order to set-up the CCD detector (image capture, display and data processing), the entire detection system and to assess the influence of experimental parameters on EL measurements, some experiments were performed on additive-free commercial LDPE films supplied by Goodfellow Ltd. This was carried out to remove the possible complicated effects of additives present in XLPE cable insulation on EL measurements. The LDPE results were used as a reference for the analysis on cables and were also compared to the ones obtained in the literature. Films of 120 μm thickness were used in the experiments following.

5.2.2 XLPE production cable insulation samples

5.2.2.1 Description of cable samples

All experiments on production cable insulation were performed on extruded XLPE cables studied in chapter 2. They were rated for system voltages of: 110kV and 400kV. They were all degassed (see chapter 2 section 2.5), which was carried out as a normal part of the manufacturing process to remove mobile by-products of the crosslinking reaction from the insulation.

One of the 400 kV cable lengths was energised prior to the EL measurements and presented elongated halo micro-defects while the other was manufactured in the same year as the former but was not energised and presented 'ordinary' halo micro-features (see chapter 2 section 2.7).

5.2.2.2 Description of the microtoming technique

XLPE films were extracted from cable samples by using an uncoiling technique. Degassed cable samples were cut into 70mm long cable sections. Prior to peeling, the conductor and the semi-conducting screens were removed from the cable samples. The

cable section was peeled to form a continuous length of tape. This was done in a lathe using a sharp cutting blade of high quality tool steel originally made for use in a conventional plane. The cutting blade was prepared in several steps and ending with diamond paste to minimise cutting marks on the film surface.

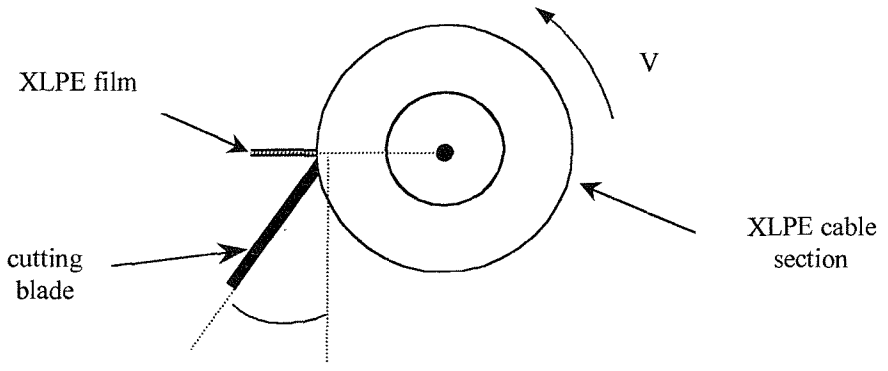

Figure 5.1: Microtoming of XLPE insulation

The cutting speed had to be adjusted to obtain the thickness of film wanted. This technique has allowed a thickness range between 100 and 200μm ± 5 %. In order to obtain good results for comparison in EL measurements, all films were cut with the same blade to ensure a similar surface roughness.

5.2.2.3 Surface roughness measurement

An estimation of the surface roughness obtained by the peeling technique was obtained using a stylus based surface measurement system (see appendix C).

There are several definitions of surface roughness. R_a is the most used international parameter of roughness. It is the arithmetic mean of the absolute departures of the roughness profile from the mean line (see figure 5.2).

$$R_a = \frac{1}{L_r}\int_0^{L_r} |z(x)|dx$$

where L_r is the sampling length.

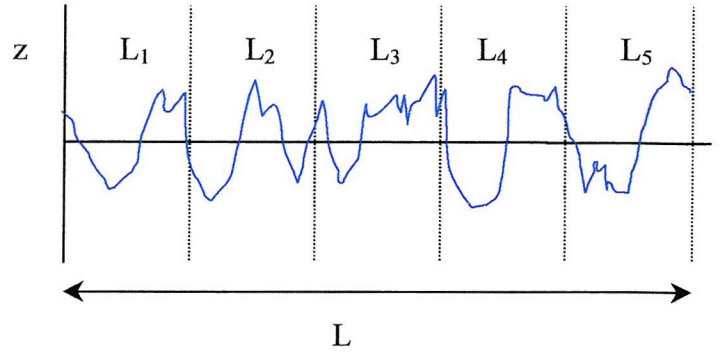

Figure 5.2: Surface roughness profile

L_1-L_5 are consecutive and equal sampling lengths. The assessment length L is defined as the length of profile used for measurement of surface roughness (containing several sampling lengths; usually five consecutive sampling lengths are taken as standard).

Inside an area of 10 mm^2 of XLPE film, ten parallel 2D scans of 2mm length were taken (see figure 5.3).

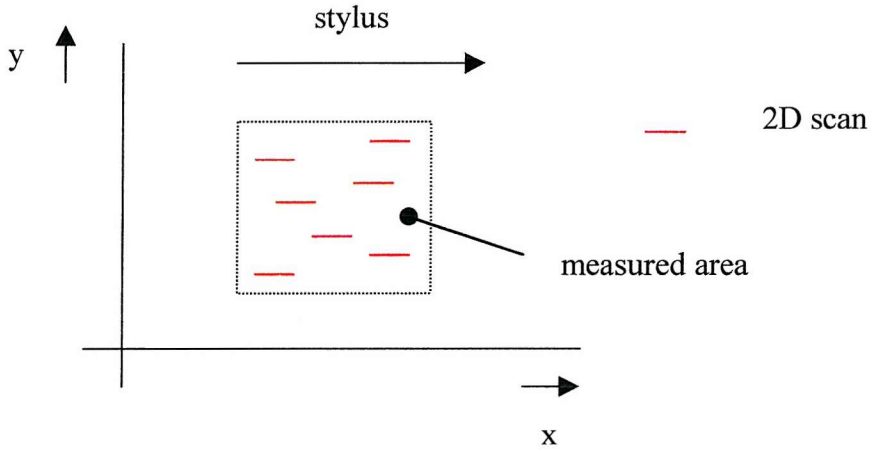

Figure 5.3: Measurements

Both surfaces of a peeled film had different surface roughness, one side being rougher than the other. A mean value of Ra was found for both sides of the film:
Ra=1.16 ± 0.05 μm and Ra=0.84 ± 0.08 μm respectively.

In order to obtain good results for comparison in EL measurements, all films were cut with the same blade to ensure a similar surface roughness and the rougher surface, once sputtered, was always used as HV electrode.

5.2.3 Sample preparation procedure

5.2.3.1 Sample arrangement

On both surfaces of each film, semi-transparent gold electrodes were deposited in a vacuum by a sputtering method using an Edwards Sputter Coater S150B.

The diameter of the gold layer was 38 mm and its thickness varied between 30 to 90nm. The first set of experiments corresponding to the imaging of EL was carried out with a relatively thick layer to ensure a good electrical contact and a good homogeneity of the gold deposition over the whole surface. Later on the thickness was reduced to 40 and then 30nm.

However, the polymer films used for comparison in the following experiments were of the same surface roughness, of the same thickness (170 ± 10μm for XLPE cable insulation samples and 120 ± 10μm for LDPE films) and of the same sputtered gold layer thickness.

5.2.3.2 Mapping of the halo region

A mapping of the halo region (figure 5.4) was made for each cable insulation studied given the characterisation carried out and presented in chapter 2. Small holes were drilled using a flat bottom drill through the insulation at the depths plotted on the diagrams. This allowed the radial position on the insulation to be determined, and hence to cut films in the clean region (near the semiconducting screens) as well as in the halo region where there was a high concentration of micro-features. For 400kV tested cable insulation, films were cut in the denser part of the halo region where the micro-features were elongated (see chapter 2 section 2.4). The figure next page represents cross sections of cable insulation (semicon layers in black), with dimensions in mm.

■ 110kV XLPE cable insulation

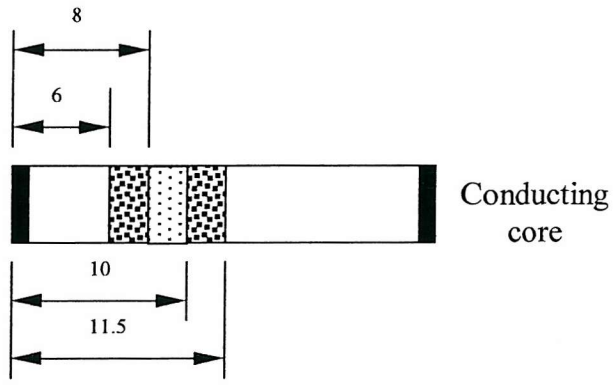

■ 400kV XLPE cable insulation tested

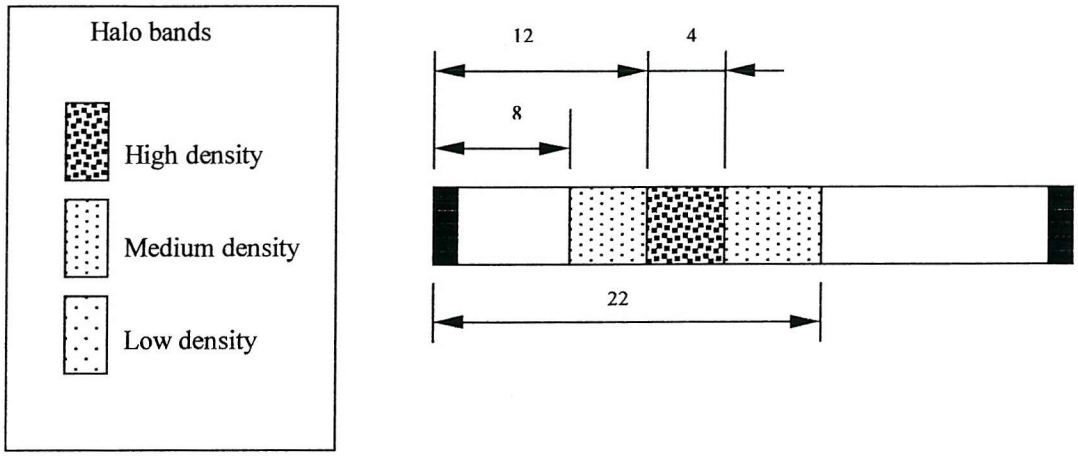

■ 400kV XLPE cable insulation untested

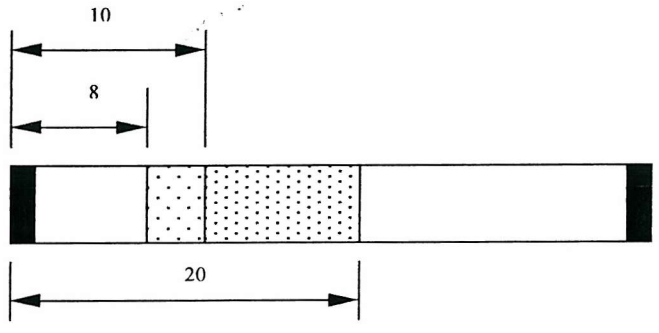

Figure 5.4: Mapping of the halo region

5.3 Imaging of the light emission

In order to ensure that the light emission when an ac voltage was applied came from the centre of the sample and not from the periphery (discharges at the edge of the gold electrodes) or from other sources of the experimental arrangement (high voltage interference such as corona discharges at any sharp points and edges within the high voltage system), some series of images were obtained at relatively low magnification.

5.3.1 Experimental procedure

Imaging of the emitting area was carried out by using the CCD detector as an imaging tool using its two dimensional CCD array. The light was collected along a direction perpendicular to the plane of the sample film. The optical coupling produced an image of the sample directly on the 512 x 411 pixels, each having a size of 19 x 19 μm^2. A square window was also attached at the front of the sample cell as a supplement to the plastic cover to ensure that any possible light coming from the edges did not perturb the measurement. Therefore the size of the emitting area was equal to the size of the observation window: 10 x 10 mm^2. The optical magnification for this set of experiments was 0.25. Taking into account the magnification factor due to the optical system, the spatial resolution was approximately 75 μm per pixel.

A long integration time was needed for imaging such a low level of light. The integration time was 10 minutes for all images presented in this section and all the images have been saved with the same level of black and white or look-up-table (LUT) level in order to allow comparison of light intensity. The LUT controlled the conversion between data values stored in the display board and displayed intensities, and gave a grey scale output intensity which ramped from black to white between two stored image data values.

Some measurements were carried out in air at atmospheric pressure while the other were performed under N_2 pressure, when the chamber was first evacuated to a rough vacuum and then pressurised with high purity nitrogen gas (see chapter 4 section 4.3.4).

5.3.2 Results and Discussion

Figure 5.5 shows the light emission from the same LDPE film for different applied ac fields in air at atmospheric pressure.

■ As the window size was 10 mm, which was about one quarter of the horizontal total image length, only the central part of the images was lit. It confirmed that the optical system and the arrangement of the plastic holder and the edges covered by silicone rubber allowed the detection of the light emitted from the centre of the sample only. When the observable area of light emission was masked, no light emission was detected in the range of voltages applied in the experiments. Therefore the emission came only from the sample and was not due to an artefact of the rig.

■ Some bright points which affect only one or a few pixels, appeared in these pictures. They were due to the excitation of the CCD by cosmic rays (see chapter 4 section 4.3.3). The lower the light emission, the longer the integration time for recording one image, and the higher was the probability of having stray signals from cosmic rays.

■ The light emission started at a threshold voltage of 2kV. Below this voltage, only the noise of the CCD detector was imaged which corresponded to white and black pixels randomly distributed. Above this voltage, the intensity increased with the applied voltage/field. The fact that the light was field dependent indicated that the polymer was involved in the light emission.

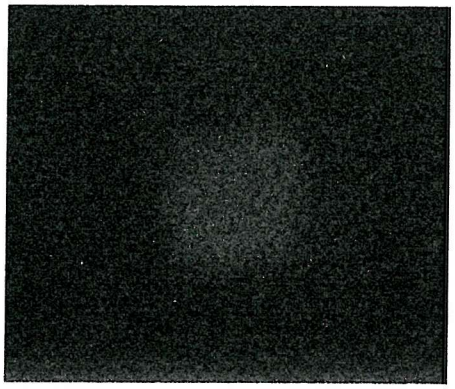

(1)

Increasing Voltage

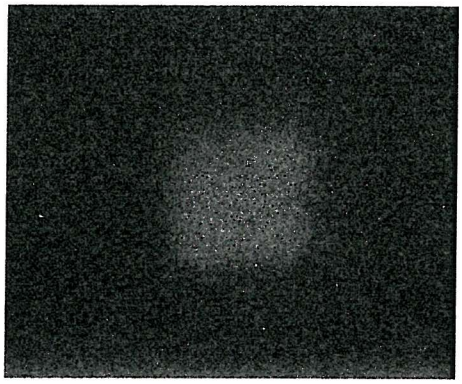

(2)

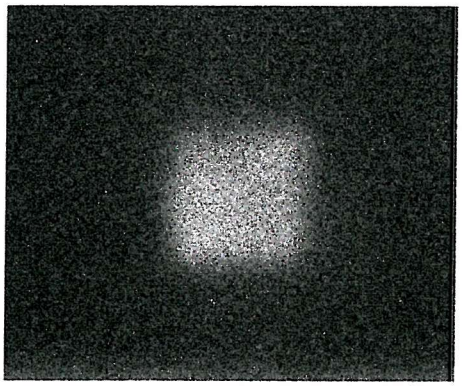

(3)

Figure 5.5: CCD images (same LUT level) in air at atmospheric pressure.
Applied ac field: (1) 20kV/mm, (2) 40.9kV/mm, (3) 52.4kV/mm

Figure 5.6 shows the light emission from another LDPE film for different applied ac fields under nitrogen conditions.

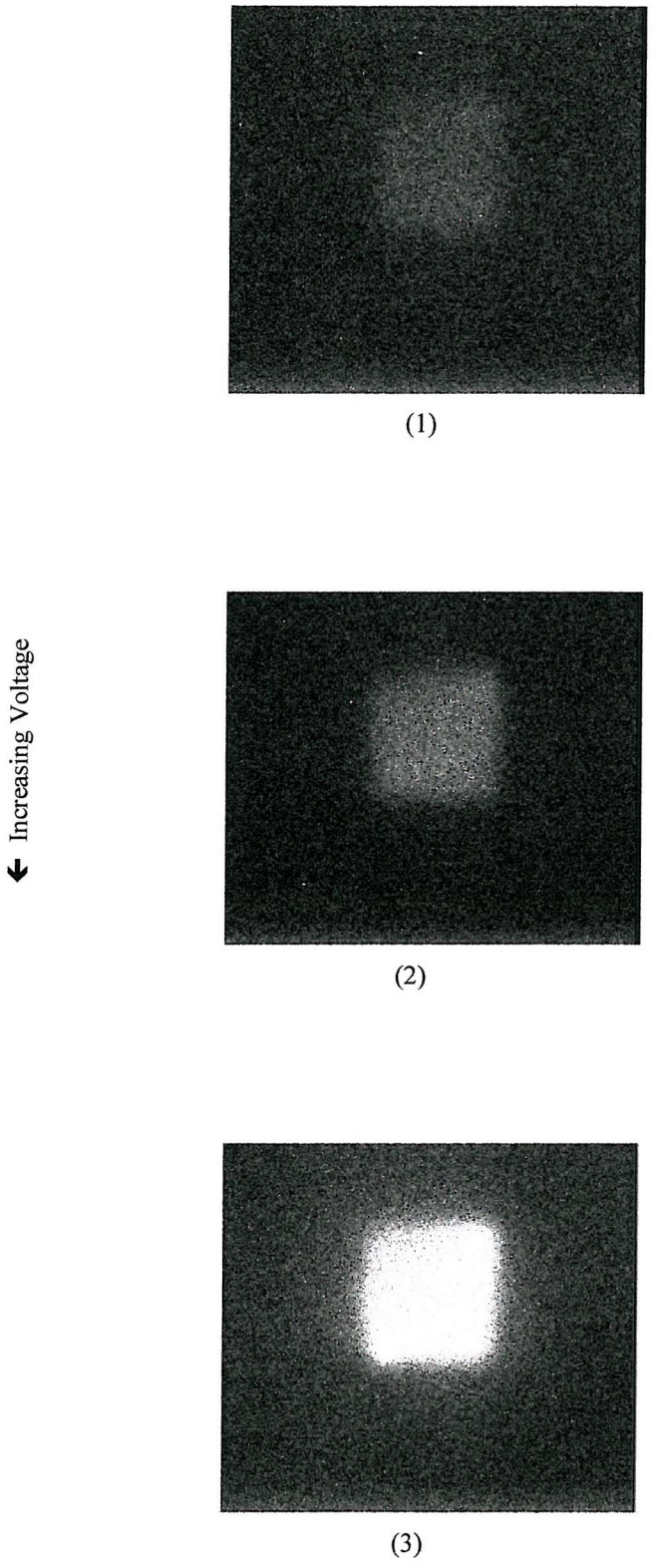

Figure 5.6: CCD images (same LUT level) under nitrogen pressure.
Applied ac field: (1)20.3kV/mm,(2) 30.4kV/mm, (3) 50.4kV/mm

■ EL intensity increased with the applied field for both experimental conditions. The intensity was significantly higher for samples under N_2 pressure than for samples in air at atmospheric pressure. LDPE films tested under atmospheric pressure were impregnated mainly with a mixture of oxygen and nitrogen. They had a higher concentration of oxygen molecules compared to the sample degassed and tested under nitrogen, and oxygen was also present at the metal/polymer interface. The reduction of the luminosity results (i) partly from the strong electron affinity of oxygen (these electronegative molecules can capture the electrons injected into the polymer and decrease the efficiency of EL), and (ii) partly from the quenching by this gas of the excited states responsible for the luminescence.

(i) $O_2 + e^- \rightarrow O_2^-$

(ii) $A^* + O_2 \rightarrow AO^{\cdot} + O^{\cdot}$ where A^* represents a molecular excited state.

Nitrogen gas, on the contrary, has a high chemical stability and does not capture electrons since it has no electron affinity so it does not interfere with the EL process. LDPE films filled with nitrogen gas behaved as though there were no gas present.

■ When looking at the whole surface (figure 5.7) by removing the square window in front of the sample cell, no erratic light due to edge effects was observed thanks to the arrangement of the plastic holder and the edges covered by silicon rubber.

The chance for the light at the edges to disturb the observation by internal reflection in the film was very small, because of the long distance involved (see sample configuration chapter 4 section 4.2.1).

The square window was an additional protection to ensure that only the light coming from the centre was detected. When carrying out experiments without covering the edges with silicon rubber, unstable light occurred due to discharges at the edges of the gold electrodes.

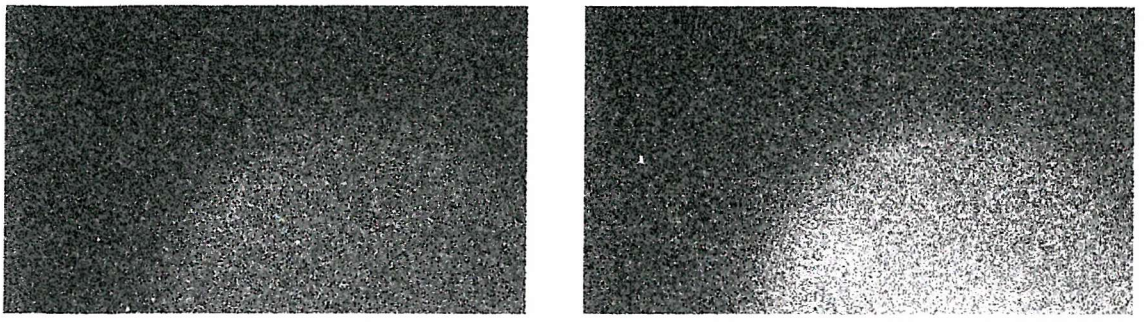

(1) (2)

Figure 5.7: CCD images on LDPE film. Applied ac field: (1) 20 kV/mm, (2) 30kV/mm

5.4 Measurements of the integral light emission

5.4.1 Experimental procedure

A 50 Hz ac voltage was applied to each sample in steps of 1kV amplitude, with 2 to 4 minutes at each step. At each voltage level, the intensity data were averaged for 0.2s (LDPE films and 110kV XLPE cable insulation) and 0.4s (400kV XLPE cable insulation). These integration times were determined by the requirement for collecting a sufficient number of photons to give a counting error of ± 5%. The CCD chip was read out as one single point which was repeated as many times as had been requested in order to obtain a plot of signal against time. This was obtained by cumulating the whole of the charge using a 'binning' function in the area defined to produce a single point (see chapter 4 section 4.3.2).

The samples used for comparison were of the same surface roughness, the same thickness and with the same thickness of sputtered gold layer. Some measurements were carried out at atmospheric pressure while the others were performed under N_2 pressure, when the chamber was first evacuated to a rough vacuum of about 10^{-3} Torr and then pressurised with 1 bar high purity nitrogen gas. Between the pressurisation and the beginning of each experiment, 10 minutes, as the calculation in chapter 4 section 4.3.4 has shown, were allowed for in order to ensure that the thermodynamic equilibrium of the polymer-gas mixture was reached.

The luminescence intensity will be presented in all the graphs in arbitrary units, which is the case for the literature when presenting light intensity data, and will correspond to the intensity of light above the CCD noise level. In chapter 4 section 4.3.2 the measurement unit of the CCD camera is explained. The CCD detector background noise level was recorded before applying the voltage and its mean value was subtracted from the value obtained with voltage applied in order to obtain the net EL. It corresponds to the sum of the electronic noise during readout, which is independent of the exposure length, the dark noise and external noise which are a function of the integration time (see chapter 4 section 4.3.3). A correction for cosmic ray removal was applied, then each point was collected twice and the lesser value was used.

5.4.2 Results and Discussion

In order to set up the detection system and to assess the influence of experimental parameters on EL measurements, some experiments were performed on additive free commercial LDPE films supplied by Goodfellow Ltd. This was carried out to remove the possible complicated effects on EL measurements of additives present in XLPE material.

Since the surface roughness of commercial LDPE films and the XLPE thin plaques used were not similar, the results obtained from each sample type were not quantitatively compared.

5.4.2.1 LDPE films

- *Behaviour of light versus voltage and time*

The 8 samples tested showed the same behaviour of light versus voltage and time (figure 5.8).

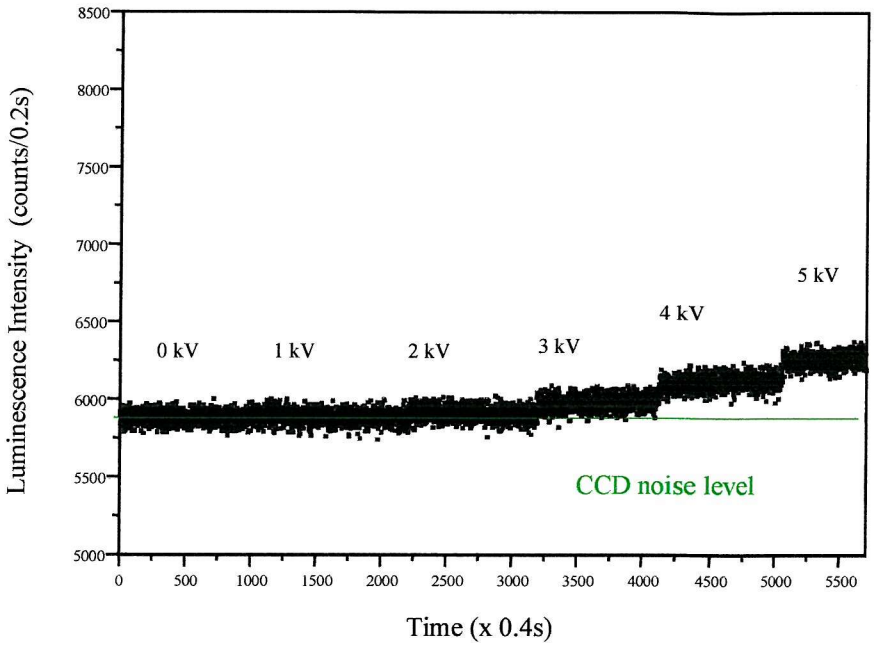

Figure 5.8: Light intensity vs ac voltage and time

■ The CCD detector noise level was recorded before applying the voltage. The level of light collected was very low and corresponded to a few counts above the noise level, less than 500 counts for an exposure time of 0.2s using a gain of 4 (see chapter 4 section 4.3.2) for a voltage of 5kV. The fluctuations in the light emission for the different stressing voltages were within the statistical error associated to the counting error of the CCD detector and therefore not significant. This error was estimated at ± 5% for the experimental parameters selected. The light was highly stable versus time under a constant voltage which is characteristic of EL emission. It does not exhibit the time instabilities of light from discharges.

■ The detectable light emission started at a threshold voltage of 2kV and then increased with the voltage. In the thesis threshold values were determined by noting the voltage for the first appearance of light emission which of course depends on the detection limit (noise level) of our measurement system.

The long-term behaviour of the light emission under a constant ac voltage is shown in figure 5.9.

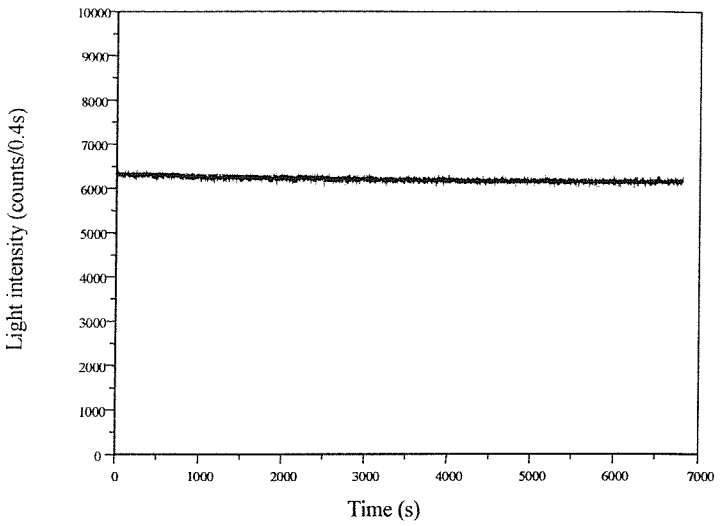

Figure 5.9: Long-term EL under a constant ac voltage of 5 kV

■ The light was highly stable versus time under a constant voltage. The level of light slightly decreased with time, this phenomenon could be explained by a decrease in luminescent centres or by quenching mechanisms occurring when their concentration reaches a critical value.

■ The characteristic of the light emitted corresponds to EL emission. As the applied field was relatively moderate (< 70kV/mm) it seems clear that EL was only due to recombination processes and not to impact processes which required a higher electric field (see chapter 3 section 3.3.3). The reported mechanism of radiative charge recombination involves trapped electrons and holes, which were injected into the sample (bulk of the polymer and/or the volume closest to the electrodes). This process was repeated with every cycle of the ac voltage and did not exhibit the high intensity and time instabilities of light from discharge activity in micro-voids which depends on the cavities' parameters such as pressure and conductivity. The increase of the voltage led to more charge being injected and hence an increase in the EL emission.

◆ *EL versus applied electric field*

The luminescence level was very low, hence the counting error of the CCD detector was the dominant error source and corresponded to an error of ± 5% on all light intensity measurements. The CCD detector background noise level (A± ∂ A) was subtracted from the value obtained with voltage applied (B± ∂ B) in order to obtain the net EL (∂ A and ∂ B are the random errors in A and B). Hence the light intensity was given by:

$$(A \pm \partial A) - (B \pm \partial B) = A - B \pm \sqrt{(\partial A)^2 + (\partial B)^2} \qquad (5.1)$$

The error bars being the same for all data points, they are plotted on only one set of data in order to obtain clearer representations.

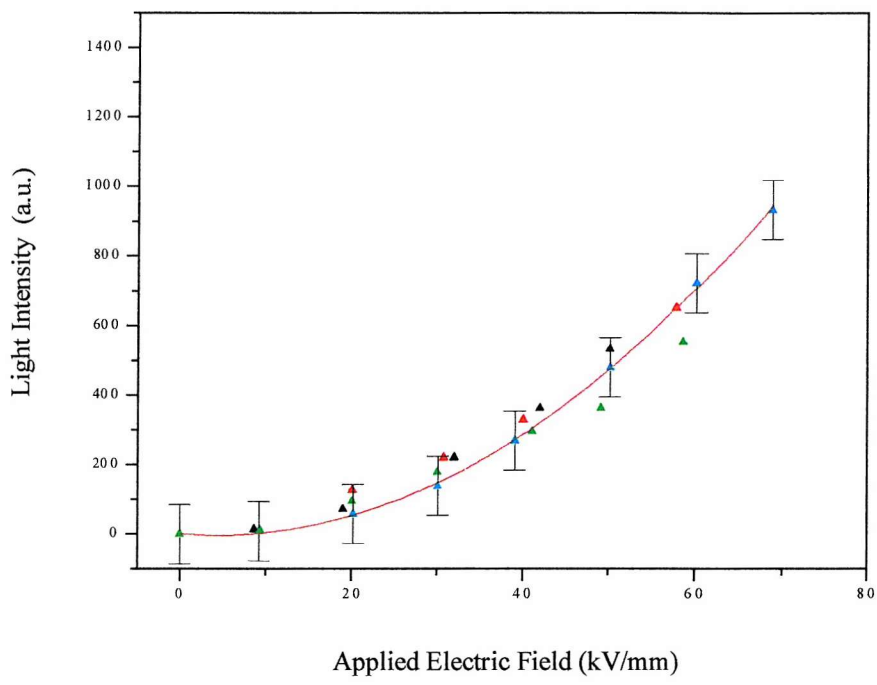

Figure 5.10: Light intensity vs electric field under N_2 pressure for four different samples

■ The light intensity from different LDPE samples of the same thickness as a function of the applied field in air at atmospheric and under nitrogen pressure is shown in Figures 5.10 and 5.11.

The light emission started at a threshold field ~8 kV/mm under nitrogen pressure and then increased with the electric stress. This value of the threshold field is comparable to the values found in the literature under high vacuum condition [11].

A better reproducibility was obtained from samples under nitrogen pressure.

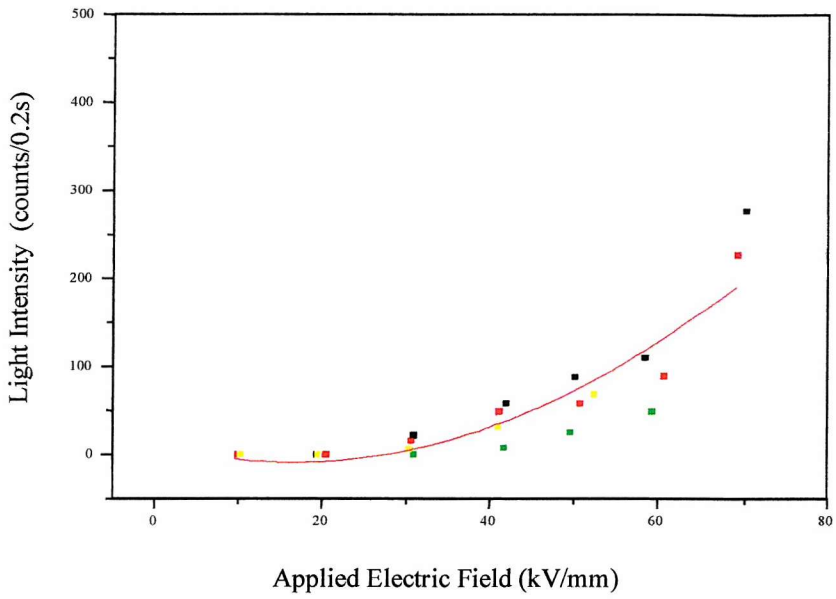

Figure 5.11: Light intensity vs electric field under air at atmospheric pressure for three different samples

■ Figure 5.12 shows the effect of oxygen on the same film and confirms what had been observed by imaging the EL emission (section 5.3.2). The effect of oxygen is to quench the excited states giving rise to less light emission and also to capture the electrons injected into the polymer which again decreases the efficiency of EL. That is why the EL inception field in air at atmospheric pressure was higher.

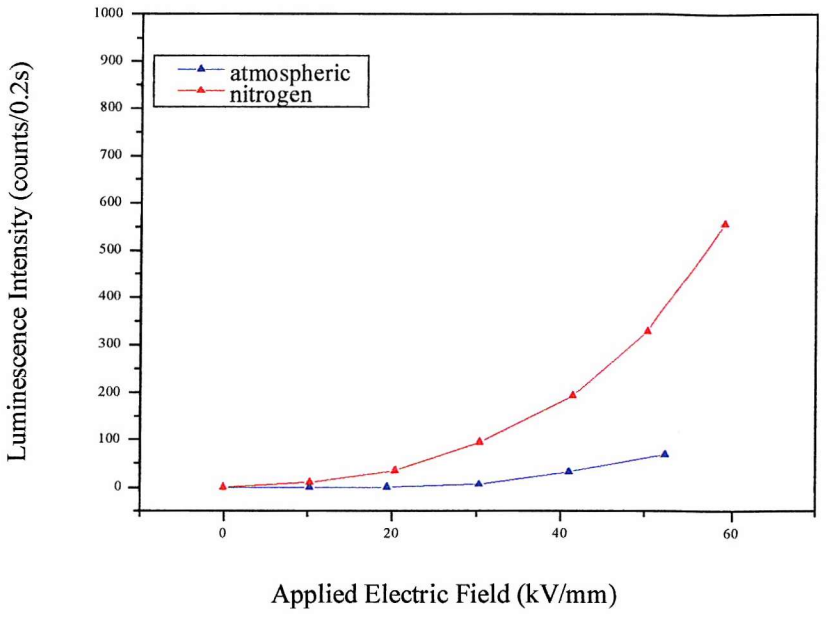

Figure 5.12: Light intensity vs electric field under atmospheric and nitrogen pressure

■ The experiment performed under atmospheric pressure on samples which were not degassed therefore gives information not just on the polymer itself but on the material-impregnated gas complex.

Because of the complicated effect of oxygen present both in the bulk of the polymer and also at the interfaces electrode/polymer, and because of the lower reproducibility obtained, it was decided to work under nitrogen pressure, the chamber being first evacuated to 10^{-3} Torr and then pressurised. The first operation was indispensable since it was important to have as little residual air as possible. Nitrogen, being a chemically inert gas of low electron affinity, does not interfere with the EL process. LDPE films filled with nitrogen gas behaved as though there were no gas present and the EL from the insulating material could be investigated more easily.

5.4.2.2 Study of production XLPE cable insulation

Several types of XLPE cable insulation were studied. This section will first present the results obtained on 110 kV cable insulation and then on the 400 kV cable insulation which was either tested or untested. For both cable rates films were microtomed in the clean region of the insulation and in the halo region where there was a high concentration of micro-features (see sample preparation paragraph 5.2.3).

5.4.2.2.1 110 kV XLPE cable insulation

- Clean region

All the films cut in the clean region presented the same behaviour of light versus voltage and time (figure 5.13): a highly stable low level of light which increased with the applied voltage. This behaviour was characteristic of EL emission.

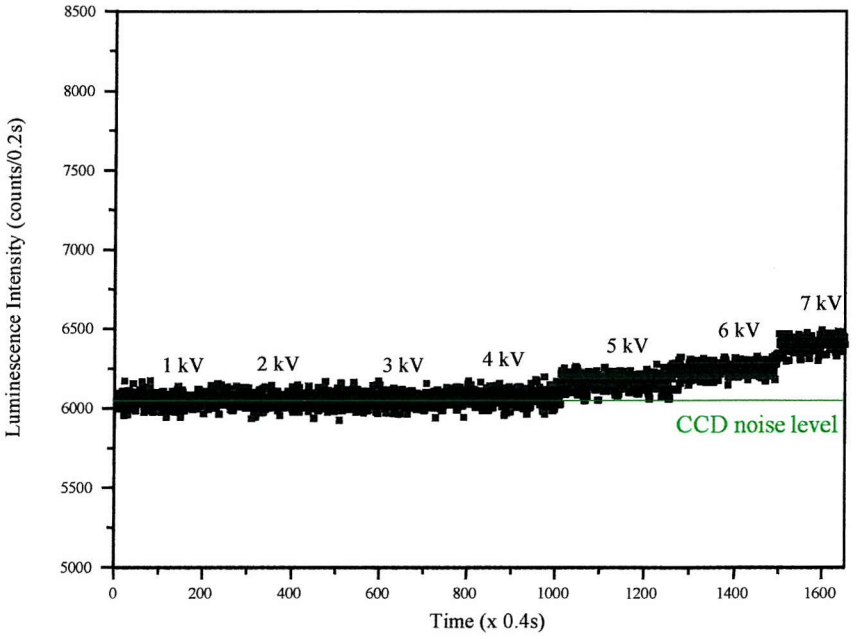

Figure 5.13: Light intensity vs voltage and time for sample in the clean region

◆ Halo region

Figures 5.14 and 5.15 show the behaviour of light for two films cut in the halo region.

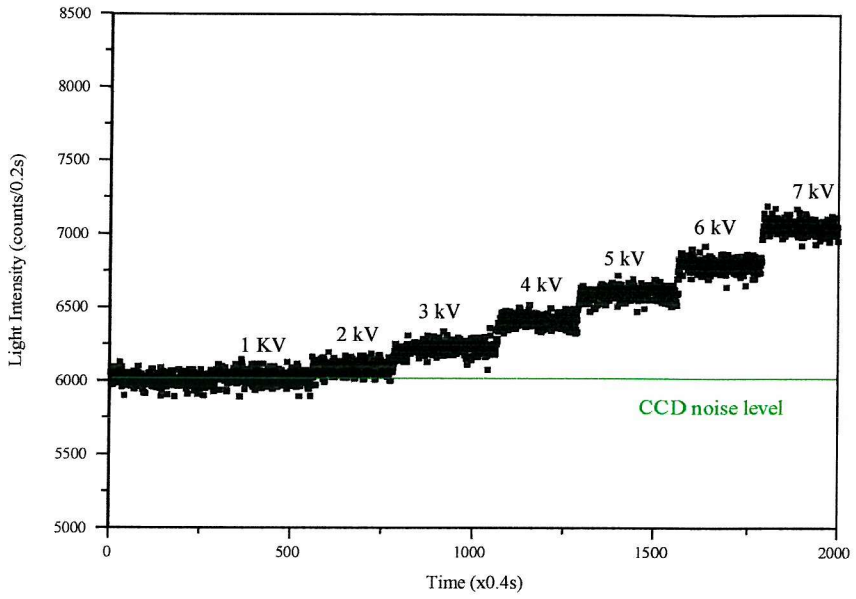

Figure 5.14: Light intensity vs voltage and time for sample in the halo region

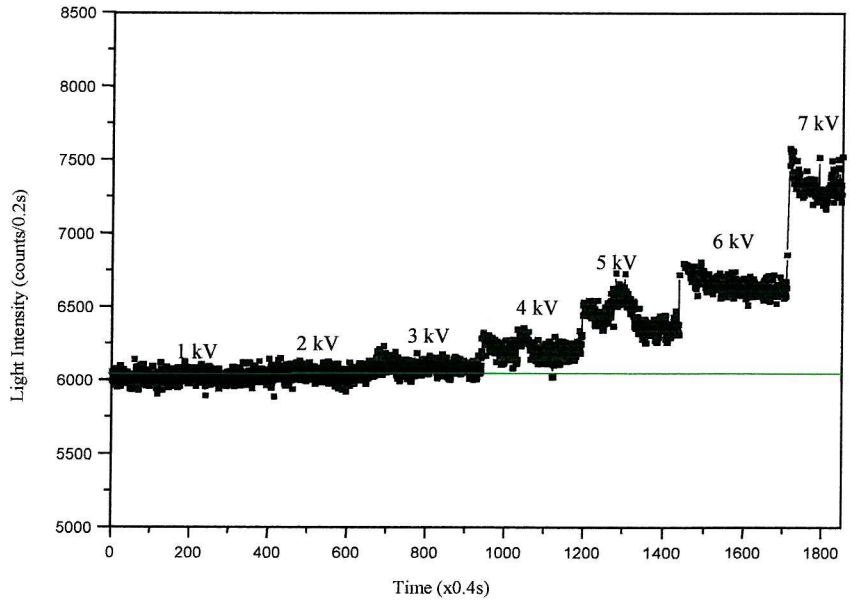

Figure 5.15: Light intensity vs voltage and time for sample in the halo region

Samples in the halo region systematically emitted more light. Some samples showed stable emission versus time at a constant voltage as in figure 5.14 while others gave a less stable scan (Figure 5.15).

■ Figure 5.16 shows a comparison of the light intensity against the applied electrical field between samples cut in the halo and in the clean region.

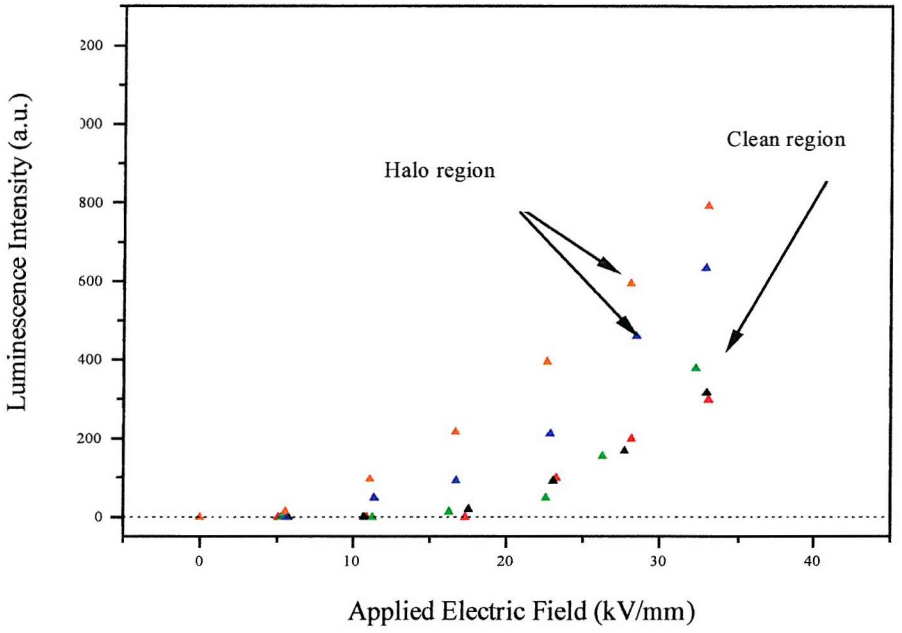

Figure 5.16: Light intensity vs electric field for five different films

The reproducibility was good for the clean region, with a larger scatter being obtained for the halo region. This would seem to indicate that the micro-features were involved in the light emission, with some films containing more micro-features than the others, due to a natural variation of the concentration of the features.

More light was emitted by the films containing micro-features. These micro-defects were likely to lead to a local field enhancement and hence more light emission. An increase in the number of interfaces due to the presence of these micro-defects may have given rise to a greater density of traps and consequently an increase in local space charge concentrations which can contribute to the EL emission (see mechanisms of EL chapter 3 paragraph 3.5).

■ Figure 5.15 shows that for this film the light emission for voltages higher than 3kV was not highly stable with time. This could be due to the beginning of another type of light emission explained later in this thesis.

5.4.2.2.2 400 kV XLPE tested cable insulation

In order to investigate further the influence of the halo micro-defects, an aged cable insulation presenting larger features (~5μm) was studied.

◆ Clean region

Figures 5.17 and 5.18 below present the characteristics of the luminescence emitted from samples microtomed in the clean region.

■ The 8 films cut in the clean region of the 400 kV tested cable insulation presented the same behaviour of light versus voltage and time, i.e. a stable low level of light which increased with the applied voltage. This was the same type of behaviour as for LDPE films and 110kV cable insulation films without micro-defects and was attributed to EL emission.

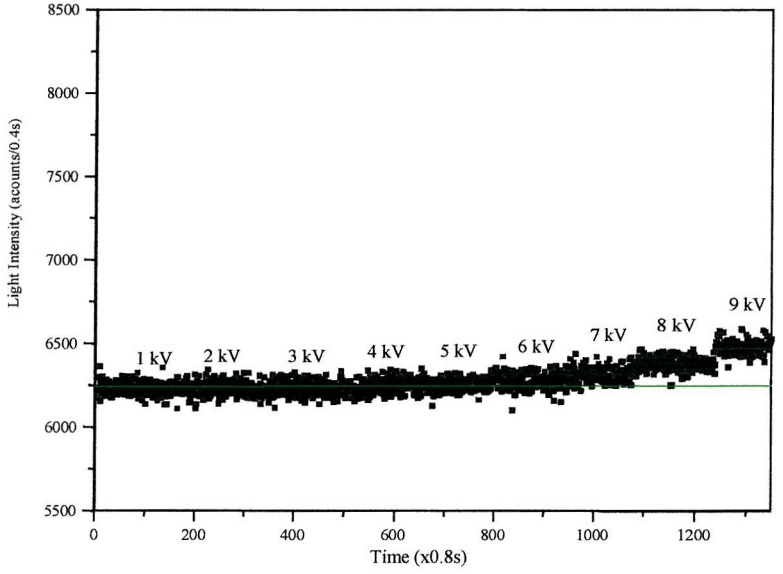

Figure 5.17: Light intensity vs voltage and time for sample in the clean region

■ A good reproducibility was obtained for films microtomed in the clean region as figure 5.18 shows.

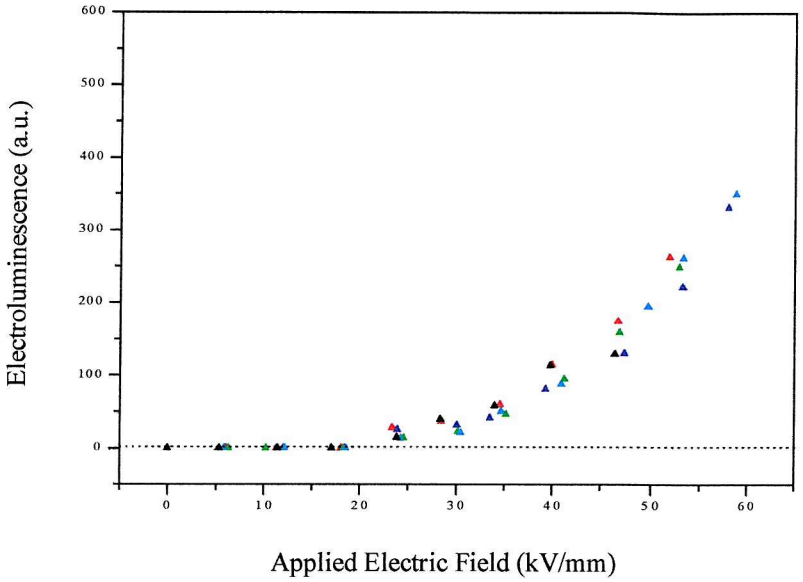

Figure 5.18: Light intensity vs electric field for five different films

◆ Halo region

For films microtomed from the halo region of the 400 kV tested cable insulation, where the micro-features were elongated in the direction of the electric field applied to the cable (see chapter 2 section 2.7), and hence in the direction of the applied field in the luminescence experiments, two different types of behaviour of the integral light emission versus voltage and time were observed when carrying out ramp test measurements.

Some samples showed stable emission versus time, which presented the characteristics attributed to EL type emission but with a higher intensity than in samples microtomed in the clean region, while the others (more numerous) showed scans which were unstable versus time. Figure 5.19 shows a typical scan obtained.

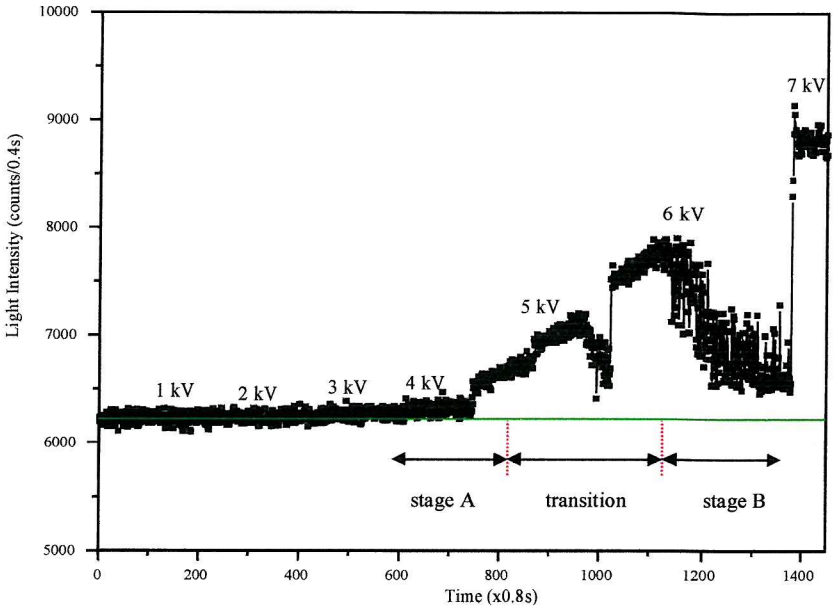

Figure 5.19: Light intensity vs voltage and time for sample in the halo region

■ Two different types of light emission responses, arbitrarily referred to as stage A and B, occurred on increasing the applied voltage:

- stage A: the light intensity was low and stable at each voltage up to 4 kV,
- transition region: the light intensity first increased at a constant voltage and then suddenly decreased sharply before the onset of stage B, the noise on the light intensity during this period was still consistent with the statistical error associated with the photon counting,
- stage B: the light emission significantly and rapidly fluctuated with time decreasing after an initial surge.

■ Our observation of two distinct types of behaviour of light emission in the time domain indicated two different types of luminescence.

The light emission at stage A was similar to EL observed in LDPE films and XLPE cable insulation samples without micro-defects. Different mechanisms can give rise to EL (see Chapter 3 section 3.3.3) hot electrons processes, excitation of the polymer molecules, or

charge carrier recombination. The latter is likely to be responsible for EL due to the magnitude of the field applied in our step-ramp stressing tests (< 70kV/mm). It is thought to be due to injection of charge into the polymer sample (bulk of the polymer and/or the volume closest to the electrodes) resulting in EL due to the radiative recombination of electrons and holes under ac voltage application.

On further increase in the field, a change in emitted light behaviour was observed. The light intensity fluctuated in time and the low level EL was rapidly swamped. This behaviour was not observed in samples without micro-defects so it is likely to be associated with the onset of micro-discharge activity from the halo micro-features present in the cable insulation sample. The onset of stage B type emission was around 5 kV or an applied field of around 30kV/mm.

Between stages A and B a transition phase was observed. Its time length and shape varied from sample to sample.

■ Spectral analysis presented in section 5.5 of this chapter showed near-UV (365nm) emission from samples where the scan was not stable with time confirming the presence of micro-discharge activity (see Chapter 3 paragraph 3.4.4).

■ The fact that some samples presented more EL and others unstable light emission could be explained as depending on whether the sample contained (initially or created during the voltage ramp-test) micro-defects of the critical size to start micro-discharge activity. The mapping of the halo region had permitted the microtoming of samples in both parts of the halo region:

- the densest part where the micro-features were elongated,
- the part were the micro-defects were of 1-1.5 microns diameter.

However, it is possible that in the densest part there still were areas where the micro-defects were small in size hence giving rise to more EL as in the halo region of virgin 110kV cable insulation (paragraph 5.4.2.2.1).

5.4.2.2.3 400 kV XLPE untested cable insulation

A few films microtomed in the clean region (without micro-defects) of this cable were analysed. The halo region, being similar to the 110 kV cable insulation's (in the size, range and shape of micro-defects) was not analysed. Figure 5.20 shows a comparison between a film microtomed in the clean region of 400kV tested cable insulation (1 year test) and a film microtomed in the untested.

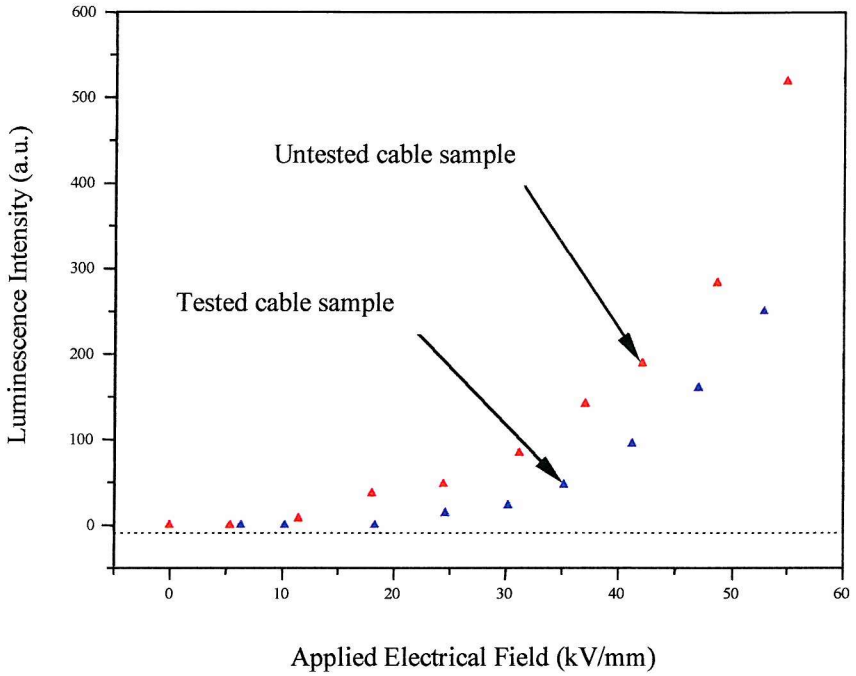

Figure 5.20: Light intensity vs electric field; comparison between tested and untested cable insulation in the clean region

EL measurement showed that slightly less light was emitted from aged samples than unaged samples for the same applied stress. This phenomenon has also been observed by other workers [101]. Ageing is likely to induce an increase in the excitation. A decrease in EL would be due to a decrease of the probability of radiative relaxation. This could be due to a disappearance of the chromophores involved in light emission or to quenching mechanisms occuring when their concentration reaches a critical value [102]. However more study would be required in order to conclude on the cause of this difference. FTIR measurements

carried out on samples microtomed from both cable insulation, aged and unaged, showed no evidence of compositional difference.

5.5 Spectral analysis of the light emission

5.5.1 Experimental procedure

The wavelength distribution of the light emission was analysed using a set of interference optical filters to obtain an estimate of the spectrum of the light emitted. Spectra were measured by using seven broad band filters (40nm bandwidth) from 365nm to 700nm. The filters were inserted in a rotating wheel which, under computer control allows each filter to be inserted into the optical path between the collecting lens and the CCD camera chip. The peak transmission of the filters varies between 37% (365nm) and 80% (700nm) (see chapter 4 section 4.2.5). In this section the samples used for comparison were of the same surface roughness, sputtered gold layer and film thickness. All measurements were performed under N_2 pressure at 1 bar, when the chamber was first evacuated to a rough vacuum of approximately 10^{-3}Torr and then pressurised with 1 bar high purity nitrogen gas.

The spectral analysis test parameters were set-up in order to collect a sufficient light intensity during a minimum integration time in order to reduce the CCD detector noise level. A suitable integration time of 10s per filter was established. The noise level for each filter being approximately identical, as the analysis of the noise has shown (see chapter 4 section 4.3.3), it was measured for two filters (600nm and 365nm) before and after the spectral analysis in order to obtain a base line. The light intensity was obtained by subtracting the level of light obtained with the application of the voltage to the noise level. For all filters, ten measurements were carried out and the mean value of the last four was taken as light intensity in order to have a stabilised value of the light level.

To ascertain that the light collected was due to EL, the total light intensity was monitored before and after the spectral analysis ensuring that the light level was stable which is the case for EL under a constant ac voltage as it has been shown in section 5.4.

The spectra are presented as bar diagrams with each bar being centred at the wavelength where the transmission is maximum. All the optical components (lens, chamber's window) have a flat response in the domain 300nm -900nm. The intensity of light at each filter was then corrected for the transmittance of the filters and quantum efficiency of the CCD detector.

5.5.2 Results and Discussion

This section will present the results obtained on additive free LDPE films followed by the results on XLPE films microtomed from production cable insulation in order to study whether the same components of the spectrum were present. The LDPE spectra will be used as a reference for the cable analysis and will also be compared to the ones obtained in the literature.

5.5.2.1 LDPE films

The field dependence of the emission is shown in figure 5.21.

An electrical field was first applied after the stable plateau was reached on the scan of the total light intensity (see section 5.4.2.1) and the spectrum was recorded. The field was then increased and a new spectrum was acquired after the total light intensity was monitored to ensure that the light level was stable.

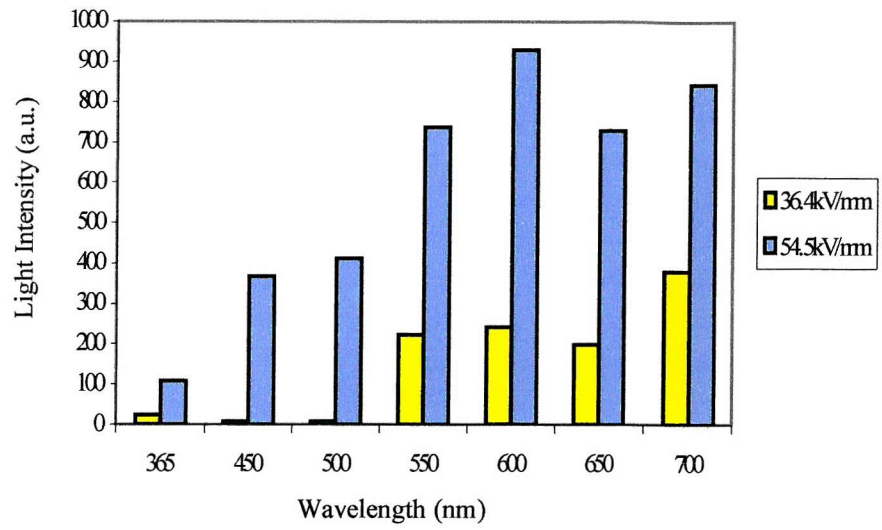

Figure 5.21: Spectra of LDPE film

■ The spectrum of light emitted from a LDPE film excited under ac voltage in an uniform field configuration showed the typical features of EL emission obtained and published by other authors for polypropylene (PP)[78], polytetrafluoroethylene (PTFE) and polyvinylchloride (PVC)[76] i.e.:

- negligible to low intensity in ranges between 365 and 500nm,
- high intensity between 550 and 650nm, peaking at 600nm,
- a second peak at 700nm.

EL in LDPE seemed dominated by phosphorescence (500-700nm) which involved triplet states which are characterised by a long life (see chapter 3 section 3.2). These triplet states may decay unimolecularly mostly by bond cleavage and rearrangements involving breaking and formation of new chemical bonds, their detection in EL is a signature of irreversible reactions [11, 25].

■ The analysis showed that the general aspect of the spectrum did not change with the applied field. The intensity of light increased with it at all wavelengths. At low field, the red component (700nm) of the spectrum was dominant which corresponded to a low emitted photon energy of 1.8 eV. As the field increased this contribution decreased in comparison to the part between 500 and 650nm which peaked at 600nm. The fact that their evolution with the field was different suggests that two different types of behaviour were involved, one between 365 and 650nm and the other in the red.

The literature assists the understanding of the phenomena. It has been shown [75] by using different metals for electrodes, that the red component of the light emission is due to a pure surface electrode effect while the rest of the spectrum is due to the EL of the polymer film. The light from the metallic electrode is due to the radiative decay of collective excitations of the electron gas of the metal so called surface plasmon (SP). SP is excited by the strong current density accompanying injection/extraction of carriers at the electrode-polymer contact. They are efficiently excited under ac stress during the charge exchange process due to polarity reversal of the voltage. They would not be excited under dc stress because the injection is space charge limited. Another possible explanation to the red component of the EL spectrum is the existence of interfacial electronic states at the metal-dielectric interface [76]. These states could be populated during charge injection, and neutralized during voltage polarity reversal, the excess energy being released by photon emission. Experiments carried out by Laurent *et al* [75] argue in favour of the SP explanation. PP films were surface grafted with acrylic acid leading to a surface layer of poly(acrylic acid), $-(CH_2CHCOOH)_n-$, chemically attached to both sides of the polyolefin film. No differences were detectable in the red domain of the EL spectrum between PP and grafted PP which shows that the surface states and the interfacial region are not involved in the emission process in that part of the spectrum. Interfacial states common to many different polymers could exist if they are due to the metal deposition procedure. They used two kinds of metal as electrodes, gold and silver, deposited either by sputtering or by thermal evaporation. Despite very different interfacial characteristics for gold and silver electrodes they obtained similar red components in the EL spectrum.

5.5.2.2 Study of production XLPE cable insulation

The results obtained on samples microtomed from 400 kV XLPE cable are presented, first in the clean region of the cable insulation and then in the halo region, and a comparison is made in order to analyse the difference, if it exists, in the spectra of the light emitted. This will enable comments to be made on the effect of the microfeatures present in the halo region on the light emitted and on the degradation of the polymeric insulation under ac stresses.

◆ *Clean region*

All the 4 slices microtomed in the clean region of the 400 kV electrically aged and unaged cable insulation presented the same type of spectrum. The figure below shows the spectrum obtained for a XLPE film sample when the applied electric field was 53 kV/mm.

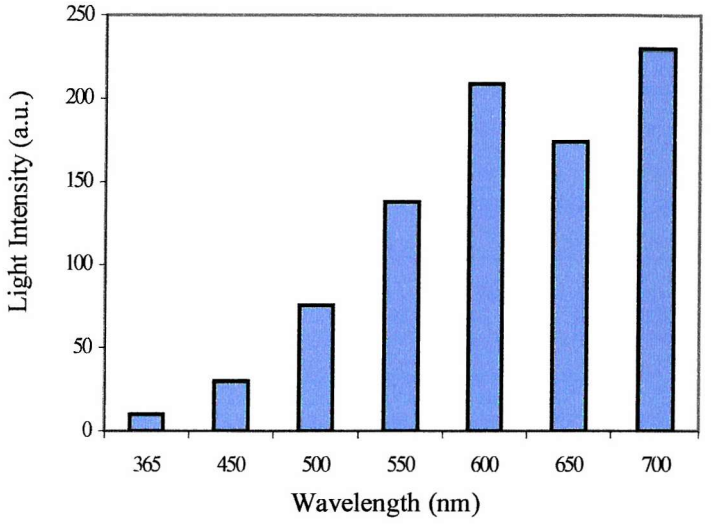

Figure 5.22: EL spectrum of XLPE film for an ac field of 53 kV/mm

■ The spectra obtained on XLPE films were similar to those obtained on commercial additive-free LDPE films (see paragraph 5.2.2.1). The two different components of EL could be clearly identified, one between 365 and 650nm peaking at 600nm and one at 700nm.

EL emission spectra at two different ac fields are shown in figure 5.23. The field dependence of the two components showed a similar trend as for LDPE films. The same conclusions can be drawn, i.e. the component of the spectra between 365 to 650 nm is associated to the luminescence of the bulk of polymer while the other is due to a pure electrode effect.

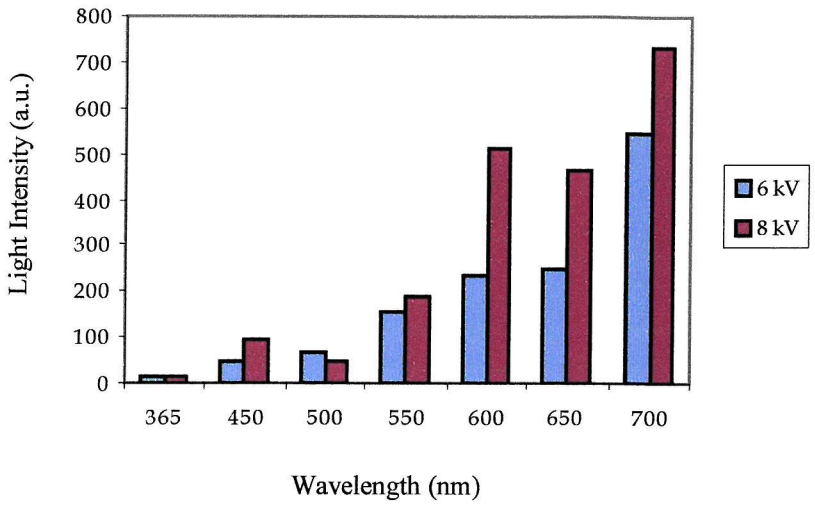

Figure 5.23: EL emission spectra for ac fields of 34 and 44kV/mm

◆ *Halo region*

For films microtomed from the halo region of the 400 kV electrically aged cable insulation two different behaviours of the integral light emission versus voltage and time were observed by carrying out ramp test measurements (section 5.4.2.2). Some samples showed stable emission versus time, which was attributed to EL type emission, while the other showed scans which were not stable versus time and we concluded on a different type of light emission. The same trend appeared also in spectral analysis.

■ The results presented first are those obtained when the total light intensity monitored before and after the spectral analysis was stable. Figure 5.24 shows the spectrum obtained from a film stress under a constant ac voltage of 8 kV.

The typical features of EL emission discussed above were present indicating that this type of emission was responsible for the light emitted. The component peaking at 600 nm was found to increase with the applied electric field which showed the same dependency as other samples (i.e. LDPE and XLPE films in the clean region). This constituted more evidence that the luminescence collected was EL.

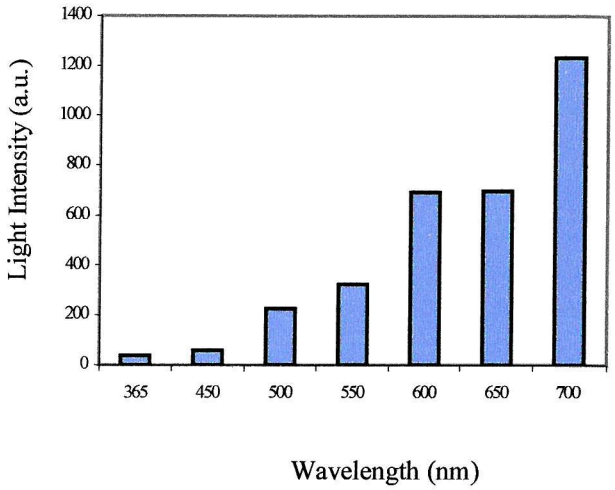

Figure 5.24: Spectrum of light at 45 kV/mm

■ For some films microtomed in the halo region the light monitored before the spectral analysis was not stable versus time. The results presented were obtained for two different films microtomed from the halo region (XLPE1 and 2).

Figure 5.25 shows the total light intensity versus time for XLPE1 under a constant voltage. The light emission was suddenly irregular and intense compared to the steady low level of the beginning.

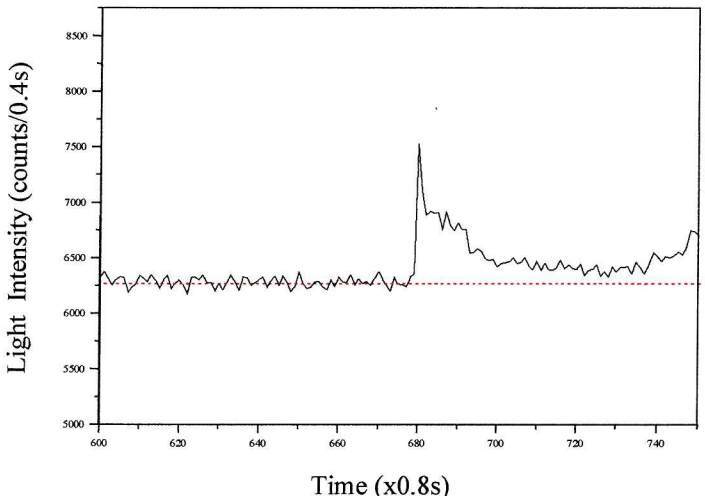

Figure 5.25: Light intensity vs time at 7 kV for XLPE1

A spectral analysis (see figure 5.26) was carried out consequently at 7 kV using only three filters (365nm, 450nm, 600nm).

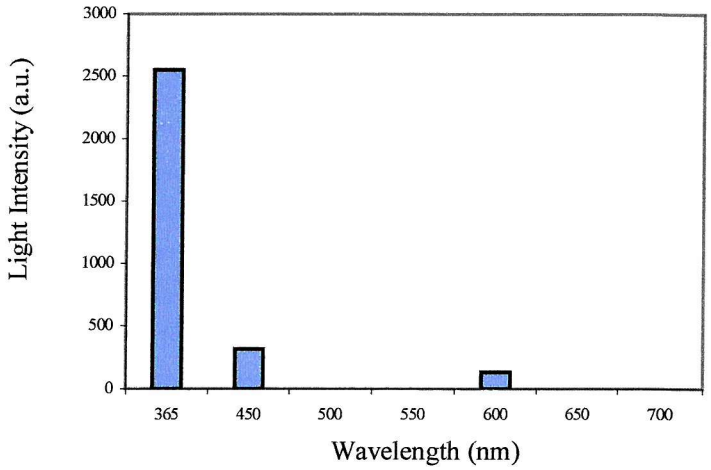

Figure 5.26: Spectrum of light at 7 kV for XLPE1

The same results were obtained for XLPE2. The light was unstable versus time for a constant voltage of 7 kV as the scan on figure 5.27 shows. The CCD detector noise level was recorded before applying the voltage to show the difference in scatter. The spectral analysis was carried out at 7 kV using 5 filters (365nm, 450nm, 500nm, 600nm and 700nm).

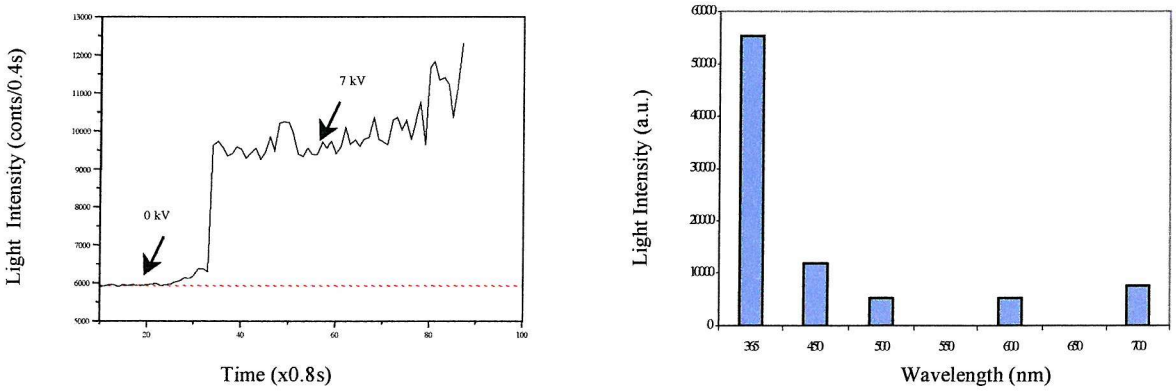

Figure 5.27: Light intensity vs time and spectrum of light at 7 kV for XLPE2

The spectral analysis on cable insulation samples containing micro-features when the light emission was not stable under a constant voltage revealed that the maximum light

was in the UV region (365nm) of the optical spectrum which could indicate an emission which was no longer due to EL.

◆ *Comparison clean/halo region*

The spectra obtained from XLPE films (electrically aged and unaged) without micro-defects were similar to those obtained on commercial additive-free LDPE films. The two different components of EL could be clearly identified, one between 365 and 650nm peaking at 600nm and one at 700nm.

For XLPE cable insulation films containing micro-features, two different behaviours were observed: if the light was stable with time at a constant voltage (type A) the same components were present but the intensity for each component was higher as figure 5.28 shows, if the light was unstable versus time (type B) then the spectral analysis revealed that maximum of light was in the UV region (365nm) of the optical spectrum (figure 5.29).

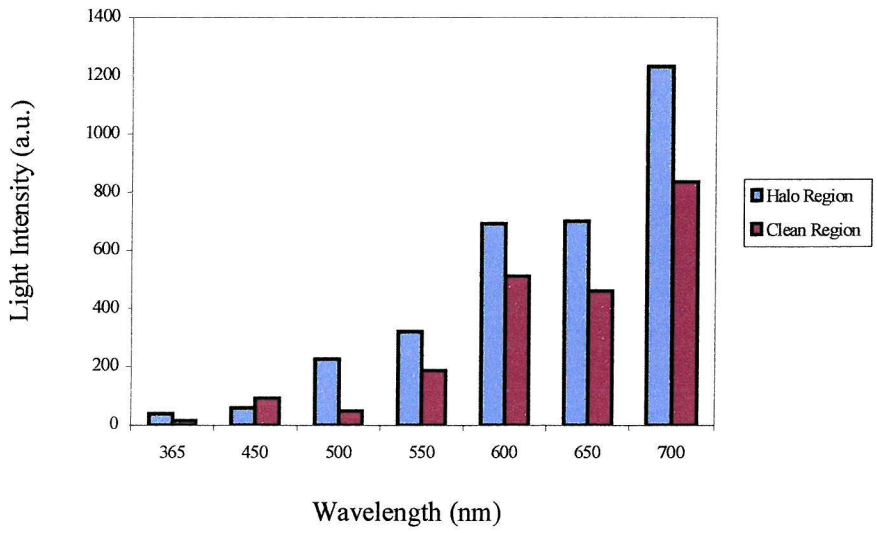

Figure 5.28: Clean/halo region (type A) spectra for 8 kV

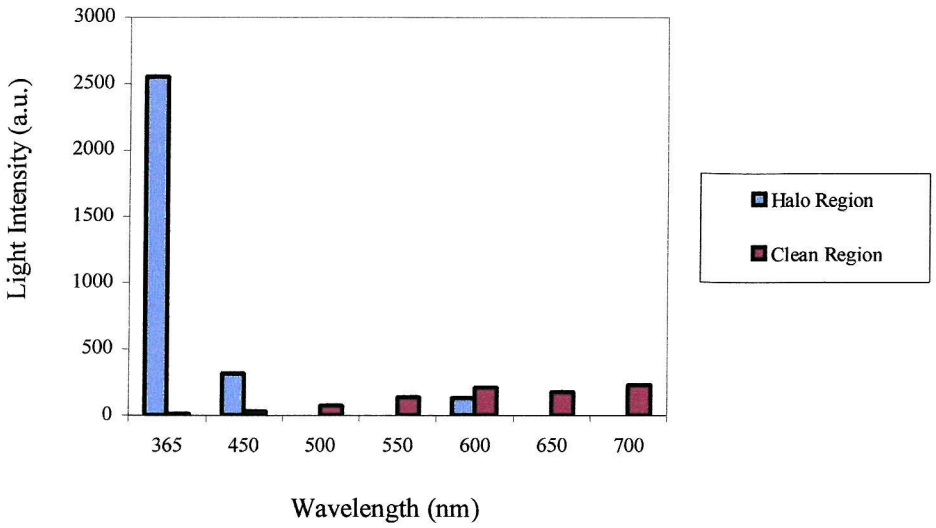

Figure 5.29: Clean/halo region (type B) spectra for 8 kV

The measurements above show clearly that two different luminescence phenomena were involved which could indicate an emission no longer due to EL but to another electrical degradation luminescence.

■ The data obtained by different authors and described in chapter 3 section 3.4.4 show that light from discharges has the maximal amplitude in the UV region between 300 and 400nm. Bamji *et al* found that during tree growth the highest peaks are at 369nm and 486nm, which are due to CO_2 and H_2 gases formed by the decomposition of the polymer due to the partial discharge. The UV emission observed in some samples containing micro-features (type B) could indicate the presence of micro-discharge activity which masked the EL. Other samples (type A) from the halo region simply presented more EL emission.

5.6 Conclusions

The experimental arrangement using the very sensitive cooled CCD detector has made it possible to successfully measure (with short time integration) and monitor the integral electroluminescence in LDPE and XLPE cable insulation samples under relatively low voltages, and to determine the spectral range as well as allowing the imaging of this very low level of light.

The performance of the system designed had been assessed and when the observable area of light emission was masked, no light emission was detected in the range of voltage applied in the experiments. Therefore the emission came from the sample and was not due to an artefact of the rig. When the sample area was imaged it confirmed that no light coming from parts other than the centre of the sample was collected.

The influence of oxygen has been analysed. Its effect was to quench the excited states, giving rise to less light emission, and also to capture the electrons injected into the polymer, which again decreased the efficiency of EL. The experiments performed under atmospheric pressure on samples which were not degassed therefore give information not just on the polymer itself but on the material-impregnated gas complex. Due to the complicated effect of oxygen present both in the bulk of the polymer and at the electrode/polymer interfaces together with the lower reproducibility obtained, it was decided to work under nitrogen pressure. This has also allowed higher voltages to be reached without discharges. Nitrogen was selected because of its small electron affinity and its high chemical stability. It did not therefore interfere with the EL processes unlike Sulfur Hexafluoride, SF_6, currently used in many high voltage application. Another possibility to study EL processes due to the polymer itself would have been to work under secondary vacuum. However it has been shown recently [37] that unlike the tests in pressurised gas, which always result in a light emission from inside the specimen for a divergent field configuration, the tests in vacuum can lead to light emission from a specimen surface.

The characteristics of EL light emission versus voltage, field and time were established on LDPE films and confirmed the results contained in literature. The light emission was low, started at a threshold voltage and then increased with voltage. The light intensity was highly stable versus time under a constant voltage. The characteristic of the light emitted corresponded to EL emission. EL emission from the polymer under the range of fields applied in this study could be explained by the reported mechanism of radiative charge recombination involving trapped electrons and holes which are injected into the sample (bulk of the polymer and/or the volume closest to the electrodes). This process was repeated with every cycle of the ac voltage and did not exhibit the high intensity and time instabilities of light from discharge activity in micro-voids which depends on the

cavities' parameters such as pressure and conductivity. The increase of the voltage led to more charge being injected and hence an increase in the EL emission.

A sample preparation procedure was therefore established to study XLPE production cable insulation and to assess the influence of the micro-features present in the halo region on the degradation of the insulation when an ac voltage was applied.

For untested 110kV type cable insulation more light was emitted by the films containing micro-features. These micro-defects were likely to lead to a local field enhancement and hence more light was emitted. An increase in the number of interfaces due to the presence of these micro-defects may have given rise to a greater density of traps and consequently an increase in local space charge concentrations which could contribute to the EL emission. A good reproducibility was obtained for samples cut in the clean region, and a larger scatter for the halo one. This indicates that the micro-features were involved in the light emission, some films containing more micro-features than others. Some films also presented less stable light emission which seemed to indicate the beginning of another type of light emission.

In order to investigate further the influence of the halo micro-defects, an aged cable insulation presenting larger features (~5μm) was studied. For tested 400kV type cable insulation all the films cut in the clean region presented the same behaviour of light versus voltage and time, i.e. a stable low level of light which increased with the applied voltage. This was the same behaviour as LDPE films and 110 kV cable insulation films without micro-defects and was attributed to EL emission. For films microtomed from the halo region, where the micro-features were elongated, two different behaviours of the integral light emission versus voltage and time were observed by carrying out ramp test measurements. Some samples showed stable emission versus time, which presented the characteristics attributed to EL type emission, with a higher intensity however than in samples microtomed in the clean region, while the other (more numerous) showed two distinct behaviours (A and B) of light emission in the time domain indicating two different types of luminescence.

(i) stage A was similar to EL observed in LDPE films and XLPE cable insulation samples containing no micro-defects. It was related to charge injection into the polymer sample resulting in EL.

(ii) stage B occurred on further increase in the field when a change in emitted light behaviour was observed. The light intensity fluctuated in time and the low level EL was rapidly masked. This behaviour was consistent with the onset of micro-discharges activity from the halo micro-features present in the cable insulation sample.

The fact that some samples presented more EL and others unstable light emissions, could be explained depending on whether or not the sample contained micro-defects (initially or created during the voltage ramp-test) of the critical size to start micro-discharge activity. The mapping of the halo region had permitted to microtome samples in its densest part where the micro-features were elongated. However, it is possible that in the densest part there remained areas where the micro-defects were small in size hence simply giving rise to more EL, as in the halo region of virgin 110kV cable insulation.

The spectra of light obtained on XLPE films without micro-defects were similar to those obtained on commercial additive-free LDPE films. EL in LDPE and XLPE seems dominated by phosphorescence (500-700nm) which involved triplet states, (see chapter 3 section 3.2) characterised by a long life. These triplet states may decay unimolecularly mostly by bond cleavage and rearrangements involving breaking and formation of new chemical bonds, their detection in EL is a signature of irreversible reactions. The two different components of EL could be clearly identified, one between 365 and 650nm peaking at 600nm and one at 700nm. At low field, the red component (700nm) of the spectrum was dominant, which corresponded to a low emitted photon energy of 1.8 eV. As the field increased this contribution decreased in comparison to the part between 500 and 650nm which peaked at 600nm. The different components of the spectrum, that between 365 and 650nm and the red component, seemed not to be controlled by the same mechanisms, which confirmed the literature result that the red component of the light emission was due to a pure surface electrode effect while the rest of the spectrum was due to the EL of the bulk of the polymer film. For XLPE cable insulation films containing micro-features, the spectral analysis when the light emission was unstable under a constant voltage revealed that light emission peaked in the UV region (365nm) of the optical spectrum which pointed to the likely presence of micro-discharge activity.

These results showed that the degradation of the insulation under ac stresses was accelerated by the presence of the halo micro-defects. The pre-degradation electroluminescence effects were stronger and evidence pointing to the likely presence of micro-discharge activity was detected in samples peeled from the area of the cable insulation containing micro-features.

Chapter 6

Conclusions and further work

6.1 Conclusions

The thesis describes how a halo effect appeared in some cable main insulation after degassification, which consisted of a circular band or bands in the bulk of the insulation concentric with the cable cross section. These appeared like a smoky or more opaque region compared to the surrounding area, the effect being present in several cables rated for system voltages of 110 kV, 132 kV, 220 kV, and 400 kV.

Staining followed by Confocal Laser Scanning Microscopy in fluorescence mode was determined to be the most suitable way to characterise the halo region. Unlike conventional optical microscopy, this technique allowed us to observe very fine details precisely thanks to a combination of the three-dimensional effect, the better resolution achieved with the confocal optical design, which cancelled the out-of-focus blurring, and finally the better contrast obtained by the fluorescence of the specific dye. These observations have revealed that the halo region consisted of a multitude of micro-features of 1 to 1.5 microns across, which appeared like isolated micro-voids, clusters of micro-voids and arrays of micro-channels.

In order to better understand what produced this effect, the influence on the halo region of the parameters of temperature and duration of the industrial degassification process were assessed. After a series of experiments it was possible to conclude that the halo effect appeared not to be due to the heat treatment during the degassification process since cable insulation specimens which had not undergone this treatment still presented this effect after a period of approximately 3 ½ months. It was most probably due to the diffusion of by-products inside the main insulation wall, this diffusion process being accelerated by the temperature. The fact that there was no halo region when the insulation was not crosslinked showed that the halo effect present in XLPE cable insulation was not due to an artefact of the antioxidant such as antioxidant agglomeration, but could be explained by the presence of crosslinking by-products as FTIR measurements seemed to indicate.

There were also indications that this halo effect was affected by electrical testing since a difference was found in its geometry in specimens originating from cables subjected to such tests. Indeed the halo region appeared more dense and wider than in a sample from the same cable before electrical testing. At the densest point in the 'halo' the micro-features were longer, about 5 μm, and oriented in the direction of the electrical field. At higher magnification, these elongated features appeared to be made of clusters of micro-voids and micro-channels arranged in the direction of the field. It would seem that in the presence of electrically-caused mechanical stresses (e.g. by Maxwell forces), the 'halo' micro-features grow and are oriented in the direction of the electric field. This phenomenon might possibly be explained by micro-void coalescence due to the presence of a mechanical stress. The stress was a tensile one, hence if imperfections like the halo micro-features were present, the energy associated with the stress might be sufficient to extend them or create crazes via micro-void coalescence in the direction of the electric field.

Following the set of observations of the halo effect to better understand its physical aspect, it was necessary to assess its significance on the degradation of the insulation under ac stress. In order to carry this out a method was required which would allow the detection in the early stages of the degradation well before partial discharges occur. The micro-voids observed being very small they were likely to induce a low level of

degradation. The bibliography study had shown that Electroluminescence (EL) measurements were known to provide such a method.

An experimental arrangement was integrally designed to carry out EL measurements on insulating samples in a uniform field configuration at room temperature under ac stress. The experimental system, using a very sensitive cooled CCD detector, has made it possible to successfully measure (with short time integration) and monitor the integral electroluminescence in LDPE and XLPE cable insulation samples under relatively low voltages, and to determine the spectral range as well as allowing the imaging of this very low level of light.

The influence of oxygen was analysed and its presence was shown to decrease the efficiency of EL through several processes. One effect was to quench the excited states, giving rise to less light emission, it also captured the electrons injected into the polymer. Hence due to those complicated effects of oxygen, present both in the bulk of the polymer and at the electrode/polymer interfaces, and due to the lower reproducibility obtained under oxygen, it was decided to work under nitrogen pressure. The latter was selected because of its small electron affinity and its high chemical stability. Another benefit of this choice is that it has also allowed higher voltages to be reached without discharges.

In order to assess the functioning of the experimental system and to provide a benchmark to allow the continuation of the study on cable samples, the characteristics of EL emission versus voltage, field and time were established on LDPE films. It was found to confirm the results contained in literature. The light emission was low, started at a threshold voltage and then increased with voltage. The light intensity was highly stable versus time under a constant voltage. The characteristics of the light emitted corresponded to EL emission as spectral analysis would later confirm. EL emission from the polymer under the range of fields applied in this study could be explained by the reported mechanism of radiative charge recombination involving trapped electrons and holes, which are injected into the sample (bulk of the polymer and/or the volume closest to the electrodes). This process was repeated with every cycle of the ac voltage and did not exhibit the high intensity and time instabilities of light from discharge activity in micro-voids which depends on the cavities' parameters such as pressure and

conductivity. The increase of the voltage led to more charge being injected and hence an increase in the EL emission.

A sample preparation procedure was established to study XLPE production cable insulation and to assess the influence of the micro-features present in the halo region on the degradation of the insulation when an ac voltage was applied. For untested 110 kV type cable insulation more light was emitted by the samples containing micro-features. These micro-defects were likely to lead to a local field enhancement resulting in more light emission. An increase in the number of interfaces due to the presence of these micro-defects may have given rise to a greater density of traps and consequently an increase in local space charge concentrations which could contribute to the EL emission. Some films also presented less stable light emission which seemed to indicate the beginning of another type of light emission.

In order to investigate further the influence of the halo micro-defects, an aged cable insulation presenting larger features (~5μm) was studied. For tested 400kV type cable insulation all the samples cut in the clean region presented the same behaviour of light versus voltage and time, i.e. a stable low level of light which increased with the applied voltage. This was the same behaviour as LDPE films and 110 kV cable insulation slices without micro-defects and was attributed to EL emission. For films microtomed from the halo region, where the micro-features were elongated, two different behaviours of the integral light emission versus voltage and time were observed by carrying out ramp test measurements. Some samples showed stable emission versus time, which presented the characteristics attributed to EL type emission, with a higher intensity however than in samples microtomed in the clean region, while the others (more numerous) showed two distinct behaviours (described as stages A and B below) of light emission in the time domain indicating two different types of luminescence.

(i) Stage A was similar to EL observed in LDPE films and XLPE cable insulation samples containing no micro-defects. It was related to charge injection into the polymer sample resulting in EL.

(ii) Stage B occurred on further increase in the field when a change in emitted light behaviour was observed. The light intensity fluctuated in time and the low

level EL was rapidly masked. This behaviour was associated with the onset of micro-discharge activity from the halo micro-features present in the cable insulation sample.

The fact that some samples presented more EL, and others unstable light emission, could be explained as depending on whether or not the sample contained micro-defects (initially or created during the voltage ramp-test) of the critical size to start micro-discharge activity.

The spectra of light obtained on XLPE films without micro-defects were similar to those obtained on commercial additive-free LDPE films. EL in LDPE and XLPE seems dominated by phosphorescence (500-700nm) involving triplet states, which are characterised by a long life. These triplet states may decay unimolecularly mostly by bond cleavage and rearrangements involving breaking and formation of new chemical bonds, their detection in EL is a signature of irreversible reactions.

The two different components of EL could be clearly identified, one between 365 and 650nm peaking at 600nm and one at 700nm. They seemed not to be controlled by the same mechanisms, which confirmed the literature result that the red component of the light emission was due to a pure surface electrode effect while the rest of the spectrum was due to the EL of the bulk of the polymer film.

In the case of XLPE cable insulation films containing micro-features, the spectral analysis when the light emission was unstable under a constant voltage revealed that light emission peaked in the UV region (365nm) of the optical spectrum, which may indicate the presence of micro-discharge activity.

The results showed that the degradation of the insulation under ac stresses was accelerated by the presence of the halo micro-defects. The pre-degradation electroluminescence effects were stronger, and evidence pointing to the likely presence of micro-discharge activity was detected in samples peeled from the area of the cable insulation containing micro-features.

6.2 Further work

In the light of the work described in this thesis, some suggestions can be proposed for future research. It would be of great interest to obtain physical thresholds in relation to charge injection/extraction at the metal/polymer interface because there are very few techniques that provide information on space charge behaviour under ac stress.

In the case of dc stress [25, 96] the onset of EL is related to a drastic change in the conduction process, current and EL being proportional above a field threshold value. Hence the dc threshold is considered as a physical threshold corresponding to the onset of hot electron effects. In this thesis only EL under ac stress has been studied and therefore also investigating EL under dc voltage would reveal valuable information.

Under ac, the situation is more complex because of the two contributions to the light emission studied, which are:

- the electrode effect (surface plasmons excited by the injection current) which dominates at low field and has a spectral component in the red;
- EL due to the material excited by charge injection/extraction which has a spectrum typical of the material under test.

This is why the threshold values derived from metallised polymer films stressed under ac are 'apparent' thresholds. Since the component of the emission due to the metallic electrode layer is in the red part of the spectrum, it is possible to reject this component using a combination of short pass filters characterised by a transmission in the range between 350nm and 650nm. Short pass filters are designed to exhibit a very sharp transition over a very narrow wavelength range from being highly transmissive to highly reflective. The characteristics of EL versus ac electric field (ramp tests) with the filtered red correction should then be analysed using the classical theories in order to investigate what could possibly be a good fit to Schottky or Fowler- Nordheim laws.

A study of the phase relationship of the light emission with the ac voltage would be interesting in order to further understand the mechanisms of EL under ac by revealing

when during the ac wave the light is emitted. In order to achieve that two possible readout scenarios of the CCD detector chip can be considered as detailed below:

i) It may be possible to read the whole CCD chip, or a selected part of it, if necessary in 1ms. It should be then possible to make one reading every cycle by shifting the image up by 512 rows to clear the image area immediately prior to shifting the charge down into the output register at the appropriate phase of the signal. This would require several cycles to give a good signal to noise ratio and would need to be repeated 20 times to generate the complete temporal response.

ii) Masking part of the CDD detector in order to achieve an image area of approximately 10x512 pixels (512 pixels long by 10 high) would also allow to achieve a 1ms time resolution. This could be obtained by for instance using a slit in a two-lens system, allowing the image to be collected on the area of the chip selected. The process would involve storing the signal in the top half of the CCD detector and slowly (10 rows per ms) shifting the signal through the active area into the bottom of the CCD and finally to the output register leaving the top of the CCD array free for the next measurement. This method would require averaging over more cycles than i) to obtain the same signal to noise ratio.

The advantage of this particular method is that it is possible to obtain a complete spectrum (temporal response) simultaneously.

Both methods would require the careful synchronisation of data collection and ac voltage under software control. A light electroluminescent device (LED) modulated at 50 Hz could be used for this purpose.

Appendix A

Cable degassification simulation

In production, cables newly manufactured are degassed at 85° C for several days depending on the cable geometry. In order to study the influence of the degassification process on the halo effect, a simulation of the degassification was carried out on cable pieces in an oven at 65°C. The aim was to study the effect of a reduction of the degassification temperature. To obtain the same conditions as in production, a calculation of the time required to de-methane cables at the chosen temperature was necessary. This calculation is presented in this appendix.

A.1 Theory of diffusion in cable

For a long circular cylinder in which diffusion is radial everywhere, the concentration C of diffusant is a function of radius, r, and time, t, only and the diffusion equation (Fick's 2nd law of diffusion in cylindrical coordinates) is:

$$\frac{\partial C}{\partial t} = \frac{1}{r}\frac{\partial}{\partial r}(rD\frac{\partial C}{\partial r}) \quad (1)$$

A solution of this equation (1) is required. Crank [115] gives the solution to equ.(1) for the problem of diffusion into a hallow cylinder, a < r < b in which the difussion coefficient D is constant, and a set of general boundary conditions is specified.

For the insulation of single-core HV cable, we have an annulus bounded by r = b and r = a .

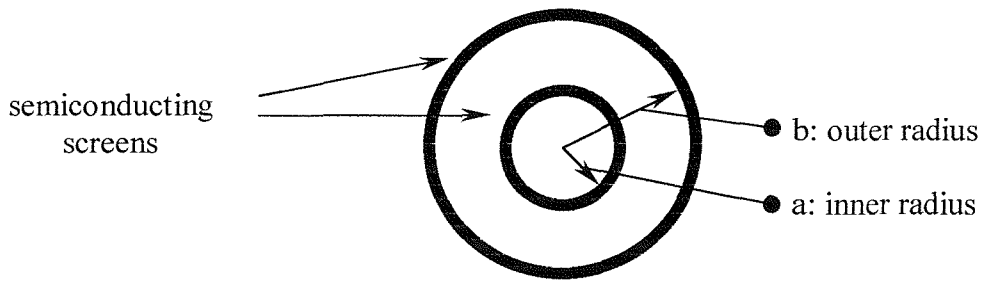

Figure A.1: HV cable section

The following assumptions are made:

- at r = a no diffusion occurs through the conductor/dielectric interface :

$$\frac{\partial C}{\partial r} = 0 \ ,$$

- $K = \frac{b}{a} > 1,$

- a high voltage cable is composed of both semiconducting screens and insulation. The calculation presented here is based upon the approximation that the diffusion coefficients of the semiconducting screens are the same as for the XLPE insulation. The error introduced by this approximation is assumed to be negligible due to the small volume of the screens.

A simplified analytical adimensional solution is obtained with the above conditions:

$$\frac{D(T).t_f}{(b-a)^2} = C_f \quad (2)$$

where C_f is a constant for particular values of b / a and of $M_t / M_0 = f$,

- M_t : total amount of diffusing substance at time t,
- M_0 : initial amount,
- D : Diffusion coefficient (cm^2 / s),
- t : time (s),
- (b – a) : insulation thickness (cm).

A.2 Calculation of time required to de-methane cable at 65 °C

The duration in production of the heat treatment for degassification is based on reduction of methane in the cable to an average of 1 % of original ($M_t / M_0 = 0.01$).

In order to simulate production degassification at lower temperature in an oven, the temperature chosen was T = 65°C.

The following table and curve [114] show the different values of $\frac{D(T).t_f}{(b-a)^2}$ for several values of M_t / M_0.

K = b / a	**$\frac{D(T).t}{(b-a)^2}$**	**F** (time multiplication factor)
3.0	1.1572	1.000
2.5	1.2366	1.069
2.0	1.347	1.164
1.5	1.4876	1.285

Table A.1: Values of $\frac{D(T).t_f}{(b-a)^2}$ for $M_t / M_0 = 0.01$

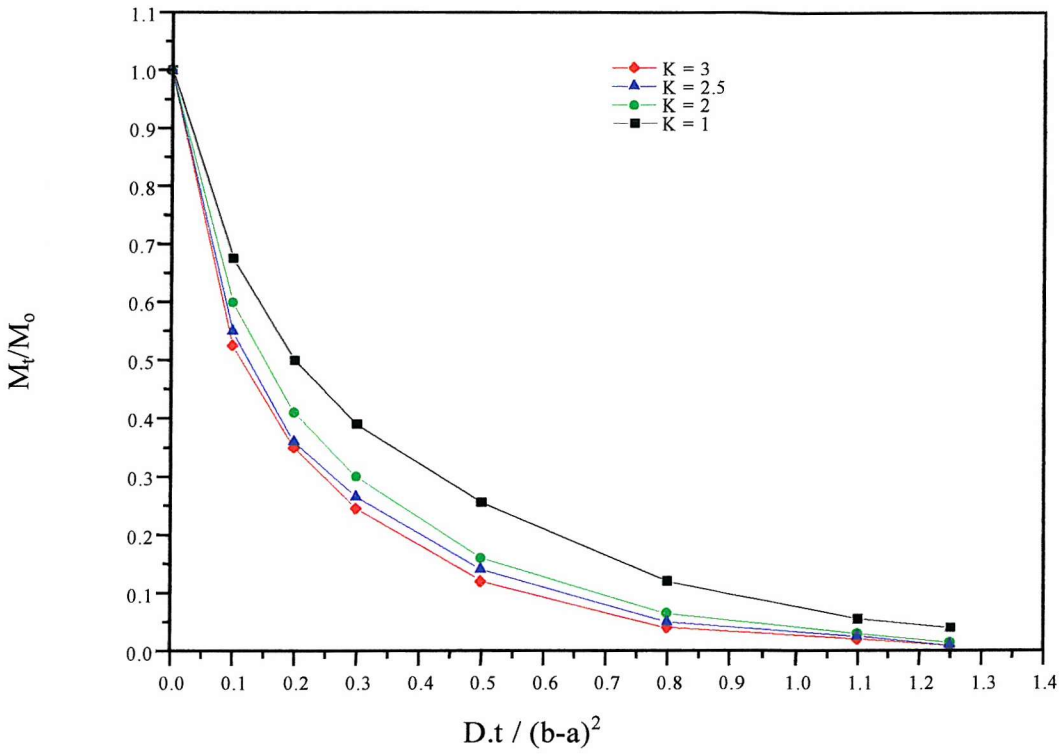

Figure A.2: Diffusion of CH_4 from XLPE cable insulation wall; curve M_t/M_0 versus $\frac{D(T).t_f}{(b-a)^2}$,[114]

For our experiment the cable's dimensions are:

a = 14 mm, b = 33.5 mm

a – b = 19.5 mm

$\Rightarrow K = a / b = 2$

$\Rightarrow \frac{D.t}{(b-a)^2} = 1.347$ (see table 1)

The diffusion coefficient of methane at T = 65°C is D = 3.7x 10^{-6} cm^2/s. Then the degassification time required at 65°C is:

$$t = \frac{1.95^2 \times 1.347}{3.7 \times 10^{-6}} = 1.38 \times 10^6 s = 384 \text{ h } 30 \text{ min}$$

Appendix B

Transmittance of the gold layer

The transmittance of the gold layer was estimated for the thickness employed, using a theoretical case illustrated in this appendix.

B.1 Principle

The calculation was made at the gold/air interface, as figure B.1 shows, based on a plane monochromatic wave $(\vec{E}_{01}, \vec{B}_{01}, \vec{K}_1)$ incident normally on the surface separating two media of index N_1 and N_2.

The incident wave will give rise to a reflected wave $(\vec{E'}_{01}, \vec{B'}_{01}, \vec{K'}_1)$ and a transmitted wave $(\vec{E}_{02}, \vec{B}_{02}, \vec{K}_2)$.

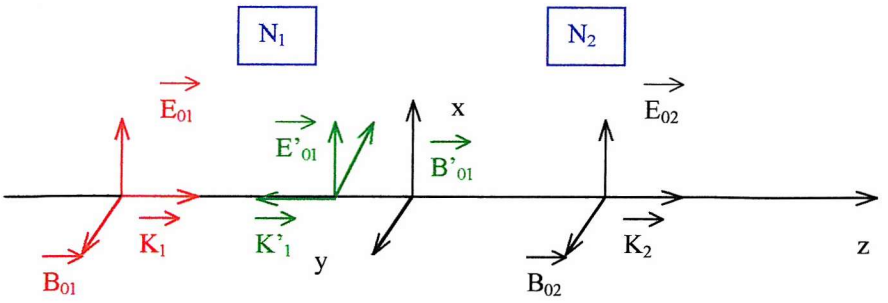

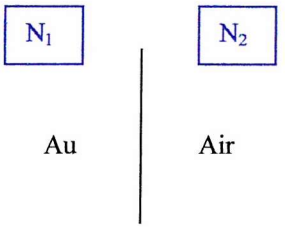

The transmittance is given by the formula [113]:

$$T = 1 - R \qquad (1)$$

where $$R = \frac{\text{reflected intensity}}{\text{incident intensity}}$$

$$\Rightarrow T = \frac{4N_1N_2}{(N_1 + N_2)^2} \qquad (2)$$

N_1: refractive index of gold, function of wavelength

N_2: refractive index of air

B.2 Result

Published values for the refractive index of gold were used [112]. This calculation is valid for a range of gold layer thickness between 25 and 50nm.

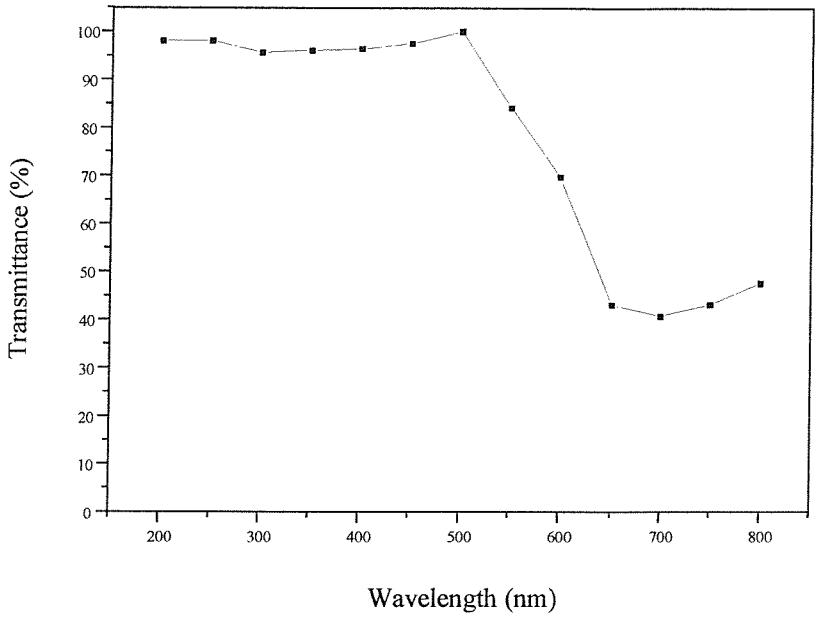

Figure B.1: Transmittance of gold layer for thickness range 25-50nm

Appendix C

Surface roughness measurements

An estimation of the surface roughness of the slices obtained by the peeling technique was obtained using a stylus based surface measurement system and the principle of these measurements is described below.

C.1 Surface roughness definition

There are several definitions of surface roughness. R_a is the universally recognised, and most used international parameter of roughness. It is the arithmetic mean of the absolute departures of the roughness profile from the mean line.

$$R_a = \frac{1}{L_r} \int_0^{L_r} |z(x)| dx \qquad (1)$$

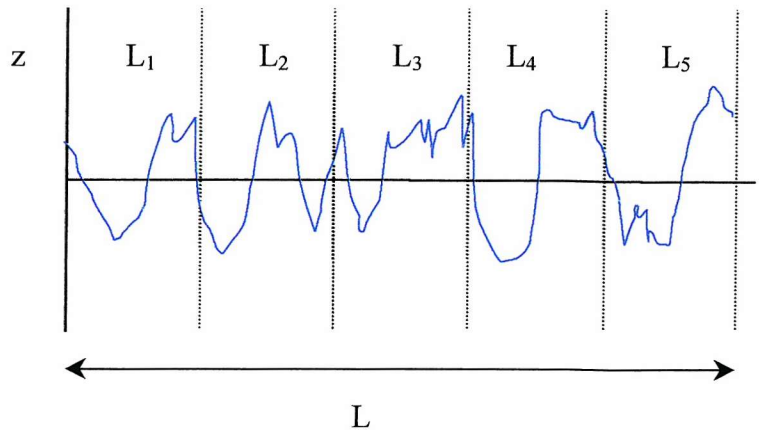

Figure C.1: Surface roughness profile, two dimensional (2D) scan

L_1-L_5 are consecutive and equal sampling lengths. The assessment length L is defined as the length of profile used for measurement of surface roughness (usually containing several sampling lengths; five consecutive sampling lengths are taken as standard).

C.2 Measurements

The surface roughness of XLPE films was measured using a contact method. The Rank Taylor Hobson (RTH) Form Talysurf series 2 is a stylus based surface measurement system at which a stylus is traversed over the surface and the vertical displacement of the stylus due to surface irregularities is measured. The movement of the stylus is recorded to a reference, normally a straight line or a plane.

Some years ago, surface measurement was exclusively two-dimensional. However, fine surface details vary on the same surface from place to place and with the direction in which the stylus is tracked over the surface. A way to get more reliable results is by taking several closely spaced, parallel 2D scans and to combine them to a 3D profile of the surface. In a 3D surface map, a trace refers to a collection of data-points along the x-axis and hence, a single trace is equivalent to a 2D measurement of the surface at a certain position. A line, on the other hand, is parallel to y-axis and connects points of several traces, one point in each trace only.

Inside an area of 10 mm^2 of XLPE film, ten parallel 2D scans of 2mm length and a 3D profile of an area of 2 mm^2 in the middle of the studied area were taken.

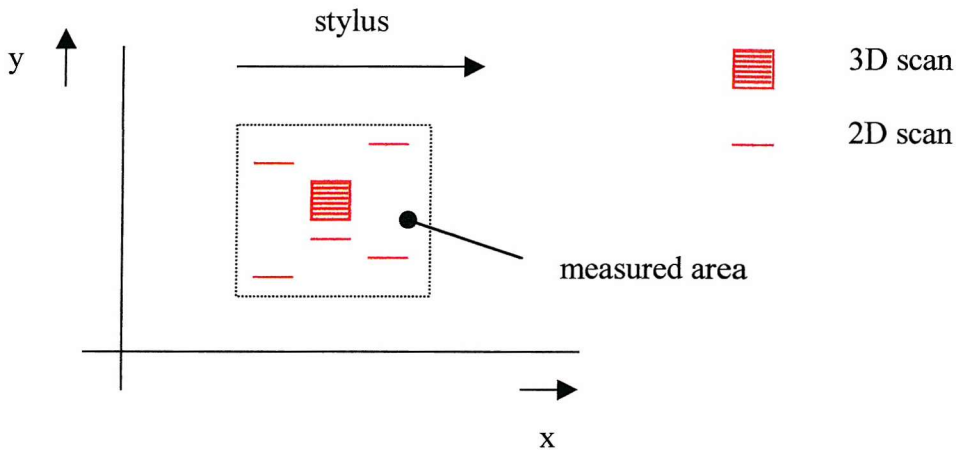

Figure C.2: Measurements

C.3 Results

C.3.1 2D scans

Both surfaces of a peeled film had different surface roughness, one side being systematically rougher than the other.

A mean value of Ra was found for both sides of the film: Ra=1.16 ± 0.05 μm and Ra=0.84 ± 0.08 μm respectively.

C.3.2 3D profile

The figures next page show the flat part only of the scanned area where we can distinguish the cutting stripes. The same value of R_a was deduced.

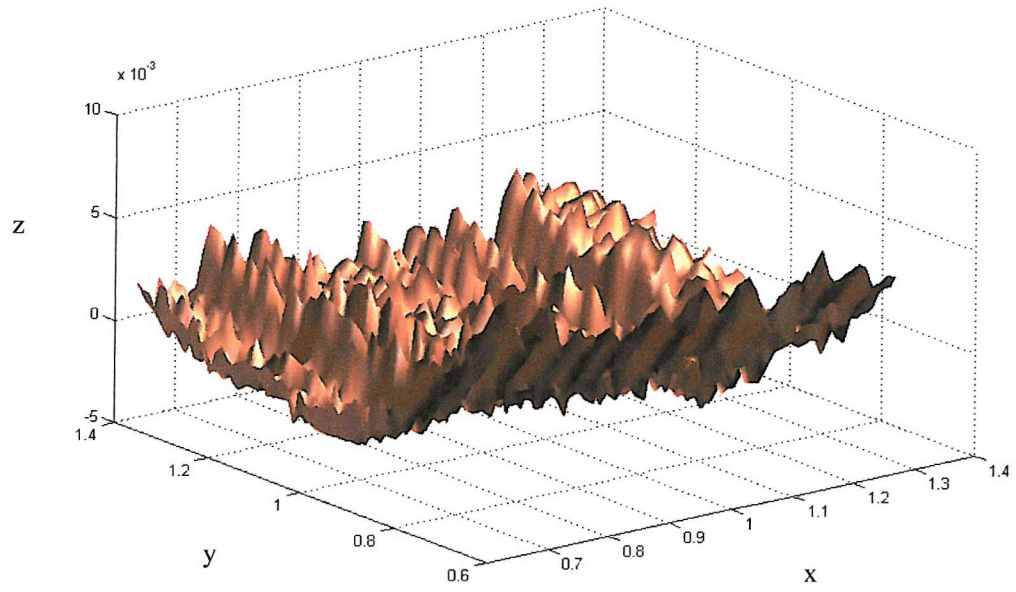

Figure C.3: 3D profile

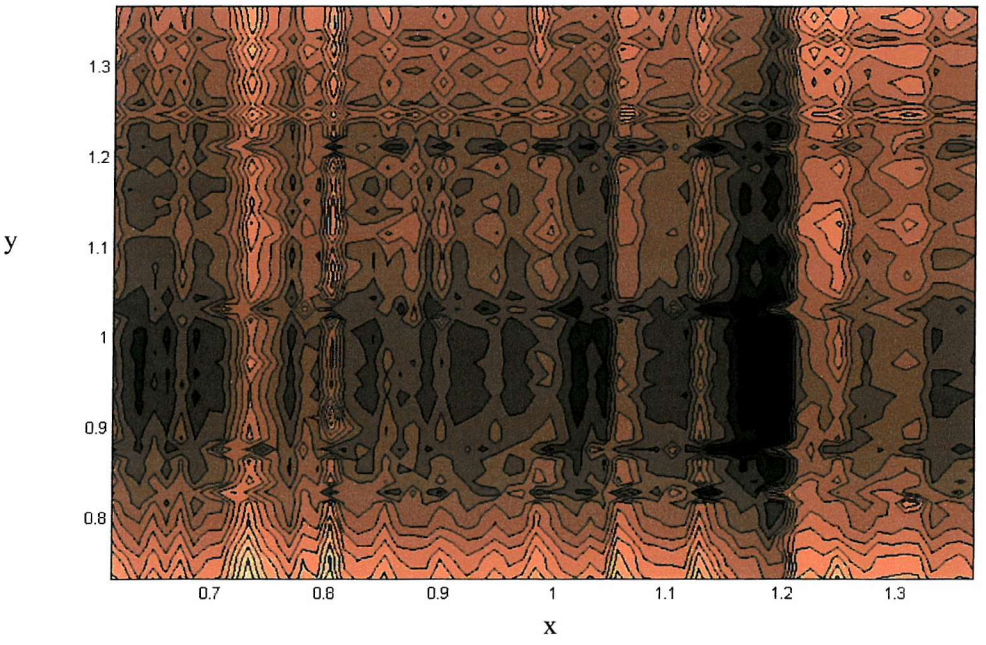

Figure C.4: contour plot of the 3D surface map

References

1. R. Arrighi, "From impregnated Paper to Polymeric Insulating Materials in Power Cables", IEEE Trans. Diel. Electr. Insul., Vol. 21, pp. 7-18, 1986.

2. A. Ishibashi, T. Kawai, S. Nakagawa, H. Muto, S. Katakai, K. Hirotsu and T. Nakatsuka, "A Study of Treeing Phenomena in the Development of Insulation for 500kV XLPE Cables", IEEE Trans. Diel. Electr. Insul., Vol. 5, pp. 695-712, 1998.

3. R. Patsch, "Electrical and Water Treeing", IEEE Trans. Electr. Insul., Vol. 27, pp. 532-542-712, 1992.

4. Pirelli Cables, Power Cables Technology Course.

5. L.A. Dissado and J.C. Fothergill, *Electrical Degradation and Breakdown in Polymers*, Peter Peregrinus Ltd., London, 1992.

6. J. Mason, Proc. IEE, Vol. 128A, pp. 193-201, 1986.

7. S.S. Bamji, "Electroluminescence –A Technique to Detect the Initiation of degradation in Polymeric insulation", IEEE Electr. Insul. Magazine, Vol. 15, No. 3, pp. 9-14, 1999.

8. N. Shimizu, C. Laurent, " Electrical Tree Initiation", IEEE Trans. Diel. Electr. Insul., Vol. 5, pp. 651-659, 1998.

9. B.R. Varlow and D.W. Auckland, "Mechanical Aspects of Electrical Treeing in Solid Insulation", IEEE Electr. Insul. Magazine, Vol.12, pp. 21-26, 1996.

10. T. Tanaka, T. Okamoto, K. Nakanishi and T. Miyamoto, "Aging and Related Phenomena in Modern Electric Power Systems", IEEE Trans. Electr. Insul., Vol. 28, pp. 826-844, 1993.

11. C. Laurent, F. Massines, and C. Mayoux, "Optical Emission due to Space Charge Effects in Electrically Stressed Polymers", IEEE Trans. Diel. Electr. Insul., Vol. 4, pp. 585-603, 1997.

12. S. Yan, K. Sheu, D.H. Damon, S.J. Huang and J.F. Johnson, "Electric Strength of XLPE Containing Acetophenone and Other Volatile Substances", Proc. IEEE Int. Symp. Electr. Insul., pp. 305-308, 1990.

13. H. Wagner and J. Wartusch, "About the Significance of Peroxide Decomposition Products in XLPE Cable Insulations", IEEE Trans. Electr. Insul., Vol. 12, pp. 395-401, 1977.

14. D.M. Tu, L.H. Wu, X.Z. Wu, C.K. Cheng, and K.C. Kao, "On the Mechanism of Treeing Inhibition by Additives in Polyethylene", IEEE Trans. Electr. Insul., Vol. EI-17, pp. 539-545, 1982.

15. L.M. Harwood and T.D.W Claridge, *Introduction to Organic Spectroscopy*, Oxford University Press Inc., Oxford, 1999.

16. A.C. Ashcraft, R.M. Eichorn, "Method for Visualization of Water Trees by Staining", IEEE Trans. Electr. Insul., Vol. EI-13, pp. 198-199, 1978.

17. R. H. Olley and D.C. Basset, "An Improved Permanganic etchant for Polyolefines", Polymer, Vol. 23, pp. 1707-10, 1982.

18. C.J.R. Sheppard and D.M. Shotton, *Confocal Laser Scanning Microscopy*, Bios Scientific Publishers, Oxford, Vol.38, 1997.

19. T.J. Lewis, J.P. Llewellyn, M.J. van der Sluijs, J. Freestone and R.N. Hampton, "A New Model for Electrical Ageing and Breakdown in Dielectrics", IEE 7th Int. Conf. on Dielectric Mat. Measurements and Applications, DMMA, pp. 220-224, 1996.

20. M.N. Arbab, D.W Auckland and B.R. Varlow, "Mechanical processes in the long term degradation of solid insulation", IEE DMMA, pp.231-233, 1988.

21. W.A. Hartman and H.L. Armstrong, "Electroluminescence in Organic Polymers", J. Phys., Vol. 38, pp. 2393-2395, 1967.

22. Z. Yang, B. Hu, F. Karasz, "Electroluminescence in Polymers", Macromolecular Symposia, Vol. 124, pp. 83-87, 1997.

23. D.A. Seanor, *Electrical properties of polymers*, Academic Press. Inc., New York, chapt.3, 1982.

24. J.N. Demas and S.E. Demas, *Encyclopedia of Physical Science*, Academic Press. Inc., New York, Vol.7, pp 438, 1987.

25. C. Laurent, "Optical Prebreakdown Warnings in Insulating Polymers", IEEE Electr. Insul. Magazine, Vol. 15, No. 2, pp. 5-13, 1999.

26. T.J. Lewis, "Charge Transport, Charge Injection and Breakdown in Polymeric Insulators", J. Phys. D: Appl. Phys., Vol. 23, pp. 1469-1478, 1990.

27. G.A. Cartwright, "The Measurement of Space Charge and its Effect on the Breakdown Strength of Solid Polymeric Insulation", PhD Thesis, 1994.

28. L.A. Dissado and J.C. Fothergill, *Electrical Degradation and Breakdown in Polymers*, Peter Peregrinus Ltd., London, pp. 217-228, 1992.

29. T. Mizuno, Y.S. Liu, W. Shionoya, K. Yasuoka and S. Ishii, "Investigation of Charge Injection in Gas-Impregnated Polyethylene by Measurement of Electroluminescence under AC Voltage" Jpn. J. Appl. Phys., Vol. 36, pp. 754-760, 1997.

30. J. Kalinowski, "Electron Processes in Organic Electroluminescence", Electrical and Related Properties of Organic Solids, Vol. 24, pp. 167-206, 1997.

31. W.W. Piper and F.E. Williams, "Theory of Electroluminescence", Phys. Rev., vol. 98, pp. 1809-1813, 1955.

32. A.S. Davydov, *Theory of Molecular Excitons*, Plenum, New York, 1971.

33. C. Laurent, C. Mayoux and S. Noel, "Mechanisms of Electroluminescence during Aging of Polyethylene", J. Appl. Phys. , Vol. 58, pp. 4346-4352, 1985.

34. F. Kabir, J.M. Braun and J. Densley, R.N. Hampton, "Light emission from Highly-stressed Polymeric Cable Insulation", Conf. Record of the IEEE Int. Symp. on Electr. Insul., pp. 37-39, 1994.

35. F. Kabir, J.M. Braun and J. Densley, "The role of XLPE Type on Electroluminescence and Subsequent Electrical Treeing", Conf. Record of the IEEE Int. Symp. on Electr. Insul., pp. 691-694, 1996.

36. J.V. Champion, S.J. Dodd and G.C. Stevens, "Long-term Light Emission Measurement and Imaging during the Early Stages of Electrical Breakdown in Epoxy Resin", J. Phys. D: Appl. Phys., Vol. 27, pp. 604-610, 1994.

37. S.S. Bamji and A.T. Bulinski, N. Shimizu, "Electroluminescence and Space Charge in Polymeric Insulation", Proc. IEEE Int. Conf. on Properties and Applications of Diel. Material, ICPADM, pp. , 2000.

38. D. Mary, G. Teyssedre, L. Cissé and C. Laurent, "Electroluminescence Emission Imaging in Insulating Polymers under Uniform Field Configuration", Proc. IEEE Int. Conf. on Cond. and Break. in Sol. Diel., ICSD, pp. 261-264, 1998.

39. T. Mizuno, Y.S. Liu, W. Shionoya, M. Okada, K. Yasuoka , S. Ishii, A. Yokoyama, and H. Miyata, " Electroluminescence from Surface Layer of Insulating Polymer under AC Voltage Application", IEEE Trans. Diel. Electr. Insul., Vol. 5, pp. 903-908, 1998

40. Z.H. Fan, M. Hiroyuki and T. Thoru, I. Tomonori and N. Takuo, "Evaluation of Electroluminescence in Polyethylene", Proc. IEEE Int. Symp. on Electr. Insul. Mat., pp. 211-214, 1998.

41. I. Tomonori and N. Takuo, Z.H. Fan, T. Thoru, S. Jun and M. Hiroyuki, "Electroluminescence in Additive-contained Low Density Polyethylene", Proc. Conf. Electr. Insul. and Diel. Phen., CEIDP, pp. 589-592, 1999.

42. D. Mary, M. Albertini,, and C. Laurent, "Understanding Optical Emissions from Electrically Stressed Insulating Polymers: Electroluminescence in Poly(Ethylene Terephtalate) and Poly(Ethylene 2,6-Naphtalate) Films", J. Phys. D: Appl. Phys., Vol. 30, pp. 171-184, 1997.

43. S.S. Bamji and A.T. Bulinski, " Spatial and Spectral Resolution of Electroluminescence in XLPE", Proc. Conf. Electr. Insul. and Diel. Phen., CEIDP, pp. 15-18, 1999.

44. Y.S. Liu, T. Mizuno, W. Shionoya, K. Yasuoka, and S. Ishii, "Light Emission before and during Prebreakdown on Polytetrafluoroethylene Surface with Metallized Electrodes under AC Voltage Application in Vacuum", Jpn. J. Appl. Phys., Vol. 37, pp. 146-150, 1998.

45. G.J. Zhang, Z. Yan, Y.S. Liu, M. Okada, K. Yasuoka and S. Ishii, "Electroluminescence from Alumina Ceramics Surface under Low AC Electric Field in Vacuum", Proc. IEEE Int. Conf. on Properties and Applications of Diel. Materials, ICPADM, pp.407-410, 2000.

46. G.J. Zhang, Z. Yan, Y.S. Liu, M. Okada, K. Yasuoka and S. Ishii, "Development Process of Surface Flashover along Alumina Ceramics under AC Voltage in Vacuum", Proc. IEEE Int. Conf. on Properties and Applications of Diel. Materials, ICPADM, pp.809-812, 2000.

47. T. Lebey and C. Laurent, "Charge injection and Electroluminescence as a Prelude to Dielectric Breakdown", J. Appl. Phys., Vol. 68(1), pp. 275-282, 1990.

48. J. Jonsson, B. Ränby, P. Canet, D. Mary, C. Laurent, C. Mayoux, "Search for Electroluminescence from Polymer Films subjected to a Homogeneous ac Field", Proc. Conf. Electr. Insul. and Diel. Phen., CEIDP, pp. 339-344, 1992

49. K. Kenzo, Y. Takai and M. Ieda, "Electroluminescence in Polyethylene Terephthalate (PET).II. AC Voltage", Jpn. J. Appl. Phys. Vol. 22, pp. 1436-1438, 1983.

50. C. Laurent, C. Mayoux and S. Noel, "Dielectric Breakdown of Polyethylene in Divergent Field: Role of Dissolved Gases and Electroluminescence", J. Appl. Phys., Vol. 54, pp. 1532-1569, 1983.

51. S.S. Bamji, A.T. Bulinski, R.J. Densley and M. Matsuki, "Degradation Mechanism at XLPE/Semicon Interface Subjected to High Electric Stress", IEEE Trans. Electr. Insul., Vol. 26, pp. 278-284, 1991.

52. S.S. Bamji, A.T. Bulinski and R.J. Densley, "Evidence of Near-ultraviolet Emission during Electrical-tree Initiation in Polyethylene", J. Appl. Phys., Vol. 61, pp. 694-699, 1987.

53. S.S. Bamji, and A.T. Bulinski, "Luminescence in Crosslinked Polyethylene of High Voltage Cables", Proc. IEEE Int. Conf. on Properties and Applications of Diel. Materials, ICPADM, pp.11-15, 1997.

54. R. W. Hare and R. M. Hill, "Space Charge in Insulators with Needle-plane Geometry", J. Phys. D: Appl. Phys., Vol. 24, pp. 398-406, 1991.

55. I. Kitani, T. Hirano and K. Arii, "Very Faint Light Emission in Low-Density Polyethylene Films under dc Field", Jpn. J. Appl. Phys. Vol. 26, pp. 639-640, 1987.

56. J.L. Augé, G. Teyssedre, C. Laurent, T. Ditchi and S. Holé, "Combined Electroluminescence and Charge Profile Measurements in Polyethylene Naphthalate", Proc. Conf. Electr. Insul. and Diel. Phen., CEIDP, pp. 516-519, 1999.

57. J.L. Augé, C. Laurent, G.C. Montanari, D. Fabiani, "Detection of DC Threshold of Polyethylene Materials through Space-charge and Electroluminescence Measurements", Proc. Conf. Electr. Insul. and Diel. Phen., CEIDP, pp. 564-567, 1999.

58. G. Teyssedre, D. Mary, J.L. Augé and C. Laurent, "Dependence of Electroluminescence Intensity and Spectral Distribution on Ageing Time in Polyethylene Naphthalate as Modelled by Space-charge Modified Internal Field", J. Phys. D: Appl. Phys., Vol. 32, pp. 2296-2305, 1999.

59. G. Teyssedre, D. Mary, C. Laurent and C. Mayoux, "Optical Emission due to Space Charge Recombination in Insulating Polymers: an Insight into Electrical Aging", in *Space Charge in Solid Dielectrics*, Ed. J.C. Fothergill and L.A. Dissado, Dielectrics Society, Chap. 26, pp. 285-302, 1998.

60. M. Kaufhold, S.S. Bamji and A.T. Bulinski, "Electroluminescence in XLPE under Impulse Voltage Stress", Annual Rep. Conf. Electr. Insul. and Diel. Phen., CEIDP, pp. 846-849, 1996.

61. K. Tohyama, S.S. Bamji and A.T. Bulinski, "Spectra of Electroluminescencein XLPE due to Impulse Voltage", Annual Rep. Conf. Electr. Insul. and Diel. Phen., CEIDP, pp. 601-604, 1998.

62. S.S. Bamji, K. Tohyama and A.T. Bulinski, "Electroluminescence due to Impulse Voltage in Cable-grade XLPE", IEEE Trans. Diel. Electr. Insul., Vol. 6, pp. 288-294, 1999.

63. S.S. Bamji, M. Kaufhold and A.T. Bulinski, "Electroluminescence Technique to Evaluate the Effect of Impulse Tests on High Voltage Cables", IEEE Trans. Diel. Electr. Insul., Vol. 5, pp. 204-210, 1998.

64. K. Tohyama, S.S. Bamji and A.T. Bulinski, "Electroluminescence in XLPE due to Impulse Voltage", DEI-99-29, pp.47-52, 1999.

65. T. Mizuno, Y.S. Liu, W. Shionoya, S. Matsushima, K. Yasuoka , S. Ishii, A. Yokoyama and H. Miyata, "Electroluminescence in Polyethylene Subjected to Impulse Voltages", IEEE Trans. Diel. Electr. Insul., Vol. 5, pp. 211-218, 1998.

66. T. Mizuno, Y.S. Liu, M. Okada,W. Shionoya, K. Yasuoka , S. Ishii, A. Yokoyama and H. Miyata, "Light Emission in PE with a Needle-like Microvoid at the Metal-Polymer

Interface under Impulse Voltages", IEEE Trans. Diel. Electr. Insul., Vol.5, pp. 536-540, 1998.

67. M. Kaufhold, S.S. Bamji, A.T. Bulinski, "Time Resolved Measurements of Electroluminescence in XLPE under Impulse Voltage Conditions", Proc. IEEE Int. Symp. on Electr. Insul., pp. 686-690, 1996.

68. K. Kojima, Y. Takai and M. Ieda, "Electroluminescence in Polyethylene Terephthalate (PET)-I-Impulse Voltage", Jpn. J. Appl. Phys. Vol. 21, pp. 860-864, 1982.

69. S.S. Bamji, A.T. Bulinski and R.J. Densley, "Threshold Voltage of Luminescence and Electric Tree Inception in LDPE", J. Appl. Phys., Vol.63 pp. 584-5845, 1988.

70. J.V. Champion, S.J. Dodd and G.C. Stevens, "Quantitative Measurement of Light Emission during the Early Stages of Electrical Breakdown in Epoxy and Unsaturated Polyester Resins", J. Phys. D: Appl. Phys., Vol. 26, pp. 819-828, 1993.

71. J.V. Champion, S.J. Dodd and G.C. Stevens, " Light Emission Studies of Electrical Treeing Processes", IEE 6th Int. Conf. on Dielectric Mat. Measurements and Applications, DMMA, pp. 201-204, 1992.

72. K. Kaminaga, N. Yoshifu, T. Uozumi, J. Yorita, S. Fukunaga, "Study on Deterioration Mechanism of XLPE Cables", Jicable'95, pp. 215-220, 1995.

73. K. Kaminaga, H. Shigetsugu, T. Uozumi, T. Haga, N. Yasuda and T. Fukui, "The Mechanism of Degradation of Polyethylene in High Electrical Fields", Proc. IEEE Int. Symp. on Electr. Insul., 1994.

74. A.R. Leighton, R.D. Naybour, L.Warren, "Light Emission and Electrical Tree Initiation in Highly Stressed XLPE and the Effect of DC Prestressing", Proc. IEEE Int. Conf. on Cond. and Break. in Sol. Diel., pp. 273-278, 1998.

75. G. Teyssedre, L. Cissé, D. Mary and C. Laurent, "Identification of the Components of the Electroluminescence Spectrum of PE Excited in Uniform Fields", IEEE Trans. Diel. Electr. Insul., Vol. 6, pp. 11-19, 1999.

76. T. Mizuno, Y.S. Liu, W. Shionoya, K. Yasuoka , S. Ishii, H. Miyata and A. Yokoyama, "Electroluminescence in Insulating Polymers in ac Electric Fields", IEEE Trans. Diel. Electr. Insul., Vol. 4, pp. 433-138, 1997.

77. T. Mizuno, Y.S. Liu, W. Shionoya, H. Miyata, A. Yokoyama, K. Yasuoka , S. Ishii, "Electroluminescence from Polymeric Halides Subjected to an ac Voltage", Proc. Conf. Electr. Insul. and Diel. Phen., CEIDP, pp. 233-236, 1996.

78. J. Jonsson, B. Ränby, D. Mary, C. Laurent and C. Mayoux, "Electroluminescence from Polyolefins Subjected to a Homogeneous ac Field", IEEE Trans. Diel. Electr. Insul., Vol. 2, pp. 107-113, 1995.

79. J. Jonsson, B. Ränby, D. Mary, F. Massines, C. Laurent and C. Mayoux, "An Interpretation of Electroluminescence of Polyolefins based on the Similarity between Electro- and Plasma-induced Luminescence Spectra", Proc. IEEE Int. Conf. on Cond. and Break. in Sol. Diel., pp. 701-705, 1995.

80. C. Laurent, F. Massines, C. Mayoux, D.M. Ryder and C. Olliff, "Comparison between Photo- and Electro-induced Luminescence Spectra of Polyethylene", Proc. Conf. Electr. Insul. and Diel. Phen., CEIDP, pp. 93-96, 1995.

81. C. Laurent, D. Mary, C. Mayoux, " Assignment of Electroluminescence Spectral Components to Molecular Transitions in Polyethylene 2,65-Naphthalate", Proc. Conf. Electr. Insul. and Diel. Phen., CEIDP, pp. 229-232, 1996.

82. C. Laurent, C. Mayoux, F. Massines, "Optical Emission due to Space Charge Effects in Polymers: an Insight into Wear-out and Breakdown Mechanisms", Proc. Int. Conf. on Space Charge in Sol. Diel., pp. 268-273, 1995.

83. F. Massines, P. Tiemblo, G. Teyssedre and C. Laurent, "On the Nature of the Luminescence Emitted by a Polypropylene Film after Interaction with a Cold Plasma at Low Temperature", J. Appl. Phys., Vol. 81, pp. 937-943, 1997.

84. G. Teyssedre, P. Tiemblo, F. Massines and C. Laurent, "On the UV Contribution to Plasma-induced Luminescence of Polypropylene", J. Phys. D: Appl. Phys., Vol. 29, pp. 3137-3146, 1996.

85. G. Teyssedre, D. Mary, L. Cissé, C. Laurent, J. Salon, "Dependence of Electroluminescence Intensity and Spectral Distribution on Ageing Time in Polyethylene Naphthalate", Proc. IEEE Int. Conf. on Cond. and Break. in Sol. Diel., ICSD, pp. 287-290, 1998.

86. G. Teyssedre, D. Mary and C. Laurent, "Analysis of the Luminescence Decay following Excitation of Polyethylene Naphthalate Films by an Electric Field", J. Phys. D: Appl. Phys., Vol. 31, pp. 267-275, 1998.

87. D. Mary, M. Albertini, C. Laurent, "Integral and Spectral Investigation of Electroluminescence in Insulating Polymers", Proc. IEEE Int. Symp. on Electr. Insul., pp. 436-439, 1996.

88. J. Jonsson, B. Ränby, F. Massines, D. Mary and C. Laurent, "Spectral Features of the Luminescence of Polyethylene Subjected to Various Excitation Sources", IEEE Trans. Diel. Electr. Insul., Vol. 3, pp. 859-865, 1996.

89. G. Teyssedre, L. Cissé, C. Laurent, F. Massines and P. Tiemblo, "Spectral Analysis of Optical Emission Due to Isothermal Charge Recombination in Polyolefins", IEEE Trans. Diel. Electr. Insul., Vol. 5, pp. 527-535, 1998.

90. G. Teyssedre, and C. Laurent, "Tunneling-mediated Recombination-induced Luminescence in Polyethylene Naphthalate", Proc. Conf. on Diel. and Related Phen., 1998.

91. G. Tardieu, G. Teyssedre, D. Mary, C. Laurent, "Analysis of Electroluminescence vs AC Voltage Characteristic of Metallized Polymers Films", IEE Proc. 8th Int. Conf. DMMA, pp. 434-439, 2000.

92. Th. Baumann, B. Fruth and F. Stucki, "Charge Injection and Electroluminescence in the Prestate of Dielectric Aging", Proc. Int. Symp. High Volt. Eng., pp.1-4, 1987.

93. R. Pietsch, "Integral and Spectral Investigations of Luminescence Light During Electrical Aging in Polyethylene", Proc. Int. Symp. High Volt. Eng., pp. 115-118, 1991.

94. S.S. Bamji, A.T. Bulinski, Y. Chen and R.J. Densley, "Threshold Voltage for Electrical Tree Inception in Underground HV Transmission Cables", IEEE Trans. Diel. Electr. Insul., Vol. 27, pp. 402-404, 1992.

95. R. Coisson, C. Paracchini and G. Schianchi, "Electroluminescence in an Epoxy Resin", J. Electrochem. Soc., Vol. 125, pp. 583-585, 1978.

96. C. Laurent, "Optical Pre-breakdown Warnings in Insulating Polymers", Proc. IEEE Int. Conf. on Cond. and Break. in Sol. Diel., ICSD, pp. 1-12, 1998.

97. K. Uchida, H. Asai, N. Shimizu and T. Takahashi, "Initiation mechanism of Electrical Tree and Deteriorated Region in Polymers", Proc. Int. Conf. Prop. Appl. Diel. Mat., pp. 240-243, 1991.

98. K. Kaminaga, T. Suzuki, T. Uozumi, T. Haga, N. Yasuda and T. Fukui, "The Mechanism of Degradation of Polyethylene in a High Electrical Field", Proc. Conf. Electr. Insul. and Diel. Phen., CEIDP, pp. 666-671, 1993.

99. N. Shimizu, J. Mori, M. Kosaki and K. Horii, "The Effect of Absorbed Oxygen on Electrical Treeing in Polymers", Proc. IEEE Int. Symp. on Electr. Insul. Diel. Phen., pp. 306-309, 1982.

100. J. Jonsson, B. Ränby, C. Laurent and C. Mayoux, "Influence of Thermal- and UV-aging on Electroluminescence of Polypropylene Films", IEEE Trans. Diel. Electr. Insul., Vol. 3, pp. 859-865, 1996.

101. D. Mary, C. Laurent, C. Mayoux, J. Berdala, R. Clavreul, "Diagnosing Power Cable Polyethylene Insulation by Electroluminescence Monitoring", Jicable'95, pp. 520-524, 1995.

102. D. Mary, C. Laurent, C. Mayoux, J. Berdala, R. Clavreul, "Aging Characterization of Cable Polyethylene Insulant by Electroluminescence Measurement", Revue Electricite et Electronique, Special Issue on Power Cables and Insulating Materials Science, pp. 79-83, 1996.

103. S.S. Bamji, A.T. Bulinski and R.J. Densley, "Degradation of Polymeric Insulation due to Photoemission Caused by High Electric Fields", IEEE Trans. Electr. Insul., Vol. 24, pp. 91-98, 1989.

104. S.S. Bamji, A.T. Bulinski and R.J. Densley, "Light Emission and Subsequent Tree Inception due to Polarity Reversal of the Local Field in Polymeric Insulation", Proc. Conf. Electr. Insul. and Diel. Phen., CEIDP, pp. 173-179, 1992.

105. S.S. Bamji, A.T. Bulinski and R.J. Densley, "The role of Polymer Interface during Tree Initiation in LDPE", IEEE Trans. Electr. Insul., Vol. 21, pp. 639-644, 1986.

106.S.S. Bamji, A.T. Bulinski, Y. Chen and R.J. Densley, "Photodegradation Versus Hot-electron Impact for Electrical Tree Inception at Low Electric Fields", Proc. Int. Conf. Prop. Appl. Diel. Mat., pp. 51-54, 1991.

107.N. Cariou-Saintemarie, A.E. Davies, J.G. Head, " Electroluminescence Measurements in Polyethylene Insulation", IEE Proc. 8th Int. Conf. DMMA, pp. 430-433, 2000.

108.N. Cariou-Saintemarie, A.E. Davies, J.G. Head, "Electroluminescence Measurements in Polyethylene Insulation under AC voltage in Nitrogen Condition", submitted to the IEEE Trans. Diel. Electr. Insul., 2001.

109. Wright Instrument CCD detector manual.

110.D.N. Batchelder, "Multichannel Raman Spectroscopy with a Cooled CCD Imaging Detector", European Spectroscopy News, Vol. 80, pp. 28-32, 1988.

111. Coherent-Ealing Catalogue.

112.P.B. Johnson and R.W. Christy, "Optical Constants of the Noble Metals", Phys. Rev. B, Vol. 6, pp. 4370-4379, 1972.

113.F.L. Pedrotti, L.S. Pedrotti, *Introduction to Optics*, Prentice-Hall Int. Inc., Englewood Cliffs, 1996.

114.Pirelli internal report, *Rapporto di lavoro 12.1-2014/10-82007*, 1982.

115.J. Crank, "The Mathematics of Diffusion", Claredon Press, Oxford, 1975.